ESTIMATING NEW ZEALAND TEMPERATURE AND ARIDITY SINCE THE LAST GLACIAL MAXIMUM FROM BIOMASS BURNING MARKERS

By

LAUREN MEREDITH WEISEL

A thesis submitted to the

Graduate School-New Brunswick

Rutgers, The State University of New Jersey

in partial fulfillment of the requirements

for the degree of

Master of Science

Graduate Program in Oceanography

written under the direction of

Dr. Elisabeth Sikes

and approved by

_____

_____

_____

New Brunswick, New Jersey

October 2015

ABSTRACT OF THE THESIS

New Zealand temperature and aridity since the Last Glacial Maximum from biomass burning biomarkers

By LAUREN MEREDITH WEISEL

Thesis director:
Dr. Elisabeth Sikes

Aridity is an important component of climate change. Wildfires linked to dry conditions can drastically alter the biomass of a landscape. Diagnostic molecules created in these fires during the incomplete combustion of plants can be used to estimate past biomass burning events. Biomass burning markers (BBM) were isolated from three sites from the South Island of New Zealand, and quantified using GCMS analysis. A record of fire occurrence based on these BBM revealed a pattern of increased aridity in the past. The central South Island was characterized by persistent dryness in the glaciation, increased wetter periods marked the Younger Dryas and Antarctic Cold Reversal, followed by drier cycles with fewer periods of wetness into the early Holocene, and persistent wetting toward the late Holocene. The southern end of the South Island showed consistent wetness from the mid Holocene to the modern. Dryness changing in longer vs. shorter and wetter vs. drier is a pattern seen from the glaciation through the early Holocene. Pollen-based temperature reconstructions in the study sites do not agree with reconstructions from elsewhere in New Zealand. These new results documenting burning in the glaciation and through the early deglaciation are a plausible explanation for bias in these temperature

reconstructions due to local aridity in the study areas of the South Island. Changes in this local aridity were likely due to the Southern Westerly Winds, which shifted north during the glaciation, then overall shifted southward toward the Holocene.

ACKNOWLEDGEMENTS

I'd like to start by thanking my advisor, Dr. Elisabeth Sikes, without whom this thesis would have been impossible – not only for the funding to complete this project, but also for the time, energy, expertise, and compassion she lent to me through the duration of my time here at Rutgers. My thesis committee, Lisa Rodenburg and James Wright, need acknowledgement as well, for their help not only during the writing of this thesis, but also during other points of my graduate career. I was lucky enough to have Jim as my professor twice, and without Lisa's support (and its finicky ASE!) this project would never have gotten off the ground. Similarly, I'd like to thank our collaborators on this project, Janet Wilmshurst and Patricia Medeiros, for helping to lay the groundwork for my research, as well as their assistance and insight into the world of New Zealand biomarkers.

My parents and boyfriend need special thanks, of course, for their love and patience during these past few years. Though I've been across the country from all of them, they still conveyed their emotional support through text, emails, and lots and lots of Skype calls.

Naturally, many other members of the Sikes lab deserve thanks as well: Anna Hermes and Becca Barnes for showing me the ropes; undergraduate researchers Amanda, Monisha, Maura, Christine, and Alyssa, for keeping me sane during my hours in lab; and Kat Allen for being a research inspiration and one of the nicest people I've had the pleasure to meet.

I would be remiss in my gratitude if I didn't thank all of the members of the graduate program in oceanography for their friendship, notably my year's cohort of Sushmita, Sarah, and Kaycee, who went through plenty of classes and trials with me, plus special shout-outs to Jack, Alex, Kevin, Katie, and Amy. In addition, I'd like to thank my close friends

Michele, Gary, Eowyn, Mike, Emma, Rina, Ella, and Mina, for helping my time in New Jersey be so much fun!

A final acknowledgement goes to Robert Sherrell, for sending the recruitment email that inspired me to come to Rutgers in the first place. It's been a great three years here, and I've learned more than I ever thought possible.

TABLE OF CONTENTS

LIST OF TABLES

LIST OF FIGURES

I. INTRODUCTION

1.1 Thesis context

In order to understand the future of climate change, first we must describe and understand past changes. The determination of past climate generally relies on indicators, or proxies, that preserve details of physical parameters, which hold the record of past events that can lead to understanding of how those events may have occurred (Meyers, 1997). To create a reconstruction of such important climate indicators as temperature, aridity, biota, or any host of other factors that make up a given area's climate, proxies must be found and their relationships to these factors reliably calibrated in order to make sense of what happened in the past.

Reconstructions of some of the factors of the climate of New Zealand since the Last Glacial Maximum (LGM) 17.8 thousand years ago (ka) exist, such as pollen proxies of temperature (Wilmshurst et al., 2007), plankton proxies of sea surface temperature (Samson et al., 2005; Sikes et al., 2002), chironomid proxies of seasonality (Vandergoes et al., 2008), and speleothem proxies of precipitation (Hellstrom and McCulloch, 2000; McGlone et al., 2004; Wilmshurst et al., 2007). However, these proxy reconstructions are presently not fully consistent with each other. Temperature as reconstructed by pollen assemblages (Wilmshurst et al., 2007), for example, suggests a different history of how the transition from the LGM to the present climate progressed in New Zealand from that derived by the changing position of glacial moraines (Putnam et al., 2010). Pollen records, a main source of climate data for the rest of this thesis, rely on the presences of pollen in the sediment record to infer by the representative plants' preferred climate range the temperature range present at the time the plant grew in the past. However, this may not be

an accurate representation if the temperatures in fact remained the same, and a past shift in plant abundances was driven instead by a concurrent change in precipitation which caused certain plants to thrive and others to migrate elsewhere. There are indications that proxies that represent temperature often are also affected by aridity in this way, yielding proxy records that can be either questionable or wrong (Wilmshurst et al., 2007). To tease apart these intertwined factors and get a better grasp of both temperature and aridity, what is needed is an independent measure of aridity to inform the pollen record of temperature. Distinguishing which plant type abundance shifts were caused by changes in temperature and which may have been caused by changes in precipitation is an important step to painting a clearer picture of the climate changes in New Zealand since the LGM.

Although single site reconstructions are useful, a complete picture of climate needs multiple records from multiple time periods. Comparing proxy records from a variety of sites can provide information that is important to regional and large-scale climate interpretation. Interpreting proxy data from several sites allows interpretation of regional climate events, making it possible to place these in a global context. An important southern hemisphere climate factor is the southern westerly wind (SWW) atmospheric circulation pattern. This is a climatic wind belt around 50°S that fluctuates in position on a north-south basis on the order of 3 degrees of latitude (Shulmeister et al., 2004). It has been hypothesized that SWW shifts influenced deglacial climate change over the southern hemisphere (Lamy et al., 2010; Toggweiler et al., 2006), and evidence for these shifts such as temperature change interpreted from Southern Alps glacial retreat has shown that the SWW have a definite impact on the climate of New Zealand (Putnam et al., 2010). In order to understand this effect, locations situated along the north-south breadth of that fluctuation

are important to study. New Zealand is one of the few landmasses that intersect that path, and it is for this reason that this thesis makes use of a latitudinal transect of sediment cores from New Zealand bogs, in addition to cores in the same region at varying longitudes.

Work towards this thesis attempts to establish an aridity record to add to existing temperature records from the South Island (Alloway et al., 2007; Newnham et al., 2012; Wilmshurst et al., 2007). Aridity is recorded through a proxy record of marker compounds produced by biomass burning. The production of these biomass burning markers is affected by the fuel and intensity of the fires in which they were created (Elias et al., 2001), which are in turn affected by cycles of both local temperature and precipitation (Westerling et al., 2003). This direct correlation makes these proxies ideal for comparing to existing records of temperature, aridity, and plant biomass to create an overall more robust climate record. In combination, these factors can be correlated to differences in the position of the SWW by the climate signal proxies this circulation pattern has left behind in the terrestrial records. This in turn sheds light on global atmospheric fluctuations since the LGM.

1.2 Overview of the study area

New Zealand is a subcontinent in the southwest Pacific Ocean (Figure 1-1), with its northern portion in the subtropical south Pacific and its southern half in the polar Southern Ocean. This creates a modern temperature and precipitation gradient between the warmer subtropical north, and the colder, more temperate south, which is under polar influences (Table 1-1). On the South Island, the Southern Alps line the west coast,

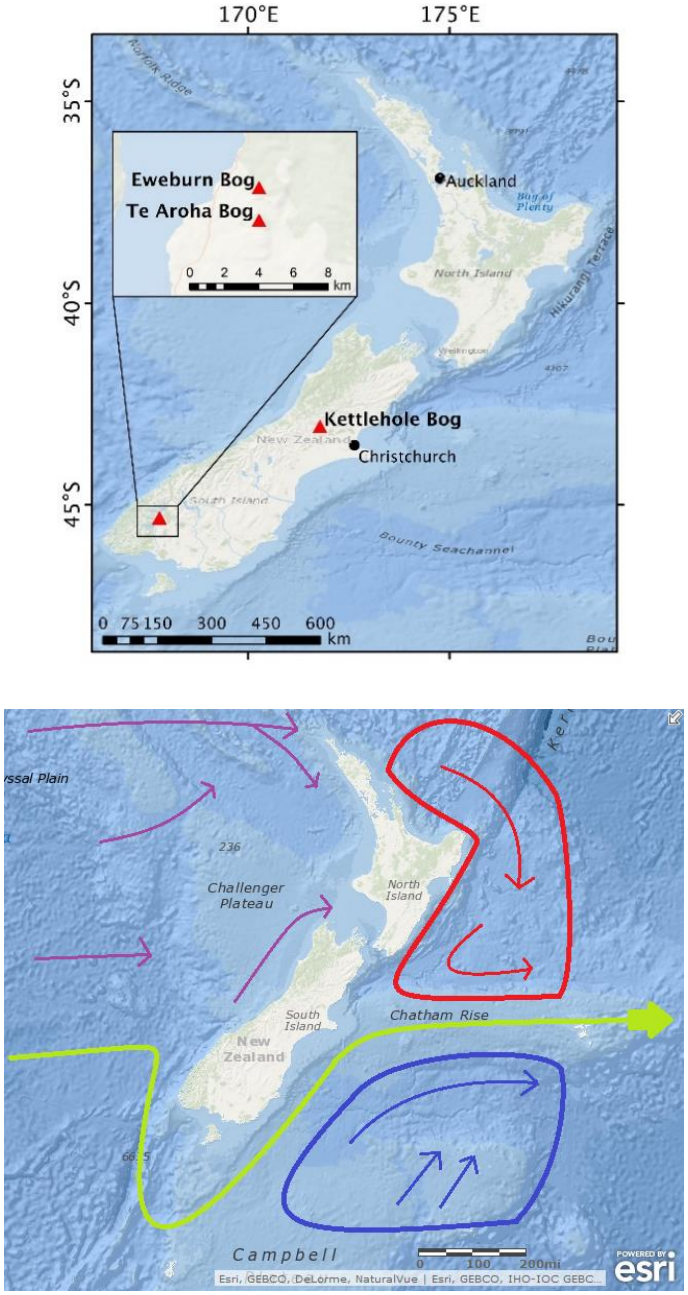

Figure 1-1: (left) Map of modern New Zealand, indicating the locations of the three study sites featured in this thesis. (right) Map of modern surface water masses surrounding New Zealand: Subtropical Front (STF) in green, subtropical water (STW) in red, subpolar water (SPW) in blue, and the Tasman Front (TF) in purple (Stevens and Chiswell, 2013). The shape and seafloor topography of New Zealand play a large part in the positions of the ocean fronts, and hence the climate, of New Zealand.

leading to a rain shadow in the warm, dry center of the Island and a consistently wet west coast (McGlone et al., 2004). While both the northern and southern portions of New Zealand receive large amounts of rain over the course of the year, the subtropical north experiences a highly seasonal gradient in monthly precipitation (NIWA, 2013). Though gradients of temperature and precipitation are both present in each of these areas over the course of a year, the temperature changes are not particularly distinct from region to region. It is the difference in annual change in precipitation between these areas that is more notable. The combination of absolute temperature and range of precipitation together set the defining characteristics of the microclimates of New Zealand.

A major force impacting these temperature and precipitation differences is the position of the oceanic fronts just offshore from New Zealand. Today, the ocean front dividing subtropical waters from subpolar water masses – known as the Subtropical Front (STF) – traverses the Pacific Ocean eastward around 40°S, until it cuts south just before Tasmania and wraps around the southern tip of New Zealand at around 45°S. After this, the STF flows northward to approximately 42°S along the South Island's eastern coast, eventually making its way northward back up to 40°S (Figure 1-1). North of the STF sits warm, salty Subtropical water (STW), while south of it lies colder, fresher Subantarctic

	Temperature (°C)					Precipitation (mm)					
	Summer		Winter			Amount				Season	
	Avg max	Avg min	Avg max	Avg min	Δ°C	Avg max	Avg min	ΔP	Total	Wettest month	Driest month
Auckland	23	14	15	7	8.5	146	65	81	1240	July	Feb
Christchurch	23	11	12	2	11	79	49	30	630	July	Feb
Te Anau	19	9	9	2	8	80	60	20	1200	May, Jan	Aug, Feb

Table 1-1: Summary of modern New Zealand temperature and precipitation from sites near core locations in this thesis.

surface waters (SAW). Farther south, the southern boundary of the SAW is the Antarctic Circumpolar Current (ACC), the global current that circles Antarctica and connects all the world's oceans (Sokolov and Rintoul, 2009).

The position of the STF on the west coast of New Zealand varies little seasonally, moving just south of the South Island during the austral summer with a slight northward shift during the winter. On the eastern coast of the island the STF is geographically constrained around the Chatham Rise and shifts very little on a year-to-year basis (Belkin and Gordon, 1996). Overall, while the STF has changed positions over the timescale of the last deglaciation, it has moved only a reported 3° south from its glacial position in the southwest of Tasmania to its modern location, and its location to the south of New Zealand and on the Chatham Rise has been relatively unchanged during this time (Sikes et al., 2002; Sikes et al., 2009a; Weaver et al., 1998). This implies that the influence of water masses on temperature and precipitation changes in New Zealand has remained relatively constant during this time. Land adjacent to STW is more likely to have a warm, wet climate, while the land adjacent to SAW will be cool and wet (Table 1-1).

1.3 New Zealand deglacial history

The climate of New Zealand has changed dramatically since the end of the last ice age. Evidence from planktonic foraminiferal assemblages and alkenones shows that overall temperatures were cooler at the end of the last glacial termination than the modern by as much as 4-5°C (Samson et al., 2005; Sikes et al., 2002). According to pollen records, LGM plant cover in the South Island consisted mainly of grasses and podocarps, small conifer trees, which could survive the cool and dry conditions present at the time. As the climate

grew overall warmer and wetter, tall angiosperm trees such as *Nothofagus* and *Dacrydium* became more dominant and spread southward to follow the more habitable climate (McGlone et al., 2004; Wilmshurst et al., 2002). While this pattern fluctuated somewhat during the deglaciation, this distribution characterized the Holocene, until the settlement of New Zealand by the Maori people around 1280AD, when the cutting and burning of tall trees for lumber and land management altered the local ecology, transforming large amounts of forest into grassland (McWethy et al., 2009).

Much of the reconstruction of New Zealand climate has been focused on the North Island and northern South Island due to plentiful regional volcanic eruptions allowing for reliable age reconstructions from tephras (Alloway et al., 2007; Sikes et al., 2013). Several lines of evidence suggest that approximately 19,000 years before present (19ka), the climate of New Zealand gradually began to warm (Alloway et al., 2007) and terrestrial glaciers began to retreat (Kaplan et al., 2010) during what is called the Last Glacial-Interglacial Transition (LGIT). This period of warming continued into a time period from 17.8-14.7ka known as Heinrich Stadial 1 (HS1). The locations and isotopic compositions of glacial moraines in the Southern Alps show that the Antarctic Cold Reversal (ACR) in New Zealand represented a short cooling period from 14.5ka to 12.9ka, interrupting the warming of HS1 (Blunier et al., 1997; Putnam et al., 2010). The ACR was immediately followed by the period of rapid southern hemisphere warming known as the Younger Dryas, which lasted until about 11.75ka (Newnham et al., 2012) and led to a so-called climate optimum, in which temperatures were warmer than the modern period, until at last temperatures cooled to their current state around 8ka (Alloway et al., 2007; Wilmshurst et al., 2007).

Some key details of climate reconstruction, such as the timing and strength of the effects of the ACR across New Zealand, are still unclear due to conflicting evidence. Key climate events such as the LGIT, ACR, and early and mid-Holocene warming events are present in northern New Zealand temperature reconstructions regardless of location and proxy (Alloway et al., 2007; Sikes et al., 2013). However, these records typically disagree on the events' specific timing, varying in some cases by 300-3000 years. In addition, the extent of warming or cooling during a given time period seems to differ from proxy to proxy, with, for example, speleothem and planktonic foraminiferan *Globigerina bulloides* $\delta^{18}O$ showing a distinct cooling of sea surface temperature (SST) from 13.5-11.6ka (Alloway et al., 2007), pollen records showing only the slightest temperature effect on pollen percentage ratio, and other planktonic foraminifera not showing it at all (Figure 1-2). More climate reconstructions across the deglaciation are needed to gain a better understanding of the timing and overall climate change during these events.

Globally, these climatic trends were quite different. The initial warming to ACR cooling to Younger Dryas warming pattern seen in New Zealand is characteristic only of the southern hemisphere. The northern hemisphere experienced an opposite climate pattern, in what is known as the oceanic bipolar seesaw hypothesis (Broecker, 1998). According to this hypothesis, the bipolar seesaw system in fact likely originated in the northern hemisphere with Heinrich Event 1 (HE1) at 17.5ka, in which a large amount of ice broke away from northern glaciers, drifted south towards key locations of North Atlantic Deep Water (NADW) formation, and melted. This resulted in a large pool of anomalous cold, fresh water that, due to being more buoyant than the saltier water

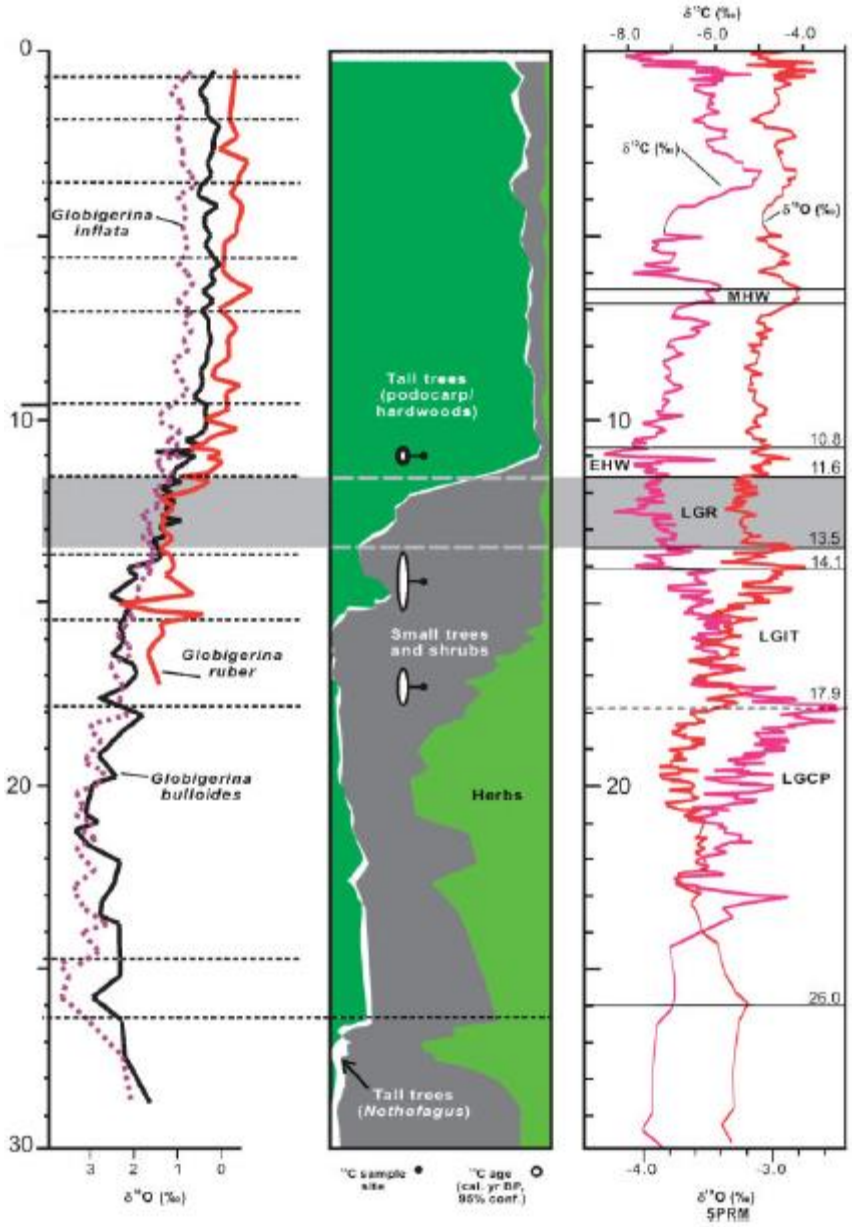

Figure 1-2: Three different paleoclimate proxies for temperature in New Zealand. Left: $\delta^{18}O$ record from planktonic foraminifera *Globigerina inflata*, *ruber*, and *bulloides* in a sediment core from off the east coast of the North Island. Center: pollen record of relative abundance of tall tree, shrub and small tree, and herb pollen in Okarito Bog on the western coast of the central South Island. Right: $\delta^{18}O$ and $\delta^{13}C$ record from speleothems in the northern South Island. Note how the different proxies react during the supposed cooling of the Lateglacial Reversal (LGR, grey bar in the figure) (Modified from Alloway et al. 2007)

around it, essentially capped those downwelling sites. Since water could no longer sink below the freshwater cap, downwelling and formation of NADW was reduced or possibly stopped completely, which greatly slowed thermohaline circulation from 17.5-14.7ka, a time period known as Heinrich Stadial 1 (HS1). While this cooled the northern hemisphere by preventing southward cold water transport, the subsequent lack of cold water being brought to the southern hemisphere led to the early initial warming of the LGIT (Broecker, 1998; Denton et al., 2010). Once this meltwater cap subsided, however, normal meridional overturning circulation was able to resume, and a period of warming occurred in the north, known in the northern hemisphere as the Bølling-Allerød (BA), while the southern hemisphere cooled, resulting in the ACR. A subsequent large meltwater pulse at 12.7ka caused the end of the ACR and the onset of the Younger Dryas stadial, bringing cold water and a climatic cooling back to the northern hemisphere at the same time as southern hemisphere warming (Denton et al., 2010).

Oceanic water masses are capable of transporting large volumes of heat between the hemispheres, but the thousand-year timescale of the thermohaline circulation means that a lag between hemispheres should be evident in the hemispheric heat budget. The glacial melting characteristic of HS1 occurred at 17.8ka, while the southern hemisphere warming believed to be associated with the subsequent lack of cold water input has been established from the EPICA Dome C ice core as occurring at about 17.5ka, only 300 years after HE1. This is a much shorter time frame than the millennial timescale of the thermohaline circulation (Denton et al., 2010). A faster mode of heat transport has been hypothesized to explain the suddenness of the onset of this southern hemisphere warming (Toggweiler et al., 2006). As circulation changed and shifted during this time, sea surface

temperature evidence as recorded by sediment molecules called alkenones show that so too did the atmosphere above them (Lamy et al., 2007). The Intertropical Convergence Zone (ITCZ), a band of warm moist air typically found north of the equator in modern times due to the heat balance between the northern and southern hemispheres, has been shown to migrate on the order of 5-10 degrees of latitude over the 3ky of the HS1 during large climate events such as the hypothesized bipolar seesaw (Lee et al., 2011). Likewise, the SWW above the New Zealand area are believed to have shifted during the LGIT (Shulmeister et al., 2004). A seesaw-led change in the coupled ocean-atmosphere system of the ACC and the southern westerly wind belt has been suggested to have provided the necessary heat flow in order to jumpstart the LGIT at the northern margin of the westerlies and the ACC in South America (Lamy et al., 2007). Since New Zealand is in the Pacific Ocean at a similar latitude to the South American study site, it is likely that the subcontinent was affected by the SWW in a similar way.

1.4 Proxy calibration

In New Zealand, regional-scale effects vary by location and proxy (Figure 1-2), leading to confusion over the accurate reconstruction of New Zealand climate. For example, one early temperature reconstruction from the North Island was obtained through pollen records, then dated in time using tephrachronology (Lowe and Newnham, 1999; Newnham and Lowe, 2000). This record seemed to show an anomalous cooling event overlapping both the ACR and the Younger Dryas, which did not agree with other terrestrial New Zealand records from the time (Denton and Hendy, 1994; Singer et al., 1998). Re-dating this same core and obtaining more accurate dating clarified that this cooling was more likely to have been associated with the ACR (Hajdas et al., 2006). This

is a case in which a proxy record was corrected by the application of new, more accurate dating, showing the possibility of inaccurate interpretations of proxy records.

Where a proxy is being utilized correctly, it may not be enough to accurately reflect expected results. Model reconstructions of pre-deforestation pollen records since the LGM using the modern analog technique resulted in 7 mean annual temperature records for different locations (Wilmshurst et al., 2007) that adhered poorly to the current understanding of the progress of New Zealand Holocene climate (Figure 1-3). The proxies discussed so far suggest that a latitudinal transect of New Zealand would indicate cold temperatures in the south and slightly warmer but still colder than modern temperatures in the north starting at the beginning of the deglaciation (Newnham et al., 2012). All of New Zealand should respond similarly to the deglacial climatic shifts described above, with warming during HS1, cooling during the ACR, warming again during the YD and optimum, and eventually cooling towards the modern (Alloway et al., 2007; Newnham et al., 2012). However, only two of Wilmshurst's temperature records (2007) in two different parts of the country, Wairehu and Longwoods, even appear to follow this trend. Most of the Wilmshurst records show temperatures consistently higher than modern even during the modern itself, with the Ajax Bog and Clarks Junction reconstructions indicating that temperatures were actually higher at the LGIT than today. The Cass Basin temperature reconstruction, which is the same location as Kettlehole Bog studied in this thesis, has a tenuous connection to nearby temperature records, which will be explored in more detail in later sections (Newnham et al., 2012; Wilmshurst et al., 2007).

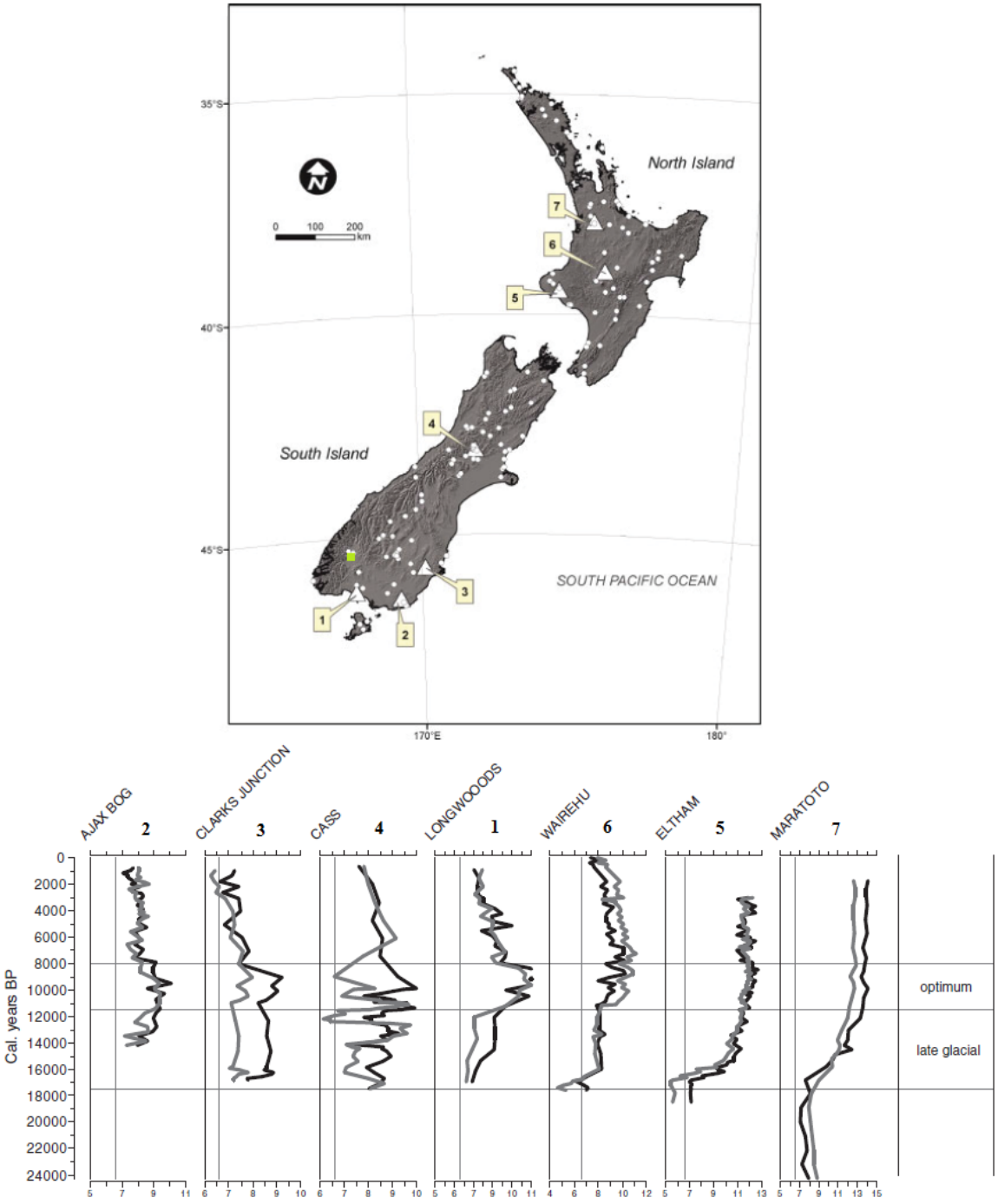

Figure 1-3: (Top) Locations of seven fossil sites for which mean annual temperature (MAT) has been reconstructed. Location 4 represents Kettlehole Bog, and the green square represents Eweburn Bog. (Bottom) MAT reconstructions for the seven fossil sites above. Vertical grey lines represent modern MAT for each site. These temperature reconstructions likely do not reflect actual temperatures for these times. (Modified from Wilmshurst et al. 2007)

Temperature is not the only factor affecting where plants will grow. Records of ecosystems over time that are based on pollen are subject to the location and abundance of the plants that produce the pollen, which is a response to both temperature and moisture. Conifers, for example, require a certain amount of moisture to grow, while grasses tend to proliferate in drier climates (Augustinus et al., 2011). The disparity between expected and simulated MAT, therefore, is a conundrum that can be addressed by obtaining a measure of moisture changes. Obtaining these measurements is the motivation behind this thesis – changes in aridity may be responsible for inaccurate temperature reconstructions due to the model's assumption that plant abundance is solely based on changes in temperature. Eweburn, Kettlehole, and Lake Te Aroha Bogs are ombrogenous, which means that they all subsist on precipitation with water flowing only outwards from the bogs, so any change in the precipitation local to the bog would have a direct effect on the ecosystem therein (McGlone et al., 2004; Wilmshurst et al., 2002). This makes these locations ideal for investigating the effects of precipitation on temperature reconstructions in New Zealand.

1.5 Study sites

The study sites selected for this thesis are in the center and south of New Zealand, covering a latitudinal range of 2.3 degrees (Figure 1-1). These sites complement and extend the latitudinal range of previous terrestrial and marine studies from the North Island at Onepoto Maar and the South Chatham Rise (Sikes et al., 2013), and the South Island at Okarito Bog (Newnham et al., 2012). The North Island terrestrial site is in the far north of the subcontinent, the South Island terrestrial site is on the central west coast of the island, and the marine site is offshore of the country to the east at about the same latitude as the Kettlehole and Okarito Bog sites. Sites farther south on a latitudinal transect of New

Zealand were selected to extend the analysis of climatic shifts in the deglaciation, since the SWW are believed to have varied in a north-south direction (Kohfeld et al., 2013; Lamy et al., 2010; McGlone et al., 2010). It is important to understand not only how climate changed in specific locations, but also how it changed over time over the subcontinent as a whole.

1.5.1 Te Anau

Two sites chosen for this study, Eweburn Bog (EB) and Lake Te Aroha (LTA), are located in the far southwestern tip of the South Island of New Zealand (Figure 1-1). Situated in Southland near Lake Te Anau, these two sites sit atop a glacial moraine hill at about 300m elevation (Figure 1-4). Radiocarbon dates on the cores from EB and LTA suggest that they extend back to 6.5 and 26.9ka respectively. The two sites are ombrotrophic bogs, which are bogs that receive their only water input from rain and only release water through runoff and slow infiltration of the underlying bedrock. The local vegetation within the bog has been dominated by *Sphagnum* moss throughout the Holocene, and other plant life there currently is primarily broadleaf trees such as *Fucospora* with some herbaceous groundcover. As is characteristic of the west and southwest South Island, broadleaf *Nothofagus* trees are dominant at this elevation, although the area has largely been deforested since being settled (Wilmshurst et al., 2003).

Eweburn and Te Aroha Bogs lie approximately 10km east of the Murchison Mountains, which divide the south of the South Island into two distinct climate regions: the west coast, which is cool and wet with low variability in temperature and precipitation, and the seasonally drier east. The sampling sites are located just at this boundary (Wilmshurst et al., 2002). The southerly location of this site is useful for determining the

influence of latitudinal fluctuation of the SWW on southern New Zealand. The Eweburn Bog core dates back only to 6.5ka, but can give us a perspective

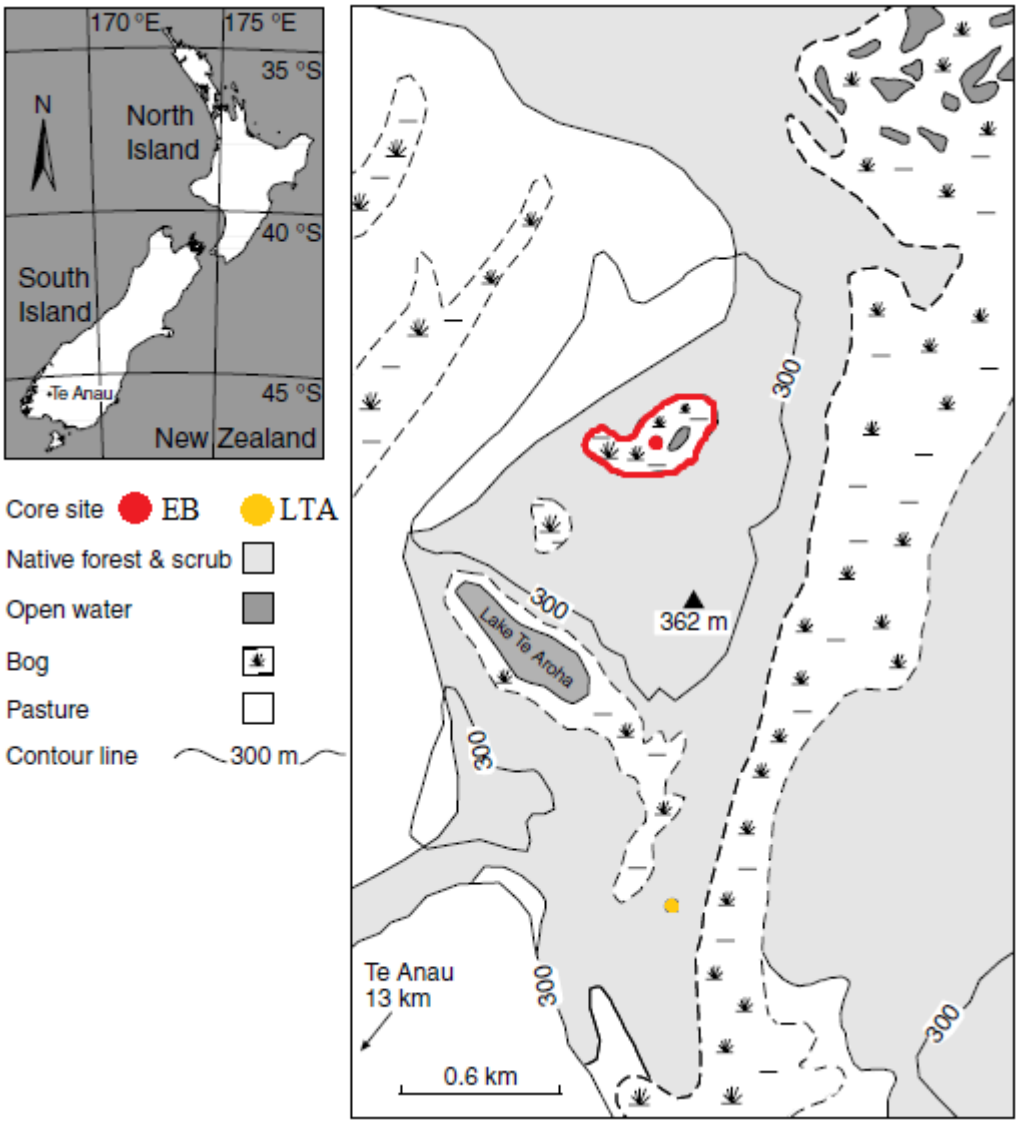

Figure 1-4: Location map for Eweburn Bog (outlined in red) and Lake Te Aroha, as well as sampling sites for both cores. (Edited from Wilmshurst et al., 2002)

on late Holocene changes in aridity. The Lake Te Aroha core has a much longer time scale overall, but with 16 points sampled, and only 12 of those placed since 18ka, its resolution is relatively low on the deglacial timescale.

Ombrotrophic bogs such as Eweburn Bog are very sensitive to surface moisture. Since precipitation is the only moisture input, these kinds of bogs are ideal for tracking precipitation through the soil moisture present because there are no competing influences of inflow. Soil moisture has been measured by identifying the tests left behind by different species of testate amoebae that live in the surface soil. Surface moisture and water table depth can be determined from the amoeba species in a given sample of peat. Where the tests of moisture-tolerant amoeba were found, the climate was likely wetter, and drought-tolerant amoeba implied drier conditions (Wilmshurst et al., 2003). However, this reconstruction is based on the number of tests found in the soil, so if significant quantities of tests from one species or another did not last in the soil, the reconstruction could be wrong. This thesis uses the same core as the Wilmshurst papers, but the new proxy of biomass burning biomarkers is needed in order to corroborate the current record.

There were no humans living on New Zealand prior to approximately 1280AD (McWethy et al., 2009), when the first Maori settlers arrived, followed by European colonists in the 19th century. These settlers began altering their local environment by large-scale forest clearing and burning, vastly altering the ecosystems over a large area of New Zealand in ways that have persisted to today. Tall trees, which had been the dominant plant type in and around Eweburn Bog (Figure 1-5), suddenly and sharply decreased around 200-300ya, coincident to the time of European colonization (Wards, 1976; Wilmshurst et al., 2002). Climate at that time was similar to the modern climate, so any changes in ecology are attributed to actions by the settlers (McWethy et al., 2009). Charcoal was also present in the soil, documenting the widespread burning.

1.5.2 Cass Basin

The third site for this study, Kettlehole Bog (KB), located in the Cass Basin of Canterbury, New Zealand, is a small bog at approximately 600m elevation east of the Southern Alps (Figure 1-6). This bog lay beneath the maximum extent of the Poulter Ice Advance during the LGM, so its sediment record begins in the early deglaciation at 17.7ka. The modern weather influencing the bog is characteristic of the subtropical climate to the north, with relatively warm summer temperatures, cold winter, and very seasonal precipitation (McGlone et al., 2004). This location is useful to this thesis due to

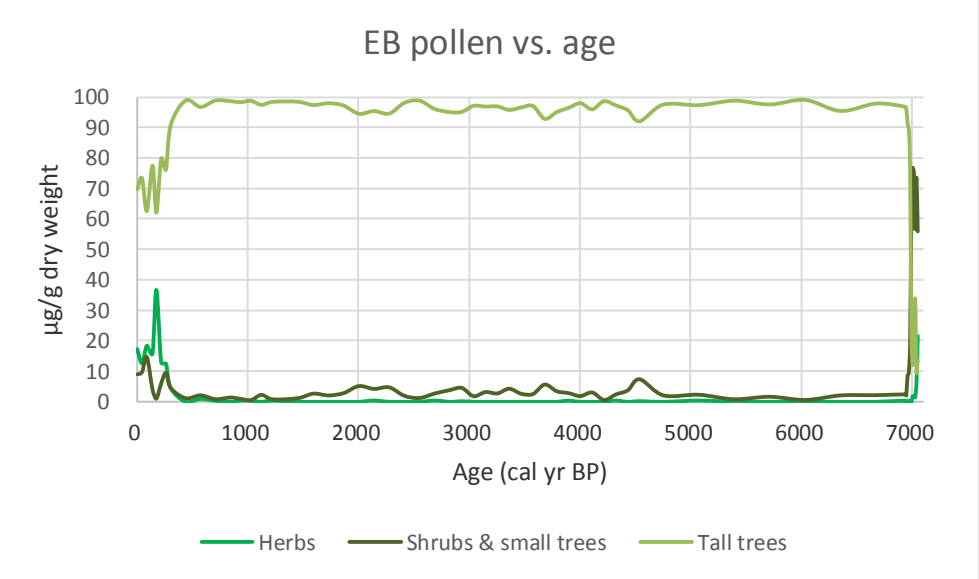

Figure 1-5: Pollen percentage diagrams of the Eweburn Bog core (Wilmshurst et al., 2002). After coming to an equilibrium after the climate optimum, plant abundance ratios remained relatively stable until European colonization and land clearing. Colors for pollen types, as well as for all future data series, will remain consistent throughout this thesis.

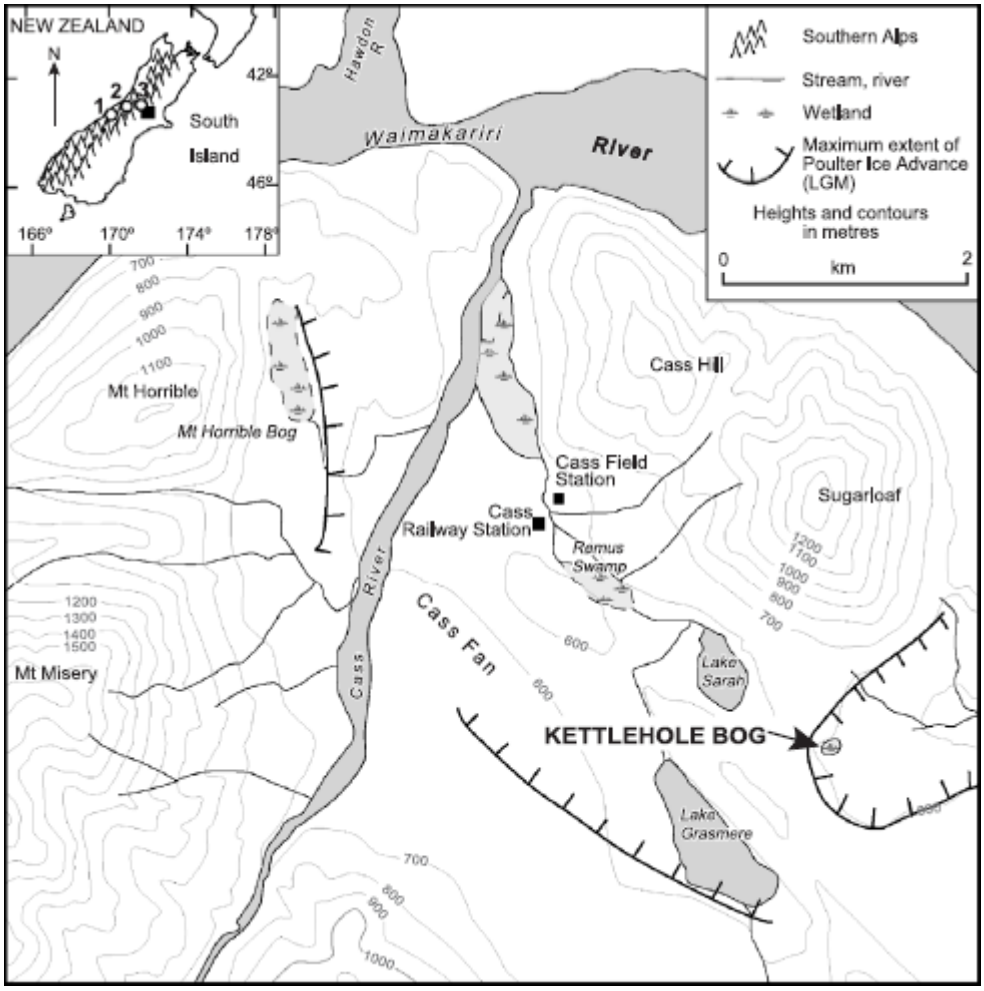

Figure 1-6: Location map for Kettlehole Bog. (Taken from McGlone et al., 2004)

its clear recording of the ACR in its vegetation, which matches some records in timing (Turney et al., 2003) while differing from others (Alloway et al., 2007). Currently, the vegetation inside the bog consists mainly of *Sphagnum* moss, in addition to a few other mosses and sedges; grasses, shrubs, and the ever-present *Nothofagus* beeches are located nearby despite deforestation within the past 800 years by anthropogenic fires (McGlone et al., 2004).

The record of vegetation has changed greatly since the glacial termination. A climate record based on the pollen record from this core has been previously published

(McGlone et al., 2004). The pollen types dominating the ecosystem at various points in the core fluctuates between trees, shrubs, and grasses, which reflects the changing climate of New Zealand (Figure 1-7). Adding an aridity record to the existing climate reconstructions for this site (McGlone et al., 2004; Wilmshurst et al., 2007) may explain the unexpected pollen abundance trends, such as why tall tree abundance dips at 11.6 and 9.7ka, and why the tall trees prevalent during the HS1 are different kinds of trees as those that appear during the Younger Dryas and beyond (McGlone et al., 2004).

1.6 Biomass burning biomarkers

The primary process to be examined in this thesis is aridity. The proxies applied in this thesis to examine this process are molecules that are produced during the burning of natural plant biomass such as trees, shrubs, and grasses. The burning-derived molecules of interest to this thesis – levoglucosan, dehydroabietic acid (DHAA), and vanillic acid –

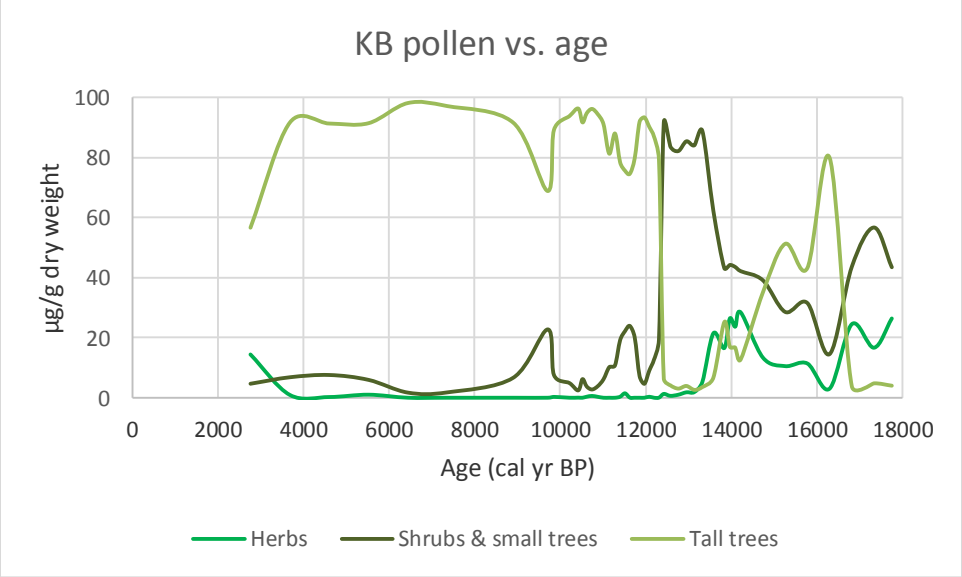

Figure 1-7: Pollen percentage diagrams of the Cass Basin core (McGlone et al., 2004). The ACR is denoted between about 14.7-12.5ka by the sudden increase in shrubs and small trees, with a corresponding decrease in tall trees.

are this particular class of burning marker, which is created when a natural molecule synthesized by a plant is pyrolyzed (burned) in a fire (Oros and Simoneit, 2001). Biomass burning markers (BBM) have been employed to study many environments worldwide (Bi et al., 2008; Elias et al., 2001; Medeiros et al., 2012). Some are created during the burning of all plants (Elias et al., 2001), and some are specific to the molecules produced by certain kinds of plants such as conifers (Saiz-Jimenez and Leeuw, 1986). Where these biomass burning markers are detected, they provide evidence that not only were the plants that created the original molecules present or nearby, but also that fires occurred where the plants were found.

The biomass burning markers DHAA, vanillic acid, and levoglucosan can be utilized to create their own record of fire prevalence, which in turn can be added to existing proxy records to synthesize a more robust climate record (Sikes et al., 2013). Levoglucosan is a product of the pyrolysis of cellulose (Figure 1-8), a complex molecule present in all kinds of plants (Simoneit et al., 1999). Molecules such as levoglucosan are useful biomass burning biomarkers because they are not created during any other decomposition process but incomplete combustion, which is the typical condition of natural fires (Kuo et al., 2008). In addition, these molecules are typically relatively inert, allowing them to survive in the atmosphere until they are preserved in soil, where they can serve as qualitative proxies of total plant biomass (Elias et al., 2001). Mannosan and galactosan, stereoisomers of levoglucosan, are the pyrolysis products of another ubiquitous plant molecule, hemicellulose. Due to the lower concentration of hemicellulose than cellulose in most plant biomass, however, mannosan and galactosan are expected to have correspondingly lower concentrations than levoglucosan, and thus

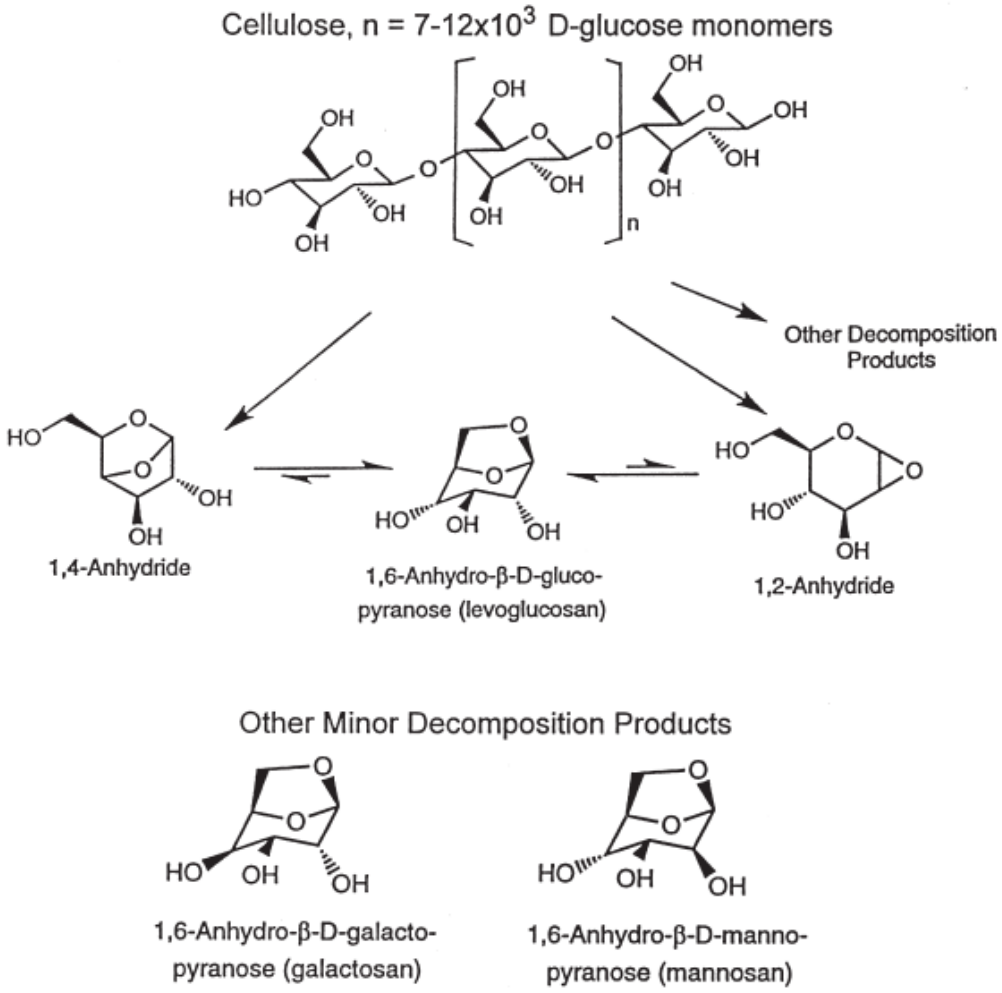

Figure 1-8: The chemical decomposition of cellulose into levoglucosan, galactosan, and mannosan during pyrolysis. (Taken from Elias et al. 2001.)

are generally not included in the realm of important biomass burning biomarkers (Shafizadeh, 1984). However, they will still be investigated in this thesis.

Vanillic acid and DHAA, which are created exclusively during the burning of conifers (Saiz-Jimenez and Leeuw, 1986), share with levoglucosan the properties of synthesis solely during biomass burning as well as inert soil chemistry. Conifers such as those of the *Podocarpus* genus, which are gymnosperms, and broadleaf trees such as *Nothofagus* species, which are angiosperms, contain approximately the same relative amounts of cellulose, hemicellulose, and lignin in their woody structures. However, the

lignin of gymnosperms is enriched in coniferyl alcohol, which is a precursor to vanillic acid in the pyrolysis process, and leads to a high concentration of vanillic acid in conifer smoke (Grimshaw, 1976; Shafizadeh, 1984). The lignin of angiosperms, however, contains very little of this precursor in favor of sinapyl alcohol, which is what makes vanillic acid an indicator of conifers specifically. Vanillic acid is produced in the combustion of lignin, while DHAA is produced in the combustion of conifer resin acids (Simoneit, 2002).

Levoglucosan levels present in a given soil sample have been correlated with the amount of plant biomass burned at the time that soil was deposited (Shafizadeh, 1984). However, different biomarkers are created in varying proportions based on the temperature of the source fire and species of wood burned, making these proxies qualitative rather than quantitative. Levoglucosan is produced in its highest concentration at relatively low flame temperatures (150-350°C) (Figure 1-9), which implies that the fires in which it is prevalent are low and smoldering (Kuo et al., 2008). A smoldering fire is a wet fire, which means that the environment around the fire was wet and likely experienced precipitation (Lobert and Warnatz, 1993). In this way, its record serves as a distinct biomarker from charcoal, which is generally produced during biomass burning from dry, hot fires (≥350°C). Charcoal is typically employed as a burning marker in cores due to its visibility to the microscope and naked eye, lending to its ease of quantification (Clark, 1982). However, since not all fires produce charcoal, it is important to also take levoglucosan into account to have a measure of both temperature ranges of fires in order to take a closer look at the aridity conditions at the times of those fires.

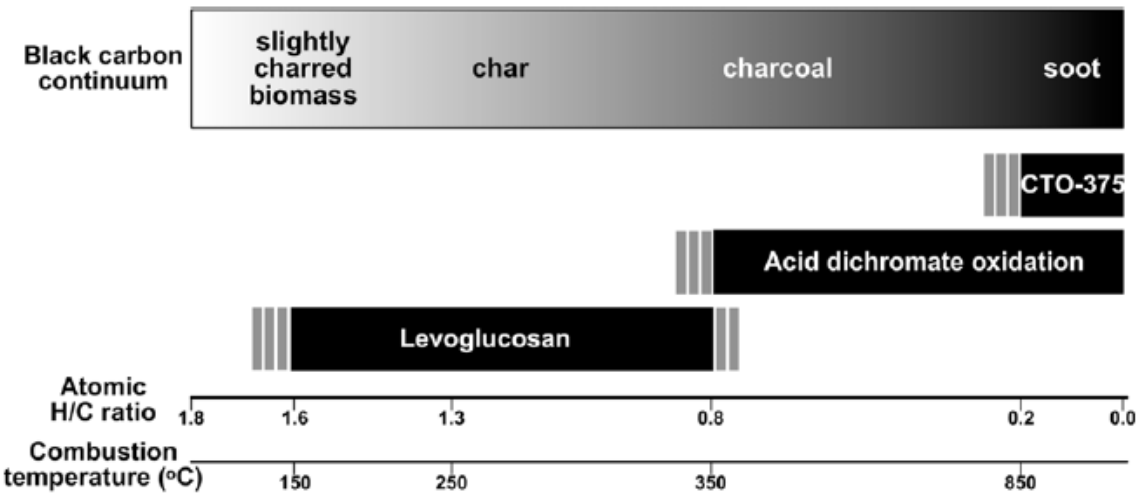

Figure 1-9: The temperature ranges of fire needed to create different species of black carbon. Levoglucosan and charcoal share very little temperature overlap, so it is likely that they are created in very different kinds of fires (Kuo et al., 2008).

DHAA and vanillic acid presence in the soil also increases with increased conifer abundance (Abas et al., 1995), and like levoglucosan they are also produced in smoldering fires (Oros and Simoneit, 2001). The varying concentrations of these molecules when compared to the levoglucosan concentration of the same sample provides a means of tracking conifer presence as a function of plant biomass, since fire will burn conifers at the same time as other plants in the same location. The typical assumption is that the hotter and drier the climate becomes in a given area, the more fires occur in that area (Elias et al., 2001). By finding these biomarkers in soil cores, and comparing their burning record to the pollen temperature reconstructions for these cores, a record of aridity can be added to the existing temperature and charcoal records. There may be cores with measured charcoal abundances that contain as-yet undiscovered evidence of past fires if the fire was wet enough to only produce levogucosan. This could cast new light on any existing aridity proxies that do not currently include levoglucosan in their analysis.

1.7 Aridity and fire prevalence

An important point in reconstructing fire intensity from compounds that indicate smoldering burning is to consider not only the temperature at which the fuel burned, but also the ecological factors that contributed to the growth of that fuel. The assumption of a direct correlation between a dry, hot climate and more fires has recently been shown to be not entirely correct in the western United States (Westerling et al., 2003). In the western US, wildfire frequency and size is directly dependent on the previous year's rainfall or temperature as deviations from the average. This is due to the two most important factors behind fire ignition and termination: fuel availability and flammability. Fuel availability is an important factor to fire ignition and frequency in places like grasslands that are warm, arid, and sparsely-vegetated, because an abundance of rain during one or more winters can cause a boom in biomass which then quickly dries out and becomes easy tinder for subsequent dry seasons. Flammability, on the other hand, is more important to in cool, moist, densely-vegetated systems, because the moisture in the area actively suppresses fire until a dry year has made the already-plentiful fuel available for burning. Thus, a fire in one particular year may not be directly due to an increase in temperature or aridity, but rather a particularly anomalous previous year or years in terms of the amount of precipitation, which promoted suitable fire conditions for the future (Westerling, 2009). Absolute temperature and precipitation numbers do not seem to be as important to high or low fire season severity as deviations from the mean. In this way, evidence of fire can show not simply that it was dry, but more importantly how aridity changed over time. As the modern climate of the South Island is similar to that of the western United States, and as

their climates changed in relatively similar ways since the deglaciation, this wildfire analysis is relevant to the climate of study in this thesis (Bartlein et al., 1998).

1.8 New Zealand context

Prior to mass deforestation during European colonization, reconstructions of overall biomass show a nearly complete forest cover along the northern, western, and southern shores of the South Island, and mainly grassland along the eastern coast and the interior (Wards, 1976). This indicates that flammability may have been a major factor behind wildfires in the regions dominated by forest (including the EB and LTA study sites) and fuel availability as an important factor behind fire in the regions dominated by grasses (including the KB study site at the LGM). This means from first principles that at times when BBM's are present in grassland areas, smoldering fires occurred there because of above-average wetness for that time, and when BBM's are present in forested areas, times of above-average dryness are indicated within already wet conditions. This is one way in which aridity can be shown to have changed in New Zealand since the LGM.

BBM prevalence varied in magnitude at specific points in time in all three study sites. The ecosystems of the sampling locations also experienced large shifts in the abundance of certain plant types since the LGM, both at similar and different times to when the BBM's changed in presence and magnitude. Since plants can be influenced by both temperature and aridity, while BBM's are solely driven by aridity, the BBM record can be used to tease apart the effects of aridity from the pollen record.

1.9 Proposed work and study sites

The aim of this thesis was to create a record of South Island burning using biomass burning markers, which can be used as a proxy of aridity. This aridity record was then

compared to published charcoal and pollen records from the same cores, in addition to two other terrestrial cores as well as one marine core, to provide correlating aridity records to existing records of temperature and burning. In this way, climate variations from the deglaciation to the Holocene can be investigated over time. This is an important research focus due to New Zealand's unique location, as it is positioned beneath the range of the Southern Westerly Wind belt. It is likely that the cause of many of the changes in New Zealand's climate since the LGM was the influence of north-south variations in the SWW (Lamy et al., 2010; Putnam et al., 2010). In addition, changing aridity with the changing climate may have affected reconstructions of temperature during this time (Wilmshurst et al., 2007).

The questions this thesis seeks to answer are:

1. What was the overall pattern of biomass burning in the South Island since the LGM?
2. How does this burning record inform how the aridity of the South Island changed since the LGM?
3. Did changes in aridity affect terrestrial pollen-based reconstructions of temperature?
4. Can we use aridity and temperature to track climatic changes since the last deglaciation?
5. Are these changes the result of atmospheric reorganization?

The new information created in this paper consists of biomarker concentration data for the three sampling sites over the times spanned by the respective core depths. This thesis will employ the three major biomass burning biomarkers found in the cores and assess how they perform as proxies of aridity, using previously published records from the North and South Islands and the Chatham Rise as context for temperature, SST, charcoal,

and ecosystem changes. Together, these records have been interpreted to investigate the potential of aridity to reconcile temperature and plant biomass location records that do not match up to each other or to expected outcomes. This has been accomplished by looking at how the North and South Islands compare climatically, how marine sea surface temperature records compare to pollen land surface temperature records, and how temperature and aridity work together to form the coherent climate signal that influenced New Zealand since the LGM.

II. METHODS

2.1 Core sampling

Three sediment cores were taken from Eweburn Bog (EB), Kettlehole Bog (KB), and a bog near Lake Te Aroha (LTA) (Figure 1-1). The 550cm EB core was taken in 1997 with a D-section corer for the top 500cm, and a Hiller borer for the bottom 50cm. The 410cm KB core was taken in 1997 20m from the northeastern edge of the bog also using a D-section corer, and the LTA core was taken in 2007 with a D-section corer as well. Immediately after sampling, core samples were transferred to plastic drainpipes and sealed into polythene bags on-site. They were then stored in a cold room at 4°C, cut into 1cm segments, transferred to airtight plastic containers, and frozen at -20°C until ready for analysis. Pollen was counted and identified for the KB and EB cores, and has been published previously (McGlone et al., 2004; Wilmshurst et al., 2002). The segments analyzed for this thesis were 23 samples from 45-485 cm depth (EB), 35 samples from 32-404 cm depth (KB), and 16 samples from 55-199 cm depth (LTA). These samples were analyzed at Rutgers University between June 2013 and May 2015.

2.2 Radiocarbon dating and stratigraphy

The ^{14}C dates reported for the EB, KB, and LTA cores (McGlone et al., 2004; Wilmshurst et al., 2002) (Table 2) were input into the Calib Rev 7.0.4 Calib Radiocarbon Calibration Program using the SHCal13 2013 southern hemisphere calibration (Stuiver et al., 2013) in order to obtain calendar ages BP (cal yr BP). Ages were interpolated between and extrapolated out from these radiocarbon dates for actual biomarker sampling depths using Matlab (Figure 2-1). These calendar dates were calculated using a newer

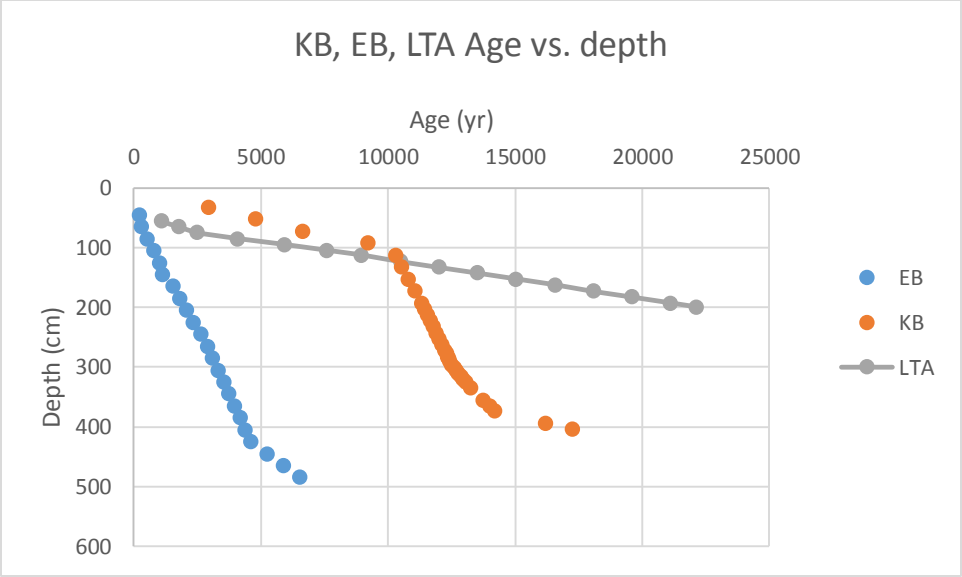

Figure 2-1: Calendar ages BP for each biomarker sample depth in KB, EB, and LTA cores. LTA extends back through the LGIT into the glaciation, while KB and EB begin after the start of the deglaciation.

calibration than what appeared in the original literature (McGlone et al., 2004; Wilmshurst et al., 2002), and hence are considered to be more accurate.

Kettlehole Bog experienced slow sediment deposition from the top of the core at 2.9ka until about 10ka, the approximate beginning of the Holocene, at which point there was a large increase in deposition rate until about 15ka, which is close to the beginning of the ACR. The deposition rate then decreased approximately back to Holocene levels until the base of the core. Eweburn Bog began with a higher deposition rate than KB at the beginning of its core 0.2ka, which decreased slightly around 4.5ka and continued unabated to the base. Only 4 samples were dated from LTA, so its age vs. depth reconstruction is essentially constant.

2.2.1 Eweburn Bog core description

Wilmshurst et al. (2002) cored and described the Eweburn Bog core as containing four distinct zones. Basal sediments were not sampled, but consisted of fine silts and

clays. The rest of the core is composed of peat. The first zone (550-495cm, ca. 11000-7000 cal. yr BP) consisted of highly humified peat, as does the second zone (495-310cm, ca. 7000-3400 cal. yr BP). Zone 3 (310-75cm, ca. 3400-400 cal. yr BP) fluctuated between highly and poorly humified peat, and in zone 4 (75-0cm, ca. 400 cal. yr BP to present) humification becomes increasingly poorer towards the surface. A more detailed analysis of core contents, paraphrased from the original publication, can be found in Appendix A3.

2.2.2 Kettlehole Bog core description

McGlone et al. (2004) cored and described the Kettlehole Bog core as containing four distinct zones as well. The basal sediments were not sampled, but consisted of stiff grey clays, atop which lay a layer of brown silty lake mud (410-340cm; ca. 16500-13500 cal. yr BP), one of olive grey silty clay (340-295cm; ca. 13500-12600 cal. yr BP), another lake mud layer (295-220cm; ca. 12600-10000 cal. yr BP), and a thick sedge-Sphagnum peat layer on top (220-0cm, ca. 10000 cal. yr BP – present). Three radiocarbon dates have been taken from nearby cores (Burrows, 1983; Moar, 1971), which agree with the radiocarbon dates taken throughout this core (Table 2-1) based on lithology, pollen, and fossil assemblages. The percent of the core made up of organic matter, measured by loss on ignition (LOI), begins at <20% in the basal clays, increasing gradually to approximately 40% by the base of the peat layer, then sharply rises to 80-90% up to about 100cm depth. After that, less organic matter is recorded (35-60%), and some silt layers are present (McGlone et al., 2004).

Core	Depth (cm)	14C Age ± Uncertainty	Cal BP Age (1σ)	Material
EB	70	287 ± 68	275-330	Plant fragments
	113	966 ± 30	859-905	*Sphagnum*
	121	1076 ± 30	926-958	*Sphagnum*
	123	**1367 ± 60**	**1257-1297**	***Sphagnum***
	138	**1304 ± 30**	**1206-1268**	***Sphagnum***
	140	1251 ± 30	1057-1186	*Sphagnum*
	142	1289 ± 30	1072-1192	*Sphagnum*
	145	1271 ± 30	1088-1181	*Sphagnum*
	148	1347 ± 30	1185-1219	*Sphagnum*
	151	1313 ± 30	1203-1269	*Sphagnum*
	156	1573 ± 30	1364-1432	*Sphagnum*
	260	2778 ± 73	2760-2887	Woody stems
	425	4158 ± 60	4529-4653	Fibrous peat
	498	6119 ± 70	6842-7017	Fibrous peat
	515	8021 ± 67	6776-7161	Peat
KB	80	6460 ± 60	7303-7419	Pollen
	95	8770 ± 75	9555-9789	Pollen
	114	**9220 ± 70**	**10244-10417**	**Wood**
	114	9270 ± 60	10290-10439	Wood
	143	9460 ± 60	10570-10727	Plant fragments
	193	9970 ± 70	11236-11407	Plant fragments
	295	10540 ± 60	12399-12559	Pollen
	340	11510 ± 70	13243-13406	Plant fragments
	375	12325 ± 70	14062-14378	Pollen
	395	13580 ± 65	16177-16418	Pollen
LTA	47	510 ± 15	504-518	Wood
	77	2606 ± 80	2492-2600	Wood
	107	8116 ± 60	8790-9093	Peat
	120	10092 ± 75	11397-11723	Peat

Table 2-1: Radiocarbon (^{14}C) dates taken from the three cores in this thesis recalculated from McGlone and Wilmshurst with the Calib 2013 southern hemisphere calibration (McGlone et al., 2004; Stuiver et al., 2013; Wilmshurst et al., 2002). Bolded dates were omitted due to conflicts in calculating calibrated ages.

2.2.3 Lake Te Aroha core description

Like Eweburn Bog, Lake Te Aroha was likely a glacial lake in the moraine hill where the two sample sites are located (McWethy et al., 2009). The bottom 35cm of this core is made up of clays from this time period, with the top 5cm beginning to be infiltrated by peat from its bog phase. From 59-135cm (1.3-12.4ka) depth, the core is entirely dark brown well-humified peat, with a large wood piece at 77cm (2.8ka) and layers of banding from 102-135cm (7.2-12.4ka). At 58-59cm (1.3ka) is a thick band of charcoal, above which the peat switches to partially-humified and slightly decomposed from 38-58cm (0.7-1.3ka), then to unhumified yellow-brown peat from 34-38cm (0.7ka). The next layer up is a brown partially-humified peat layer from 25-34cm (0.5-0.7ka), containing many fibrous roots. The section from 15-25cm (0.3-0.5ka) is missing, but the 0-15cm (0-0.3ka) segment contains *Sphagnum* moss that was alive and growing at the time of core sampling.

2.3 Extraction and wet chemistry

Upon arrival at Rutgers in 2011, samples were frozen at -20°C until processing. First, the samples were freeze-dried, then individually homogenized with a mortar and pestle. After this samples were loaded into *Dionex* Accelerated Solvent Extractor (ASE) cells according to the following order: 0.7µm GF/F filter (25mm), ~500mg CN sorbent (Supelco Discovery SPE normal CN phase), 0.7µm GF/F, ~1 cm Ottawa sand (Fisher Scientific), sediment sample, 6µL internal recovery standard (nonadecanone), with the remaining top space filled with Ottawa sand (Figure 2-2). The internal standard was added on top of the sample so as to be rinsed through the sample and be subjected to the

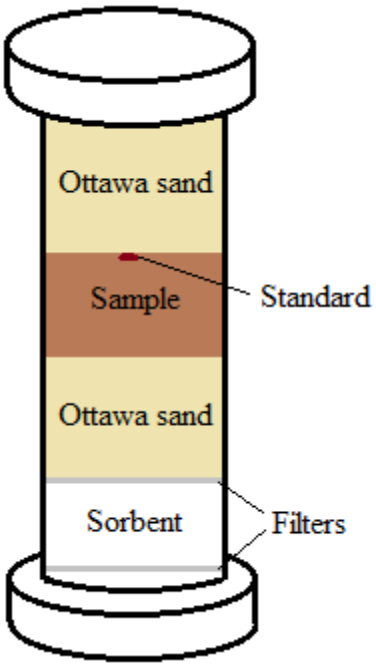

Figure 2-2: An illustrated diagram of the contents of an ASE cell, used for the total lipid extraction process.

same conditions as the sample within, and therefore hypothetically have a similar percent recovery as the extracted biomarkers.

Once the samples and standard were loaded into the ASE cells, the next step was solvent extraction. The lipids were ASE extracted using a method from the literature (Sikes et al., 2009b). Eight samples per core were first extracted in 2:1 v:v dichloromethane:methanol (DCM:MeOH) for initial testing purposes, with the addition of 6µL per sample of an internal standard, nonadecanone, for quantitation purposes. After the initial run of samples, this solvent mix was determined to not fully extract the target biomarkers, so the same samples were extracted again in 4:1 DCM:MeOH plus standard. The remainder of the samples were extracted using the 4:1 solvent mix plus standard, as it extracted a much larger quantity of the desired compounds. A new portion of unused sediment from 10 samples selected from KB and EB, some of which had been extracted in the initial inferior solvent mix, were later processed using the correct solvent mix from the

start, in order to provide a measure of quantitative biomarker extraction; the process is detailed below. All samples were extracted using the same ASE method, consisting of two ten-minute cycles at 150°C and 1000psi, to obtain a total lipid extract (TLE). Once extracted, the TLEs were concentrated via vacuum evaporation using a RapidVap, and half of each TLE was archived.

In order to best resolve polar compounds for identification on a nonpolar column, derivatization using bis(trimethylsilyl)trifluoroacetamide (BSTFA) is a standard process. BSTFA substitutes a silyl group in place of the polar group, such as –OH, of many organic compounds, the general reaction of which is pictured below (Figure 2-3). For analysis in this study, a 5% fraction of each TLE was taken for derivatization and quantification by blowing down the whole TLE to dryness under ultra-high purity nitrogen (Airgas UN1066), redissolving the TLE in 500µL of DCM, and then taking 5% (25µL) for further analysis. Each 5% fraction was again blown to dryness under nitrogen, and 50µL BSTFA + 1% TMCS (Thermo Scientific TS-38831) plus two drops of pyridine (Fisher Scientific P368-500) were added to each. The samples were then incubated at 70°C for two hours, blown down a final time, and redissolved in 25, 50, or 100µL of toluene depending on the desired concentration of the sample. The end volume was

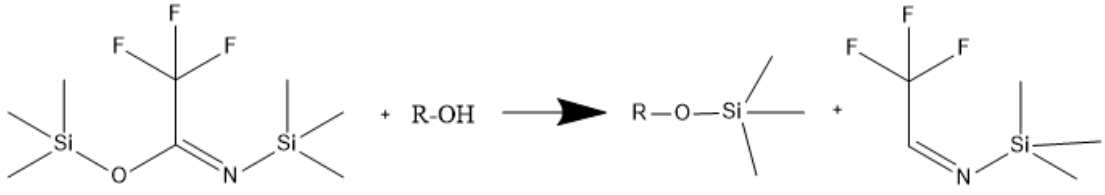

N,O-Bis(trimethylsilyl)trifluoroacetamide

Figure 2-3: The general chemical reaction for the derivatization process using BSTFA.

varied to match the detection limits of the GCMS and to optimize peak height and shape, as an overly concentrated sample overloads the column and detector which precludes accurate quantification.

2.4 Instrumental analysis and data

Instrumental analysis was conducted by gas chromatograph-mass spectrometry (GCMS). 1µL of each derivatized sample was injected into and analyzed by a Shimadzu GCMS-QP2010 gas chromatograph/mass spectrometer in order to identify and quantify biomarkers. Samples were injected onto a Shimadzu SHR5XLB 30m column with a 0.25mm internal diameter and 0.25µm thickness, with helium as the carrier gas. For all biomarker analyses, the GCMS was in splitless mode with an injector starting temperature of 60℃ held for one minute, after which it increased by 5℃ per minute until reaching 320℃, which it then held for 40 minutes. The MS ion source was set to 240℃ in scan mode, with 106.4kPa column pressure, 8.4mL/min total flow, 1.67mL/min column flow, and a linear velocity of 47.2cm/sec. Biomarkers were identified by retention time, molecular ion, and other major ion fragments (Table 2-2), and quantified using Shimadzu-provided software (Figure 2-4).

Calibration and quantification of the data was performed as it was acquired, in order to determine whether adjustments to the sample concentration or to the tuning of the GCMS were required. The GCMS was tuned periodically in order to ensure optimal performance and consistent data quality, and response factors were found for the internal standard and for levoglucosan to allow for accurate comparison of results. Once the tuning was completed, pure samples of levoglucosan (provided by collaborator Patricia Medeiros) and 2-nonadecanone (Thermo Scientific) were injected into the GCMS at three

Molecule	Retention Time (min)	Molecular Ion (m/z)	Major Ions (m/z)
Galactosan	22.4	333	**73**, 204, 217
Mannosan	22.9	333	**73**, 204, 217
Levoglucosan	23.3	333	**73**, 204, 217
Vanillic Acid	25.3	312	267, **297**, 312
Nonadecanone	32.3	282	43, **57**, 71
DHAA	37.3	372	**239**, 357, 372

Table 2-2: The biomarkers investigated in this thesis, in addition to the internal recovery standard 2-nonadecanone, in order of retention time. Retention times and characteristic ions for biomarkers are for the derivatized molecules. Bolded ions are the 100% relative intensity ions. (Simoneit, 2002)

to five different concentrations each, ranging from 4 to 800ng/µL. The concentrations were then plotted against the integrated areas of the resulting GC spectrum peaks, and the slope of the line created in this way became the response factor for that compound. Each time the GCMS was tuned, response factors were recalculated, to account for instrument calibration drift.

Calibration of biomarkers for percent recovery was calculated according to the following equation:

$$Recovery = \frac{\left(\frac{A_N}{RF_N}\right) * \frac{1\mu g}{1000ng} * \frac{V}{\%_{tot}}}{Y} * 100\%$$

A_N is the integrated area under the nonadecanone peak, RF_N is the nonadecanone response factor, V is the total volume the 5% fraction was brought up in before injection, $\%_{tot}$ is the fraction of the TLE the sample represented (5%), and Y is the theoretical yield of nonadecanone in the sample (6µL). A similar calculation was performed in order to quantify the amount of each biomarker present in each sample:

$$\text{Quantity} = \frac{\left(\frac{A_B}{RF_B}\right) * \frac{1\mu g}{1000ng} * \frac{V}{\%_{tot}}}{S}$$

A_B is the integrated area under the peak of the biomarker in question, RF_B is the biomarker response factor, V is the total volume the 5% fraction was brought up in before injection, $\%_{tot}$ is the fraction of the TLE the sample represented (5%), and S is the mass of the dry weight of the original sediment sample in grams. The levoglucosan-specific response factor was used to calculate responses for the stereoisomers levoglucosan, mannosan, and galactosan and used in the quantifications of all three biomarkers. Vanillic acid and DHAA were also quantified using this response factor, as it was assumed to be more accurate than the response factor for nonadecanone due to a greater similarity in chemical composition of vanillic acid and DHAA to levoglucosan than to nonadecanone.

2.5 Nonadecanone

Nonadecanone was added to each sample to provide a quantitative marker for surrogate recovery. Between the steps of ASE, nitrogen blowdown, and GCMS, it was possible that some sample could be lost or diluted along the way. Adding a known quantity of an independent molecule that was highly unlikely to be in the sample from the start provided a means to track any change to the initial sample's concentration.

Upon quantification of the biomarkers and the internal recovery standard in each sample, it became clear that the standard had not performed according to expectations. Nonadecanone concentration in GC spectra varied greatly between samples, even between samples that had been ASE extracted, derivatized, and GCMS analyzed on the same day under the same conditions. The calculated percent recoveries of the standard across samples varied an unacceptable amount, from zero to one hundred percent (Figure 2-5). No correlation could be found between standard concentration and any laboratory method or sediment type. For this reason, percent recovery was not calculated for the compounds

of interest. Compound abundances are reported as concentrations calculated from dry weight of the original sediment assuming consistent recoveries across all samples.

2.6 Compound identification

After injection of the compound into the GCMS, the results were displayed in a format that required interpretation. The GC spectrum displayed relative amounts of all compounds detected by the GC, and the mass spectrum showed concurrent mass ions that were picked up by the instrument's ion detector (Figure 2-4). The approximate GC retention times of the compounds of interest were known from initial analysis (Medeiros and Simoneit, 2008; Simoneit et al., 1999) of the samples in 2013, prior to the start of this thesis work, and each peak near a given relative retention time was checked for the presence of its associated biomarker. Biomarker presence was confirmed through the mass spectrum, in which characteristic patterns of mass ions could be used to identify specific compounds, at times with help from the software compound library. Vanillic acid, for example, was easily identifiable by its pattern of five mass ions from 237-312 m/z (mass to charge ratio) in a specific ratio in the mass spectrum (Figure 2-4E), including the major mass ions 267, 297, and 312 m/z (Table 3). DHAA was also easily recognizable by its own characteristic mass ion pattern, when it was present.

As stereoisomers, levoglucosan, mannosan, and galactosan were very similar both in retention time and mass spectrum fingerprint. Levoglucosan and mannosan have a higher abundance of the 204 m/z mass ion than the 217 m/z ion, but in galactosan this is reversed, making it relatively easy to distinguish from its stereoisomers. In addition, the sample of pure levoglucosan provided by Patricia Medeiros provided a confirmation of the typical retention time and mass spectrum needed to definitively identify levoglucosan in the bog

samples. The 333 mass ion has been reported to be one that all three stereoisomers have in common (Simoneit et al., 1999), however it was only identified in some of the samples.

Nonadecanone was difficult to identify in the bog samples. It was often not present at the expected retention time, while plausible breakdown peaks containing similar mass ions were present at other times. It is likely that the nonadecanone added to the samples chemically reacted in some way within these samples, despite nonadecanone having been used successfully as an inert internal standard in similar previous applications (Sikes et al., 2013). The mechanism behind this potential reaction is not known.

2.7 Re-extraction of samples

To examine reproducibility of results in these bog sediments, 10 sub-samples from the original suite were selected as duplicates and run as independent analyses through the data collection process. This assisted in determining quantitative reproducibility of the procedure, and to analyze the differences in surrogate and biomarker recovery between using the 2:1 and 4:1 solvent mixes. Two KB and three EB samples selected had been previously ASE extracted in the 2:1 solvent mix, and the remaining five samples had been previously ASE extracted in the 4:1 solvent mix. A new portion of sediment was taken from the original 10 core samples, and the same freeze-drying, BSTFA, and GCMS processes as the first portion were performed on the new portion. Each new sample portion was ASE extracted in the 4:1 DCM:MeOH solvent mix regardless of the solvent mix used to extract the first sample portion.

The initial and duplicate concentrations for each biomarker in each core sample (Figure 2-6) were averaged, and the standard deviation and standard error were calculated from this (Table 2-3). Each standard error and standard deviation per compound per core

were then averaged in order to calculate an estimate of how well each compound was extracted in each core ("mean error" and "error range" respectively). The mean error and error range of the samples originally extracted in 2:1 vs. 4:1 DCM:MeOH were also calculated separately, in order to investigate how the two approaches differed in compound extraction.

Overall, EB samples had higher error than KB samples, but relative compound error was different between the two cores. Vanillic acid had the lowest overall error in EB and mannosan the highest, while in KB levoglucosan was recovered with the least error and galactosan the most. EB had a higher 4:1 error than 2:1, while in KB the 2:1 error was higher than the 4:1.

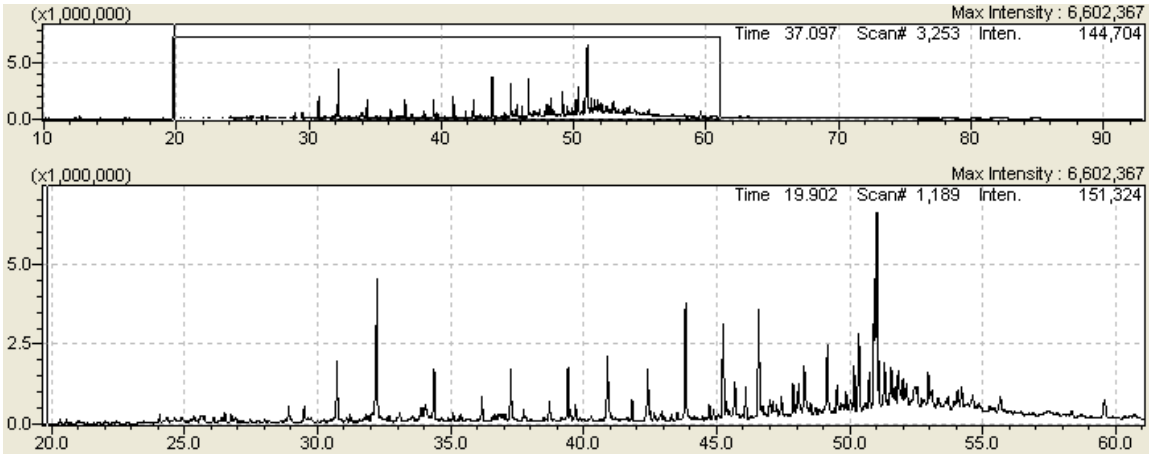

Figure 2-4A: Whole sample GC spectrum

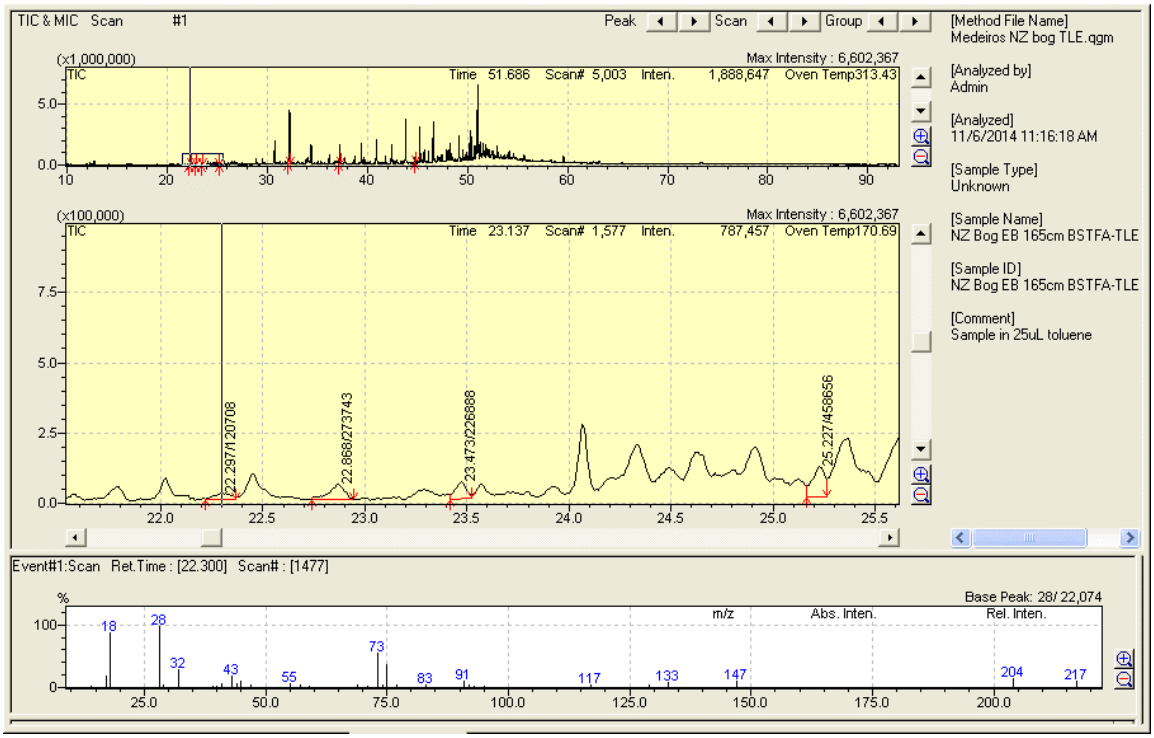

Figure 2-4B: Galactosan GC spectrum and MS mass spectrum

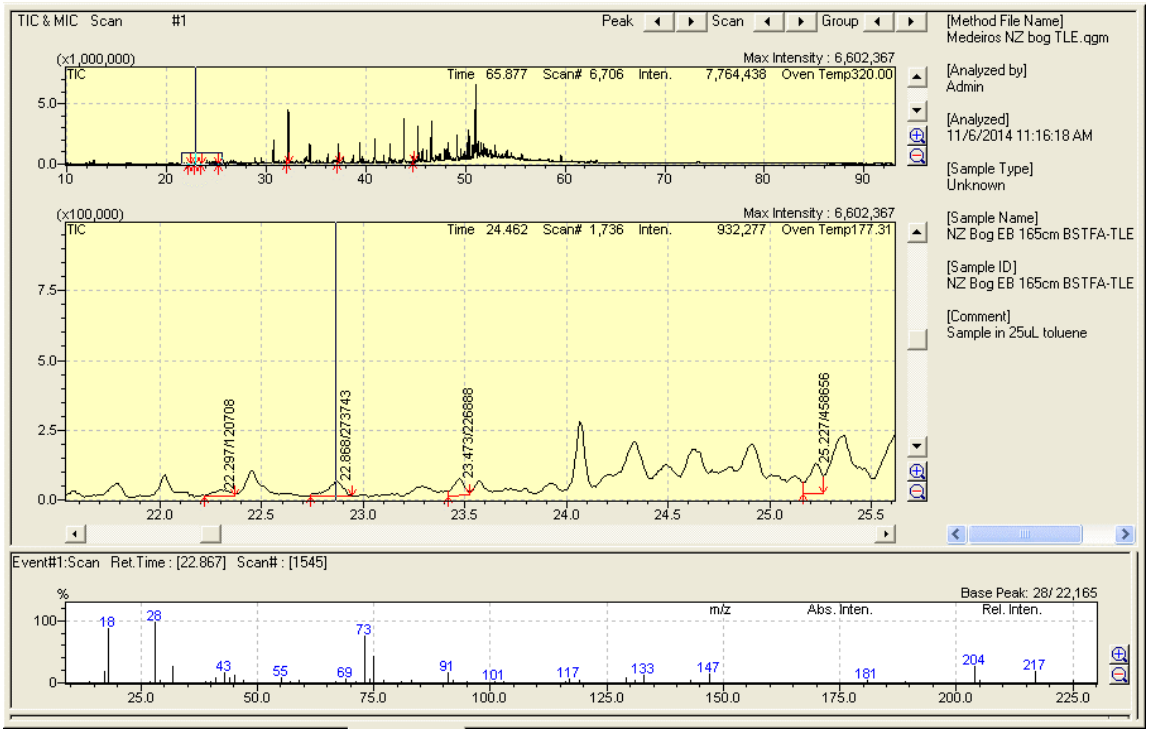

Figure 2-4C: Mannosan GC spectrum and MS mass spectrum

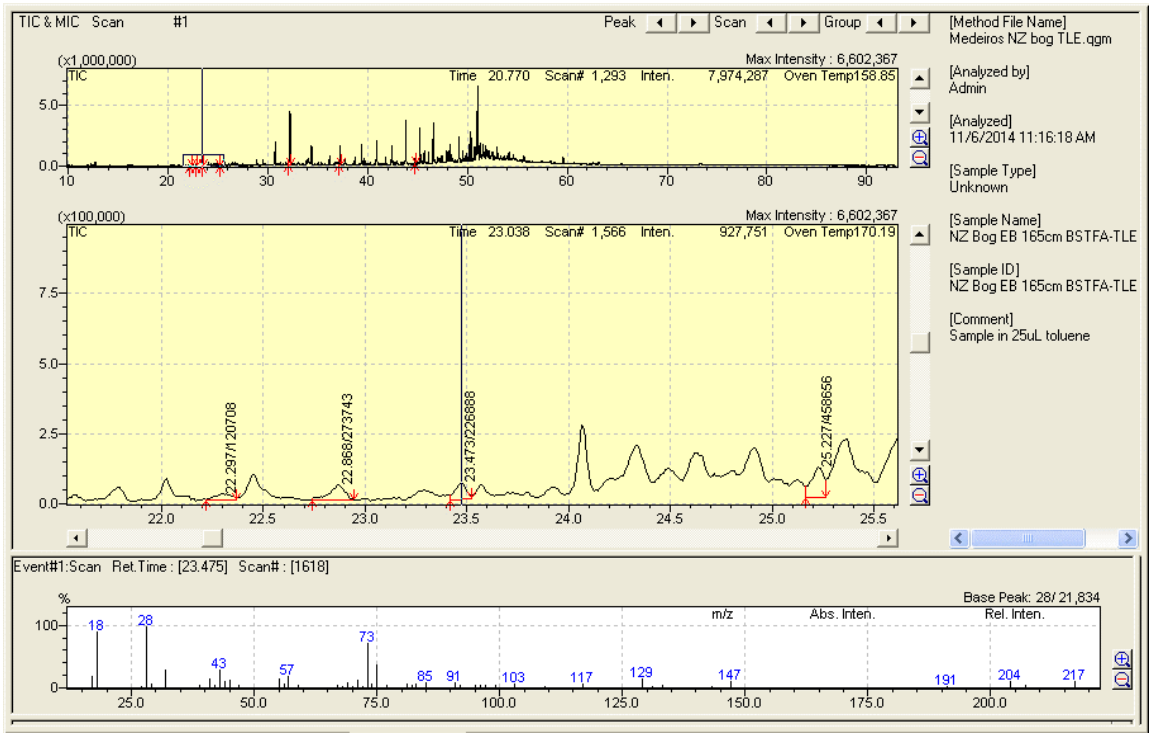

Figure 2-4D: Levoglucosan GC spectrum and MS mass spectrum

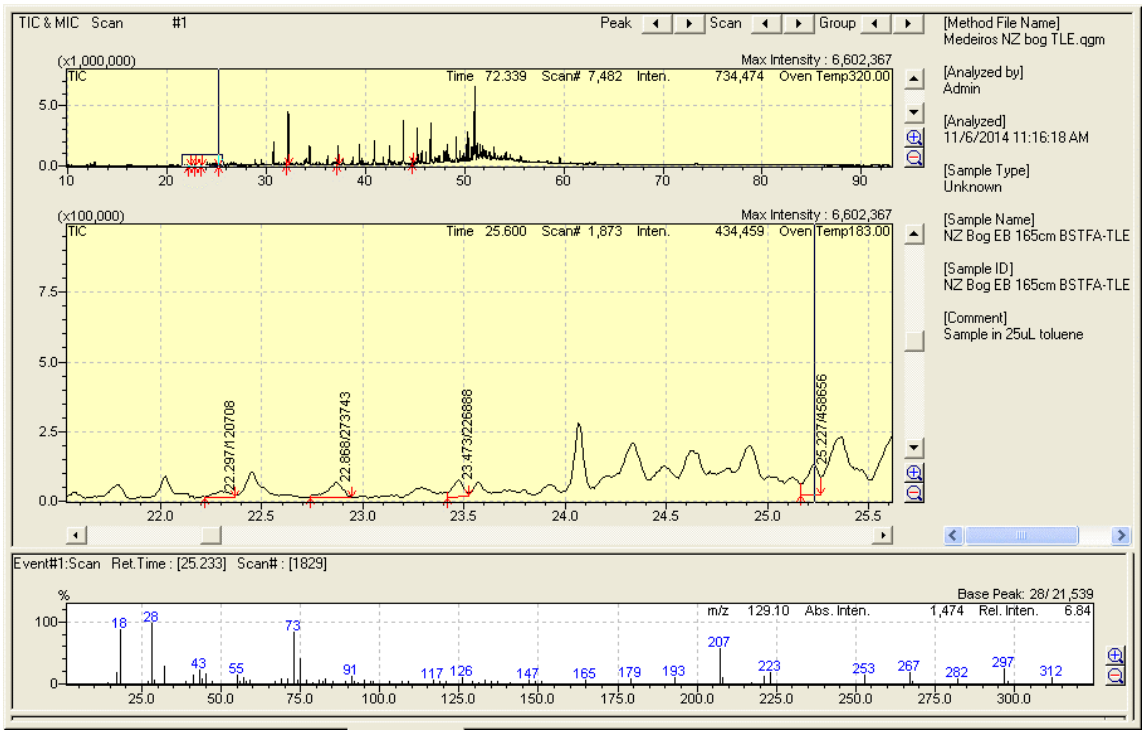

Figure 2-4E: Vanillic acid GC spectrum and MS mass spectrum

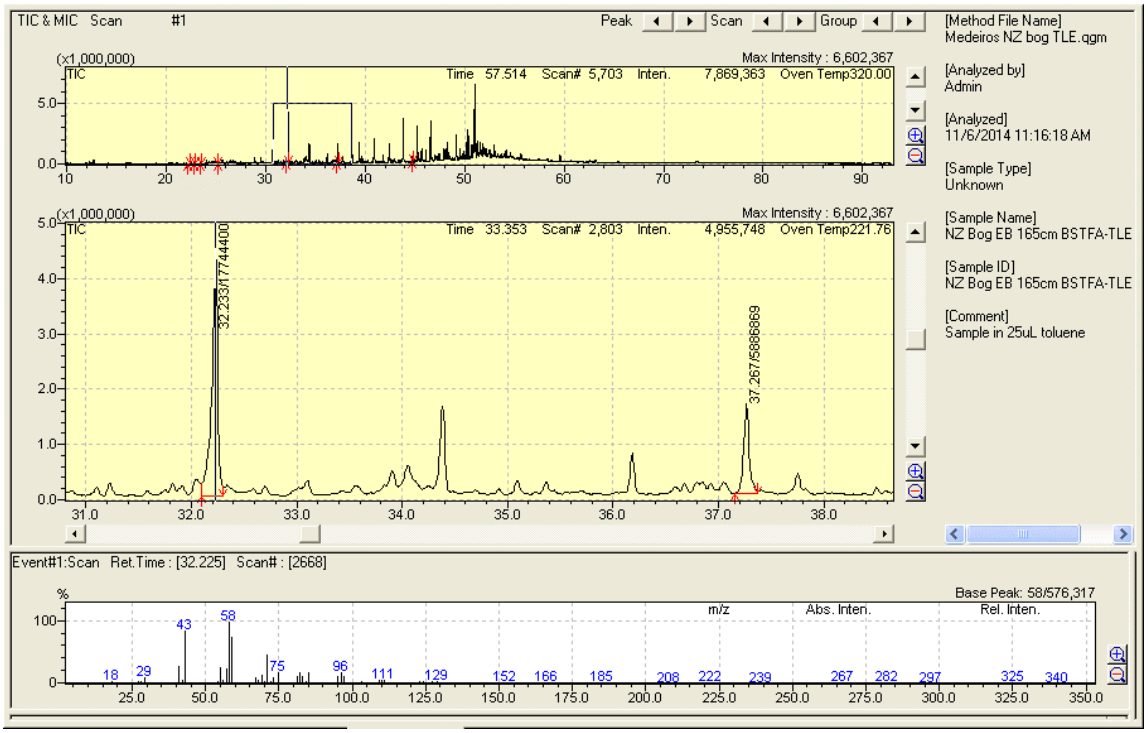

Figure 2-4F: Nonadecanone GC spectrum and MS mass spectrum

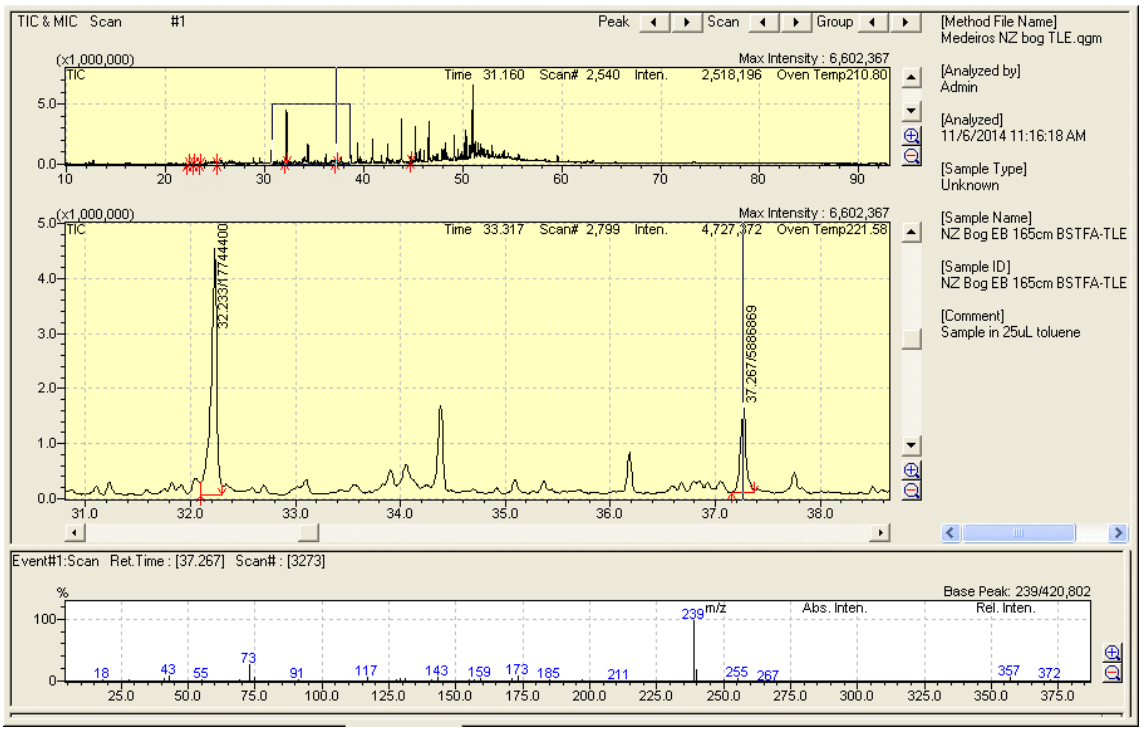

Figure 2-4G: DHAA GC spectrum and MS mass spectrum

A typical GC spectrum for the bog samples analyzed in this thesis, with the region of interest magnified in the inset (Figure 2-4A). Following this are both GC spectra and MS mass spectra for each biomarker and standard, in order of retention time (Table 2-2). All graphs shown in this figure are from one sample, EB 165cm. Biomarkers were identified as peaks in GC traces by identifying key mass ions in the MS mass spectrum.

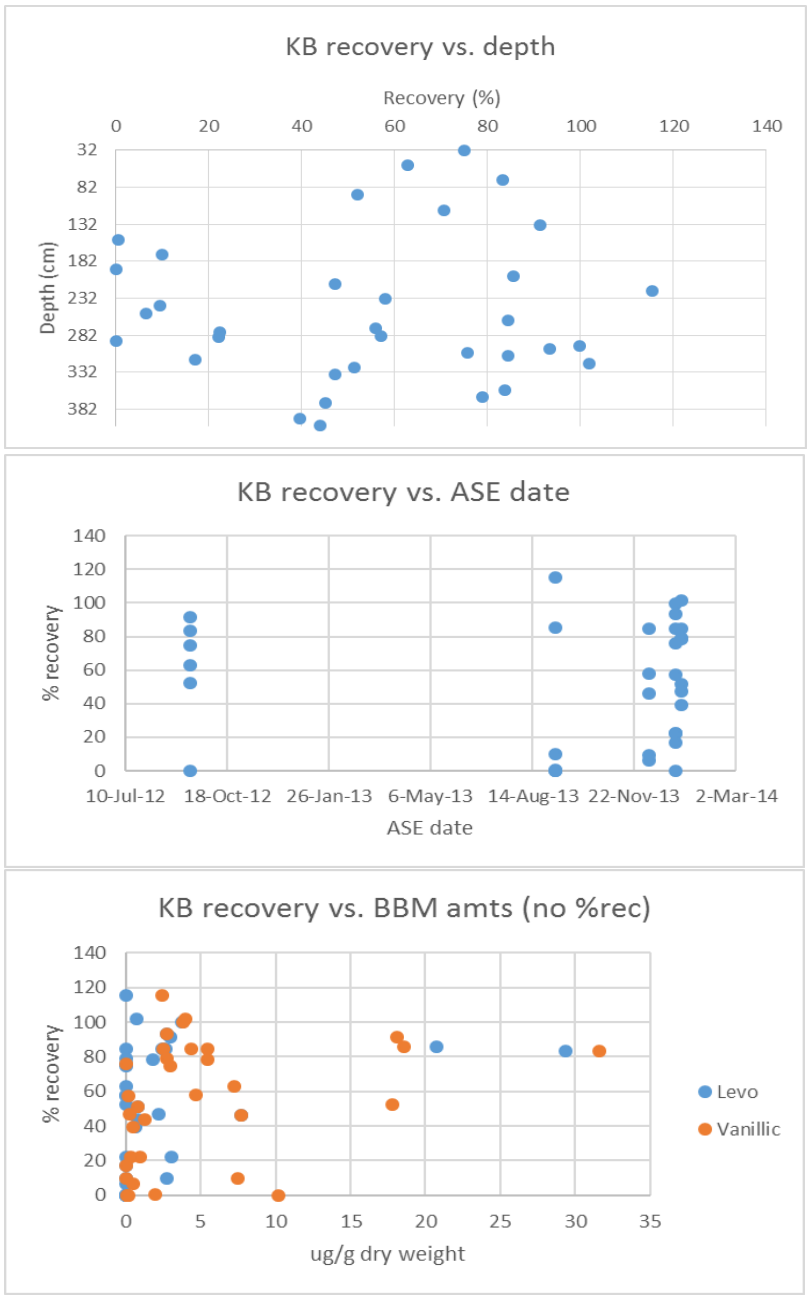

Figure 2-5: The three graphs all represent data from Kettlehole Bog.

Top: Percent recovery of KB samples as a function of core depth. While clusters of similar recoveries are evident (0-20%, 25-60%, 70-100%), these clusters are evenly split over the length of the core. There is no correlation between recovery and core depth.

Center: Percent recovery of KB samples as a function of the date they were run on the ASE. Multiple recoveries are reported every day ASE extraction was performed, and recoveries are evenly distributed over each day. There is no correlation between ASE date and recovery.

Bottom: Percent recovery of KB samples as a function of biomass burning marker (BBM) mass per gram dry weight of sample, without percent recovery applied. Levoglucosan and vanillic acid are featured. Recoveries are evenly spread over the most common range of BBM concentrations. The outlying high BBM concentrations also have no commonality of percent recovery. There is no correlation between BBM amounts and recovery.

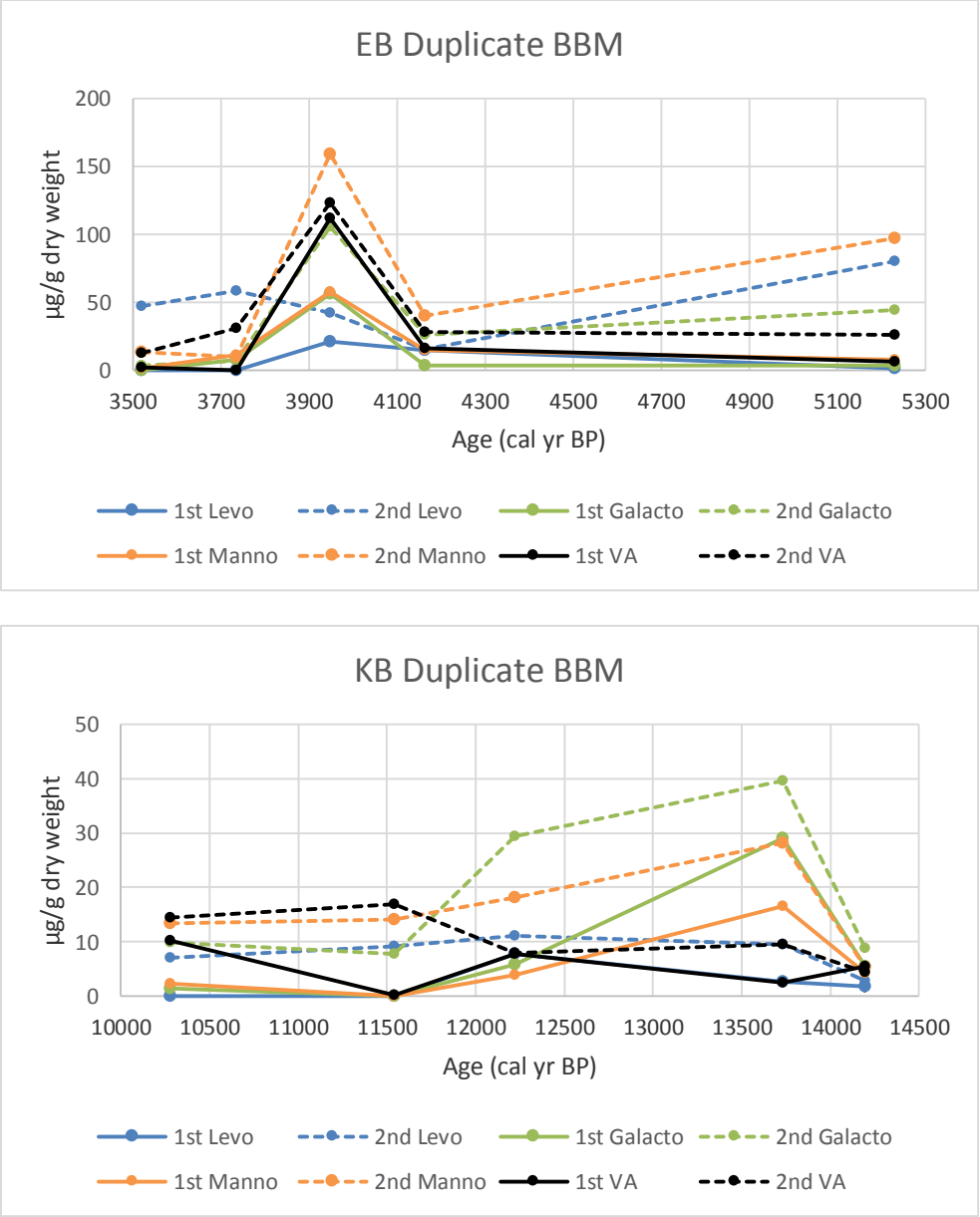

Figure 2-6: Amounts of biomarkers vs. age in initial samples (1st) and duplicate sub-samples (2nd). Levo = levoglucosan, Manno = mannosan, Galacto = galactosan, VA = vanillic acid. The colors of galactosan and mannosan have been changed here for ease of differentiation.

Core	Error (µg/g)	Levoglucosan	Mannosan	Galactosan	GML	Vanillic acid
EB	Mean error	14.6	16.2	8.2	38.7	6.0
	Error range	20.6	22.9	11.6	54.8	8.4
	2:1 Error	16.2	13.7	7.5	37.0	7.4
	2:1 Error range	11.6	13.2	5.9	26.1	2.7
	4:1 Error	12.1	20.0	9.2	41.3	3.9
	4:1 Error range	4.8	15.8	8.0	19.1	0.2
KB	Mean error	2.0	3.7	3.8	9.4	2.1
	Error range	2.8	5.2	5.4	13.3	2.9
	2:1 Error	2.9	4.4	2.9	10.2	3.7
	2:1 Error range	0.4	0.5	0.1	0.8	2.2
	4:1 Error	1.3	3.2	4.4	8.9	1.0
	4:1 Error range	0.8	2.0	3.0	5.3	1.0

Table 2-3: Error calculation. GML = the sum of galactosan, mannosan, and levoglucosan. DHAA was not present in any of these samples.

III. RESULTS

3.1 Biomass burning markers in South Island bogs

Radiocarbon dates used to establish stratigraphy were converted to calendar years using IntCal13. These calendar ages were in turn used to convert depth down core to ages (Figure 2-1). The biomarker abundances could then be related to calendar ages in order to establish changes in their abundance through time and across the varying climate of the deglaciation (Figure 2-5). The cores overlap very little in time, providing concurrent data from just 6.5-3.3ka. This means that in general, interpretation of biomarkers, temperature, and aridity are from one core or the other, but not both at once. While the LTA core extends over the entire time period since the deglaciation, its resolution is too poor for in-depth analysis due to having only 12 sampled points in 17.7ka. For this reason, it is being shown in this section in order to corroborate a general consensus among the biomarker abundances of the three cores, but will not be featured in subsequent discussion.

The biomass burning markers levoglucosan, DHAA, and vanillic acid, as well as the burning product stereoisomers of levoglucosan, mannosan and galactosan, were collectively used to create burning records for three locations in the South Island of New Zealand. These can be directly compared to the more traditional biomass burning indicator, charcoal (McGlone et al., 2004; Wilmshurst et al., 2007). Both biomass burning markers (BBM) and charcoal are produced in fires, but the smoldering conditions present in lower-temperature fires producing BBM's imply greater moisture was present, whereas charcoal implies hotter burning conditions (Kuo et al., 2008).

Levoglucosan, its stereoisomers, and vanillic acid were frequently present in in all three cores, whereas DHAA was found very infrequently; only 4 samples across two sites,

KB and EB, contained DHAA. Previous work has shown levoglucosan to consistently have the highest concentration among the three stereoisomers (Elias et al., 2001), levoglucosan, galactosan, and mannosan, but in this study each had interchangeable patterns of high concentrations amongst themselves throughout these two cores.

3.2 Kettlehole Bog

The Kettlehole Bog core provides a 50-200yr resolution record of the deglaciation from 14.1-10.2ka due to a high sedimentation rate of 66.8cm/kyr. Between 17.2-14.2 and 10.2-2.9ka, the sedimentation rate was very low (9.9cm/kyr and 10.6cm/kyr respectively), resulting in few analyses and low-resolution records during these parts of the core (Figure 3-1 top). This prevents a detailed comparison to the EB Holocene BBM record where the two records overlap between 6.6-2.9ka.

Levoglucosan, mannosan, galactosan, and vanillic acid showed their highest levels between 15-10ka, with the compound that was in higher abundance varying without any discernable pattern (Figure 3-1 bottom). Levoglucosan had only one major peak of 20.8 µg per g dry weight of sample at 11.4ka, with the rest of its occurrences being small intermittent peaks of 0.7-14.5 µg/g throughout the core. Galactosan showed large peaks of 39.6 µg/g dry weight at 13.7ka, 29.4 µg/g at 12.2ka, 23.6 µg/g at 11.4ka, and 33.5 µg/g at 10.5ka, with intermittent smaller peaks of 0.3-11.5 µg/g throughout the core. Mannosan, in a similar pattern to its stereoisomers, had large concentrations of 28.2 µg/g dry weight at 13.7ka, 18.2 µg/g at 12.2ka, and 25.8 µg/g at 11.4ka, with other smaller peaks of 0.3-13.4 µg/g throughout the core. Vanillic acid peaked with 18.6 µg/g dry weight at 11.4ka, 18.1 µg/g at 10.5ka, and 17.8 µg/g at 9.2ka, with peaks of smaller

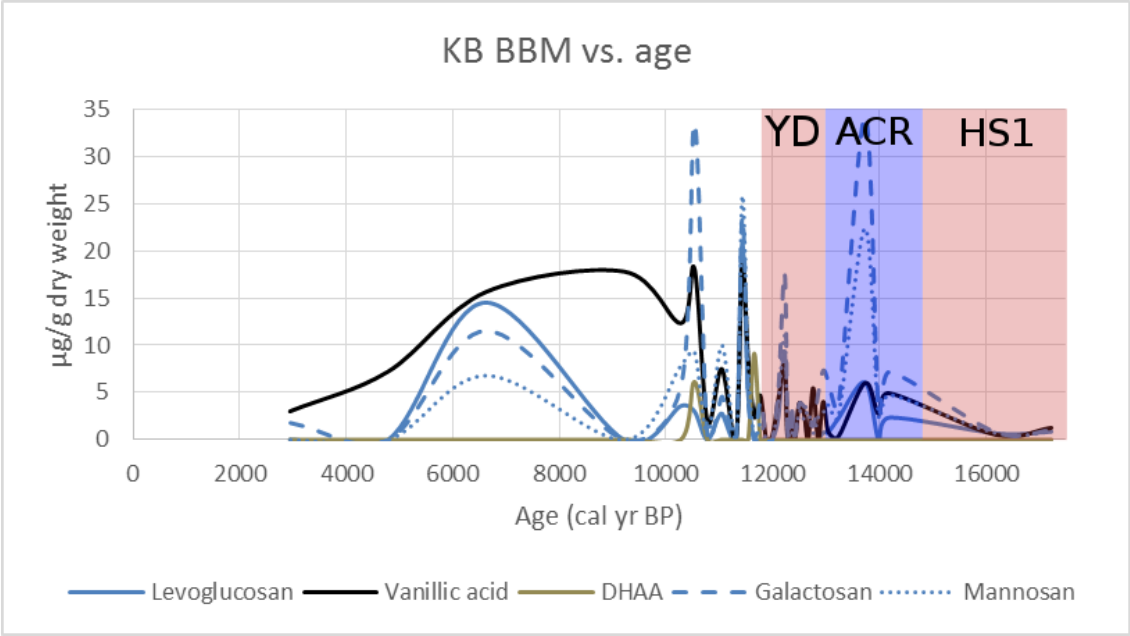

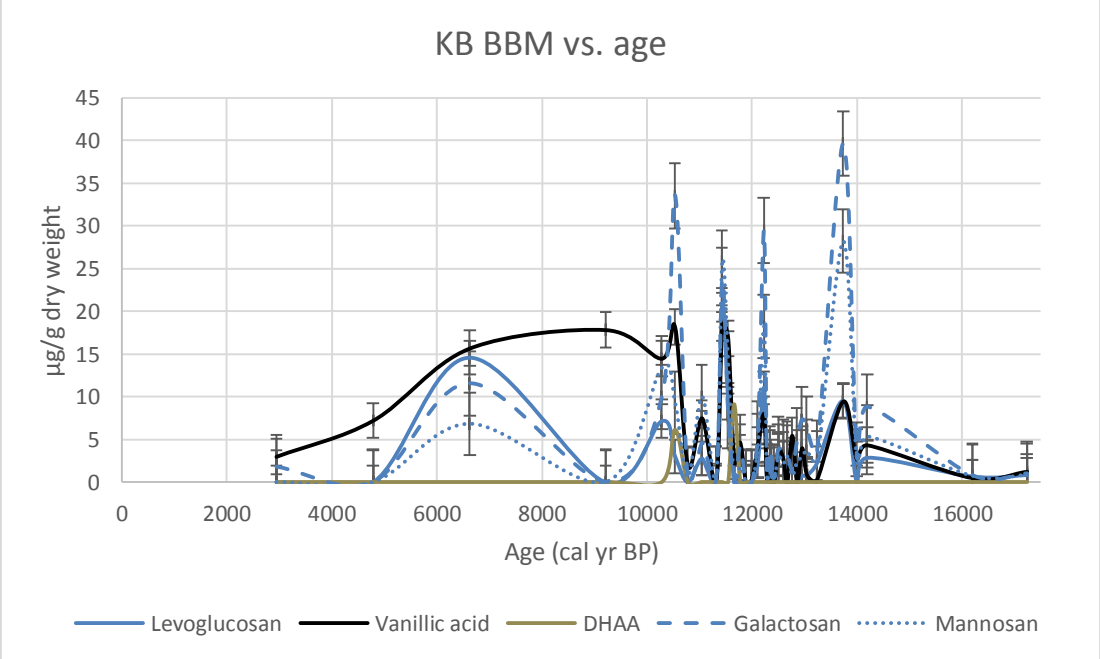

Figure 3-1: The biomass burning markers for Kettlehole Bog generated in this thesis, according to age. Levoglucosan is expected to be consistently higher in concentration than mannosan and galactosan, but this is not the case. Top: deglacial millennial events superimposed for ease of dating. Bottom: mean error added as error bars for more quantitative data analysis.

abundances throughout. DHAA occurred two times in the core, with 13.8 µg/g dry weight at 12.2ka, 9.1 µg/g at 11.6ka, and 6.1 µg/g at 10.5ka.

Kettlehole Bog also has a charcoal record, with its highest levels occurring earlier than 15ka (Figure 3-2). Most notable is the large charcoal peak of 480 particles at 17.3ka. Charcoal presence decreased rapidly after this, with moderate peaks of between 70-120 particles from 15-14ka, reducing to between 10-47 particles by 12.6ka. After this time, most other charcoal occurrences are very low, between 0.3-2.8 particles.

Overall, the burning indicators show a shift from low biomarker levels and a large amount of charcoal present at the end of the glaciation to moderate charcoal and increased biomarker abundance during the early deglaciation. BBM's rose in stages, first in the ACR and then the Younger Dryas, as charcoal amounts drop.

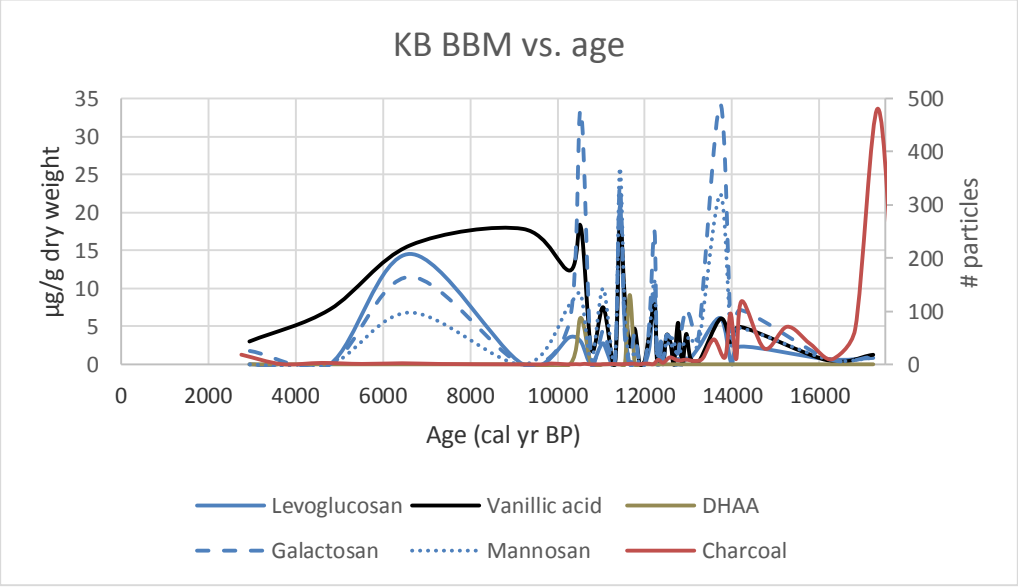

Figure 3-2: Kettlehole Bog biomass burning marker concentrations generated in this thesis and charcoal records (Wilmshurst et al., 2002) plotted against time. Charcoal is plotted on the right vertical axis, while all other biomarkers are plotted on the left vertical axis.

3.3 Eweburn Bog

The Eweburn Bog core provides a 200yr resolution BBM record of the later Holocene, from 6.6ka to 200 years before the present. The sedimentation rate was 31.2cm/kyr from 6.6-5ka, and 81.9cm/kyr from 5-0.2ka. BBM appear in increasing quantities around 5ka. The top part of the record includes BBM evidence from just before the colonization of the country by European settlers ~150ya.

All five BBM were present in this core. As in the KB core, levoglucosan and its stereoisomers were largely present in the same samples in association with each other but had maximum abundances at different times (Figure 3-3). Levoglucosan had significant peaks of 38.4 µg/g dry weight at 5.8ka, 101.6 µg/g dry weight at 4.6ka, 31.8 µg/g at 3.9ka, 49.7 µg/g at 3.3ka, and 35.8 µg/g at 0.3ka, with abundances between 10.1-80.1 µg/g from 6.5-3.3ka, and smaller amounts at various other points. Vanillic acid showed notable concentrations of 32.6 µg/g at 6.5ka, 48.2 µg/g at 4.6ka, 117.5 µg/g at 3.9ka, 70.9 µg/g at 3.3ka, 20.3 µg/g at 1.1ka, and 53.9 µg/g at 0.2ka, with smaller amounts at various

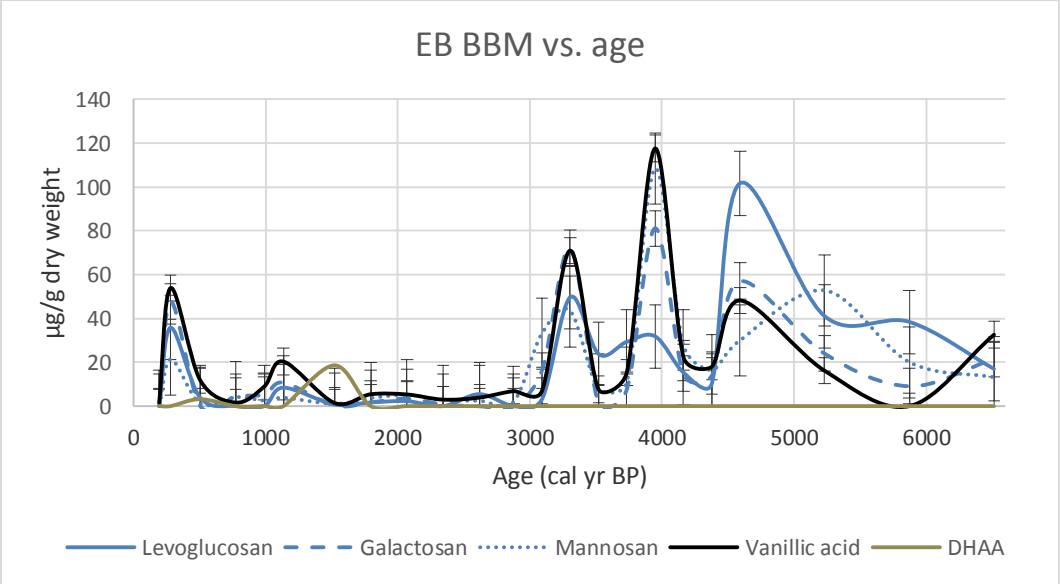

Figure 3-3: The biomass burning markers for Eweburn Bog generated in this thesis, according to age. Levoglucosan is expected to be consistently higher in concentration than mannosan and galactosan, but this is not the case.

other points. DHAA was only present in two samples with concentrations of 18.5 µg/g dry weight at 1.5ka and 3.2 µg/g at 0.5ka. Mannosan had concentration spikes of 52.7 µg/g dry weight at 5.2ka, 108.3 µg/g at 3.9ka, and 43.2 at 3.3ka; and galactosan showed large concentrations of 57.0 µg/g at 4.6ka, 81.1 µg/g at 3.9ka, and 72.1 µg/g at 3.3ka.

Biomass burning markers and charcoal did not typically occur in high concentrations at the same depths in the core (Figure 3-4), which is consistent with previous studies suggesting that different types of fires produce charcoal as opposed to biomarkers like levoglucosan (Kuo et al., 2008; Sikes et al., 2013). Charcoal was rare in the core, with peaks of 2.7 particles per 250 counts of charcoal found at 7.0ka, 8.3 particles at 2.0ka, and 10.6 particles at 0.2ka, and the rest of its occurrences as occasional peaks of 0.4-0.8 particles (Wilmshurst et al., 2002).

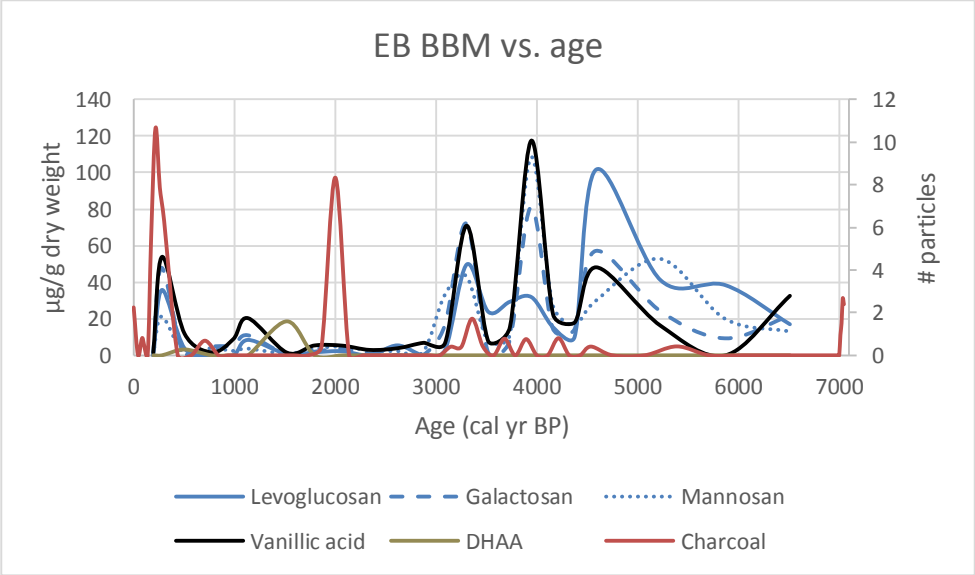

Figure 3-4: Eweburn Bog biomass burning biomarker concentrations generated in this thesis and charcoal records (Wilmshurst et al., 2002). In general, biomarkers showing evidence of cooler fires occur deeper in the core (7-3ka), while charcoal as evidence of hotter fires occurs more recently (4ka-top).

Overall, there was a trend of higher concentrations of BBM across the time period of 7-3ka, with highest levels at 5-3ka. A smaller series of BBM peaks with a charcoal peak are present at 2-1ka. This pattern suggests a period of wetness in the Eweburn Bog area between 3-2ka.

3.4 Lake Te Aroha Bog

Lake Te Aroha is near in location to Eweburn Bog, and provides a lower resolution record of the deglaciation from ~18ka to present that ties the two higher resolution records together. The low sedimentation rate of 6.8cm/kyr resulted in about 2m of deposited sediment over approximately 21ky. Twelve samples from the core were available for analysis.

Levoglucosan, its stereoisomers, and vanillic acid were identified in the core, but DHAA was not present. Neither charcoal nor pollen records are available for this site. Additionally, the age record is tentative, as only four radiocarbon dates were taken that were deemed to be reliable (Figure 3-5).

The LTA core contained relatively high BBM concentrations compared to the other cores. Levoglucosan and its stereoisomers had greatest abundance early in the deglaciation, with a large spike of 208.6 µg/g of galactosan, 217.4 µg/g of mannosan, and 50.7 µg/g of levoglucosan at 15.0ka. The abundances of all three of these molecules gradually decreased toward the modern, ending at their lowest peak at 1.8ka with concentrations of 18.1 µg/g, 31.8 µg/g, and 27.7 µg/g, respectively. Vanillic acid gradually increased over time, with no peak greater than 7 µg/g until 10.5ka, at which point its first significant peak of 47.6 µg/g appeared. Vanillic acid had two major peaks

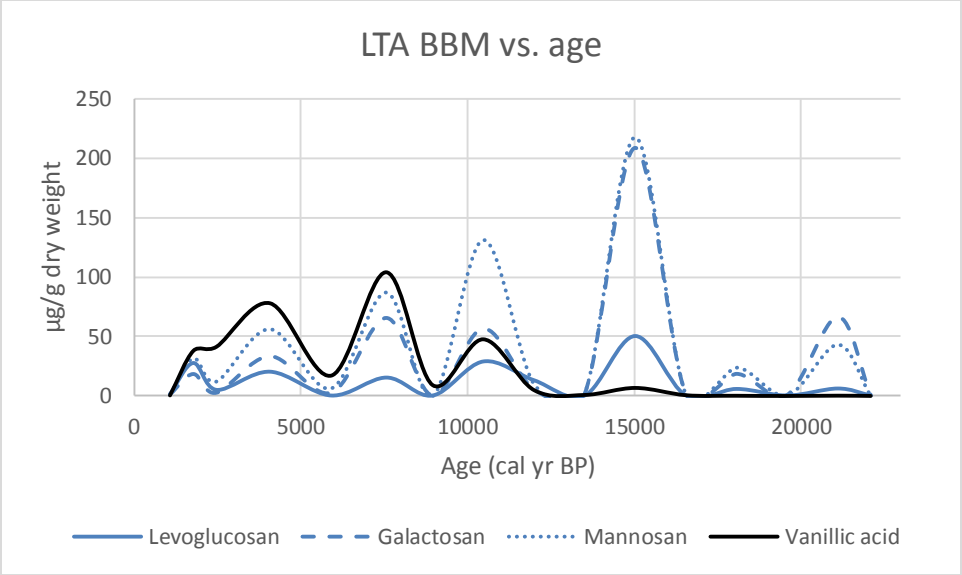

Figure 3-5: Lake Te Aroha Bog BBM to depth. No DHAA was identified in the core.

of 104.0 µg/g at 7.6ka and 77.9 µg/g at 4.1ka before also decreasing to 37.8 µg/g by 1.8ka.

3.5 Summary

Overall, the trends for this core are for low levels of all biomarkers until a large spike in levoglucosan and its stereoisomers at 15.0ka. After this, levoglucosan, mannosan, and galactosan gradually decrease until the top of the record, while at 10.5ka vanillic acid abundance overall increased to the top of the core. The overlapping of the EB and KB cores between 6 and 3ka seems to imply a coordinated decrease in biomarker abundance from 3.9ka to today. The LTA record reinforces the trend seen in KB and EB, by showing low levels of biomarkers in the LGM, steadily increasing in BBM concentration until approximately 7.6ka, and decreasing again after that time, until a slight resurgence in the modern with anthropogenic burning. Taken together, these three records show low levels of smoldering fires at the very beginning of the deglaciation, an increase in these kinds of fires from about 10.5-3.9ka, and a decrease towards today (Figure 3-6).

Charcoal was recorded in high quantities at the end of the glaciation and beginning of the deglaciation in KB, and then waned up-core. In contrast, biomass burning biomarkers began to appear and increase shortly after the start of the deglaciation around 17.5ka in both KB and LTA. This suggests that at the beginning of the deglaciation in New Zealand, there was a decrease in the hotter fires that produced charcoal in favor of the smoldering fires that produce vanillic acid, DHAA, and the stereoisomers levoglucosan, mannosan, and galactosan. In general throughout all three sites (Figure 3-6), BBM's showed increased abundance over time until about 3.9ka, when they gradually decline through the late Holocene. The only exception to this is at the most modern point of 200ya in EB, possibly due to forest clearing by burning during European colonization.

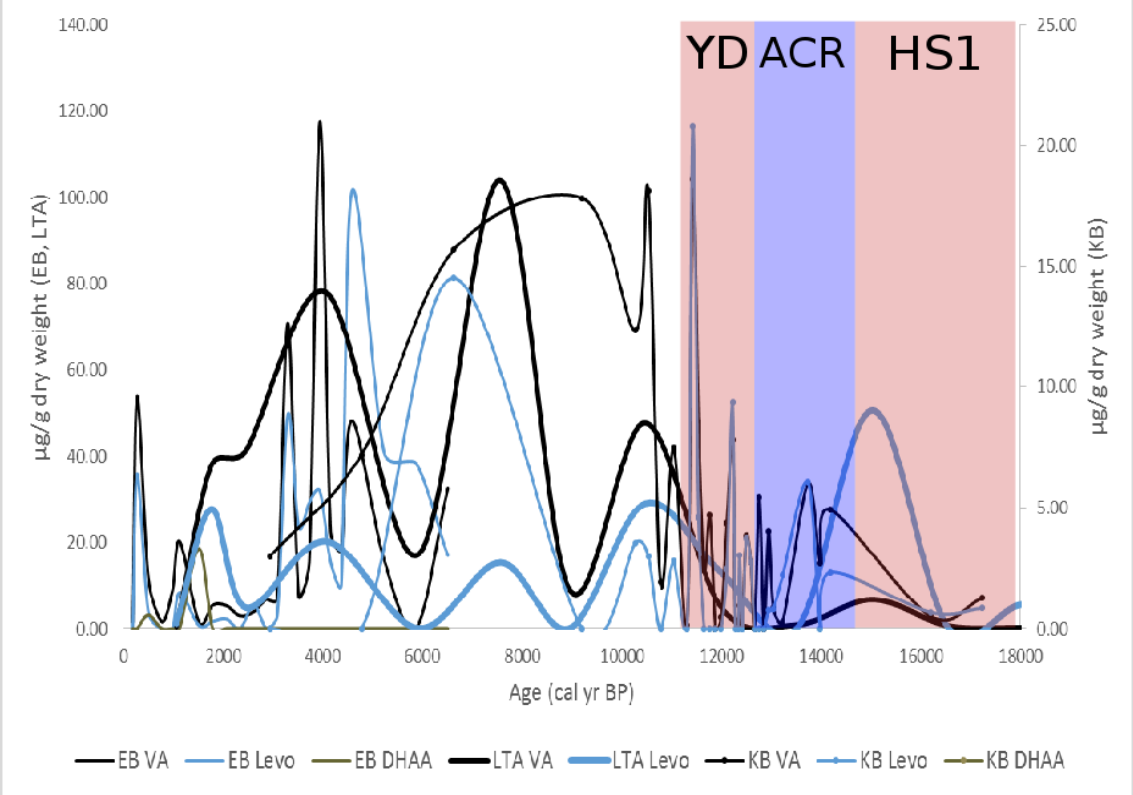

Figure 3-6: Mass per gram dry weight of vanillic acid, levoglucosan, and DHAA from KB, EB, and LTA cores as a function of time, showing millennial deglaciation events. There is no DHAA present in the LTA core, but otherwise all three BBM records seem to conform.

The two points at 6.6ka represent potential outliers in levoglucosan and vanillic acid concentration that have been removed from the overall record.

IV. DISCUSSION

4.1 Burning and the floral ecosystem

The dichotomy between the formation conditions of charcoal, which is produced by hot fires, and the burning biomarkers in the levoglucosan stereoisomer family, which are formed in smoldering fires, can be used to understand the burning record in three New Zealand sites. Charcoal abundance and levoglucosan abundance have been shown to provide a qualitative measure of how hot fires burned (Kuo et al., 2008). Charcoal particles present in a core are indicative of a hotter fire (≥350°C), which more likely occurred in a drier, if not hotter, setting (Elias et al., 2001). The presence of levoglucosan indicates cooler (150-350°C), more smoldering fires, which likely occurred in wetter but not necessarily cooler conditions (Kuo et al., 2008; Sikes et al., 2013). Also of consideration is the fuel that is burned in these kinds of wildfires. The conifer burning markers vanillic acid and DHAA in New Zealand trace the burning primarily of plants in the *Podocarpaceae* (podocarps), the major conifer family in New Zealand (Wilmshurst et al., 2007). Conifer BBM's are created under the same sorts of condition as the levoglucosan stereoisomers (Oros and Simoneit, 2001), so they also serve as a qualitative marker for conifer abundance of cooler smoldering fires.

Recent fire studies suggest the possibility of an interactive fire-plant relationship. This work highlights the differential ability of plants in the northern hemisphere to rebound after fires, indicating that fires influence the spread and growth of certain kinds of plants over others (Rogers et al., 2015). In boreal forests of North America and Eurasia, species-level characteristics of trees can determine their success in fire-prone regions (Rogers et al., 2013; Rogers et al., 2015). More frequent burning alters plant ratios in favor of trees

that can avoid or resist fire, such as tall conifers that grow sufficiently tall to avoid fatal crown burning. Although conifer trees contain highly flammable pitch, which burns readily, a tall crown and thick bark enables the trees to survive and quickly reproduce in the cleared forest area (Rogers et al., 2015). The New Zealand-native rimu tree (*Dacrydium cupressinum*) is a conifer known for having a crown much taller than the canopy of surrounding trees (Wassilieff, 2012), so it may represent a fire resister. Similarly, broadleaf trees are more resistant to fire due to the higher water content in their leaves than in the needles of conifers (Rogers et al., 2013). By extension, the *Nothofagus* genus of broadleaf trees common in the South Island may be fire resisters. Furthermore, after a fire has burned away competition, surviving trees quickly repopulate the burned area, which may explain a shift in tree abundance after a burning event (Rogers et al., 2015).

The assumption that constant and persistent dryness is conducive to more burning is simplistic (Westerling et al., 2003). The most important factor leading to more burning today in North America is fuel type, which is driven by cycling between abnormally wet and dry years. It is the shift from drier-than-average to wetter-than-average or vice versa that is directly responsible for burning, which is reflected in these cycles of wet vs. dry times. In the northwestern United States dry grass- and shrub-lands, a year with wetter than average spring and summer has been shown to correlate strongly to burning during the next year's dry season (late summer to early fall), regardless of the amount of precipitation in that next year (Westerling et al., 2003). This is because grasses and shrubs, known as fine fuels, proliferate very quickly during wet years. In a generally dry environment, the availability of fuel is a more important factor to burning frequency than the increased flammability that a drier than average year provides (Rogers et al., 2013; Westerling,

2009). Within tall conifer forests, wetter than average springs and summers also allow local grasses and shrubs to proliferate. A subsequent drier than average year will cause these fine fuels to burn, which then act as tinder to fuel burning of trees, as burning in heavy fuels such as wood is much harder to induce during any wetter time (Westerling et al., 2003). It is assumed that opportunities for fire ignition such as lightning strikes are relatively consistent from year to year (Westerling et al., 2011). The northwestern United States experiences similar temperature and precipitation ranges to those of New Zealand (Bartlein et al., 1998; Wilmshurst et al., 2007), allowing analogies to be drawn to temperate New Zealand climate. The grass or shrubland ecosystems are similar to the ecosystem reconstructed from pollen of the Cass Basin of South Island at the end of the glaciation.

By analogy to these northern hemisphere ecosystems (Westerling et al., 2003), the presence of burning events may have been due to a pattern of cyclical dryness. In New Zealand, shrubs require more warmth and moisture in order to grow preferentially over grasses. Shrubs are short-lived, and can survive brief periods of dryness on the interannual scale but prefer wetter growing seasons. New Zealand trees inhabit environments still warmer and wetter than shrubs. However, once trees are established they can survive multiannual to decadal scale droughts due to higher stress tolerance (Wilmshurst et al., 2002). Therefore, persistent dryness with very short, mild wet cycles on the seasonal to interannual scale are likely to both promote the growth of grasses and shrubs as well as cause the most burning of these plants, which have life spans on that time scale. Smoldering fires would likely be most common in climatic cycles with longer wet periods and shorter, sparser dry times, which are the conditions in which tall trees are more likely to grow. These variations over time would cause feedbacks between increasing wetness

that affected the ecosystem and conditions that were dry enough to allow for fires. Aridity alone is enough to shift ecosystems, regardless of fire influences.

Seasonality is a factor in many temperature reconstructions from proxies (Meyers, 1997). Sea surface temperature from alkenones, for example, typically records spring-summer temperature, since that is when the plankton that produce the alkenones bloom (Sikes et al., 2005). Plant abundances are largely determined by winter minimum temperatures, since cold winters as opposed to warm summers are typically the deciding factor in whether a location is habitable for a particular kind of plant (e.g. Vandergoes et al., 2008). Burning is linked to summer dryness, because fires tend to occur during the late summer and early fall, typically the driest parts of the year in New Zealand (NIWA, 2013). A wet spring conducive to growth may also be followed by a dry summer, which may not affect burning ignition in grass or shrubland but could be a factor in the outbreak of forest burning. The temperature records based on pollen used in this thesis have been calibrated to reflect mean annual temperature (Wilmshurst et al., 2007).

4.2 The deglaciation record: ecology, temperature, and climate of Cass Basin

The Cass Basin site of Kettlehole Bog provides a detailed record of climate of the central South Island from the deglaciation ~18ka to the early Holocene ~8ka. For clarity, the HS1 time period has been split into two periods, the end of the glaciation (17.7-16.8ka), and the early deglaciation (16.8-14.7ka).

There are a number of paleoclimatic records from the South Island, and a terrestrial record of temperature from Okarito Bog is relevant to this analysis both for its proximity to Cass Basin and its reconstruction which generally agrees with other temperature reconstructions for the time and general area (Alloway et al., 2007; Denton et al., 2010;

Newnham et al., 2012). Okarito lies on the western edge of the South Island, and is roughly latitudinally equivalent to Kettlehole Bog. It is on the upwind side of the Southern Alps, and the precipitation there today is about 5000mm per year, relatively consistent year-round with a slight summer maximum and winter minimum (Vandergoes and Fitzsimons, 2003). This is in contrast to Cass Basin, which is on the eastern side of the mountains in their rain shadow, with a mean annual rainfall of 1300mm and seasonal precipitation having a strong maximum in the winter with a highly seasonal variation of temperature (McGlone et al., 2004).

The Kettlehole Bog temperature reconstruction differs from the Okarito Bog reconstruction, and a suspected cause for the discrepancies in the reconstructions is the differences in the precipitation patterns between cores' locations. A past seasonal or interannual perturbation in the persistently wet environment of Okarito Bog is unlikely due to the moderating influence of the ocean on the local climate, apart from occasional katabatic winds (Newnham et al., 2007). When examining the perpetually wet, but reliable, Okarito Bog record, the variability of Cass Basin's precipitation becomes suspect. We examine the KB record in the context that aridity may in fact be influencing the reliability of the modern analogue technique of pollen temperature reconstruction (Wilmshurst et al., 2007).

4.2.1 End of the glaciation (17.7-16.8ka)

The late glaciation, at the base of the Kettlehole Bog core, contains high levels of charcoal and low amounts of BBM's, which indicates that there was significant burning of hot fires (Figure 4-1). The pollen present shows that this was the time in which grasses were at their highest abundance, in addition to large amounts of shrubs and few trees, which

is an ecosystem pattern indicative of a persistently or annually dry climate (McGlone et al., 2004; Westerling et al., 2003; Wilmshurst et al., 2002). Low amounts of moisture on the annual to interannual timescale promoted grass growth. Grass burns hotter than most other heavier fuels, and this is evidenced by charcoal peaks in the KB core correlated to peaks in grass abundance. Hot fires link to grassland fuel.

Following evidence of persistent dryness at and just after the LGM, there was a sharp dropoff in charcoal abundance and a shift in plant abundance ratios away from grass and shrubs and towards tall trees at 17.3ka. This ecosystem shift indicates that the Cass Basin area likely became wetter if not warmer. The temperature reconstruction in Cass Basin suggests that the temperature at this time warmed by 1°C, while the reconstructed temperature from Okarito Bog suggested that the climate remained cool for another 100 years (Newnham et al., 2012). With this relatively small temperature change, the fact that plant type ratios in the pollen record changed after 17.3ka indicates that perhaps increased wetting during this time drove ecosystem change more strongly than temperature. Angiosperm shrubs were likely the burning fuel through this period, based on their prevalence in the pollen record (Figure 4-2) and preference for wetter conditions if not warmer temperatures than grasses (Alloway et al., 2007).

By comparison to other temperature reconstructions that indicated a relatively constant temperature for the time (Alloway et al., 2007; Newnham et al., 2012), the shift from grasses and shrubs toward tall trees suggests a change from the cooler, drier climate that may have again been driven more by increasing moisture than temperature. The

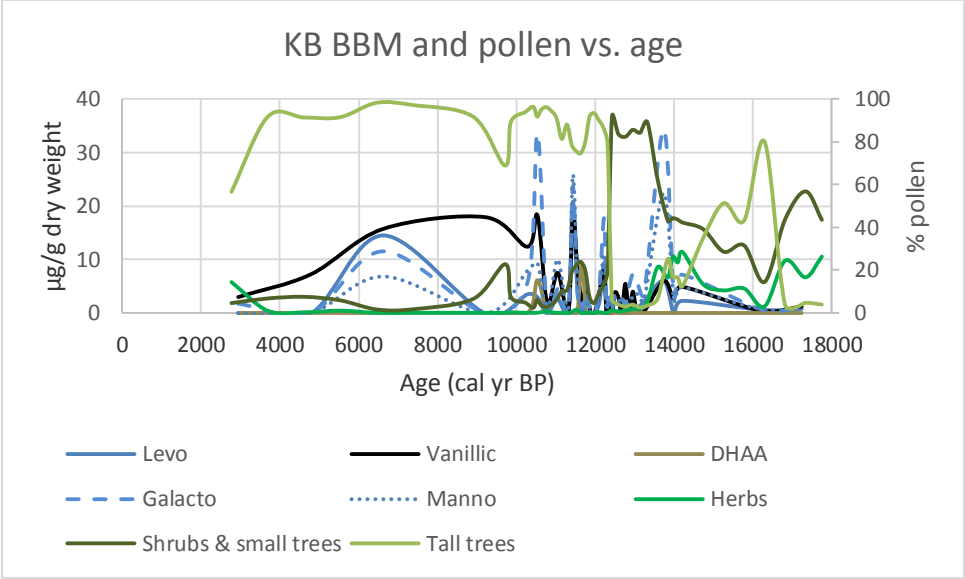

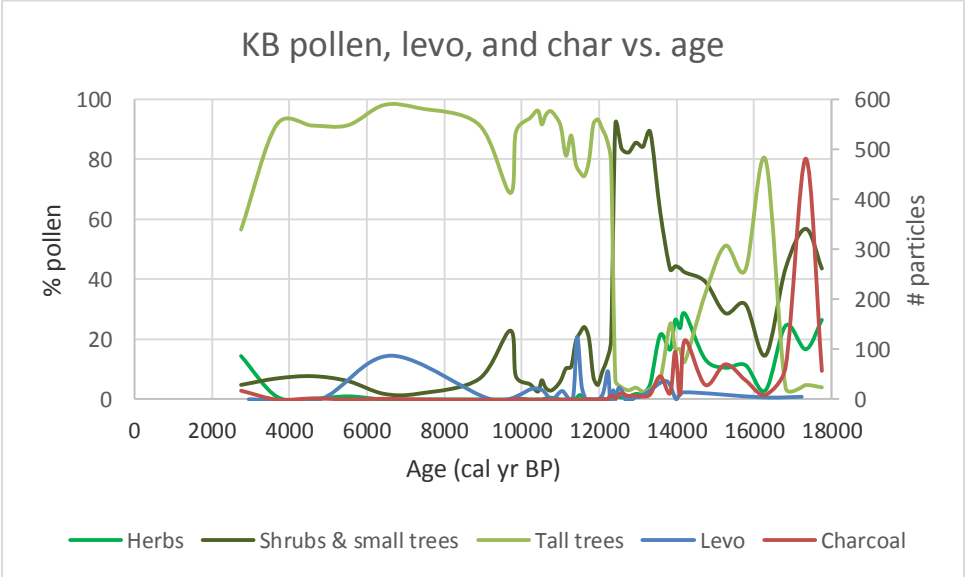

Figure 4-1: Kettlehole Bog pollen ratios to age contrasted against all three major biomass burning biomarkers (top), and against levoglucosan and charcoal (bottom). The rapid shift from shrubs and small trees to tall trees at 12.5ka may be the cause of increased DHAA abundance.

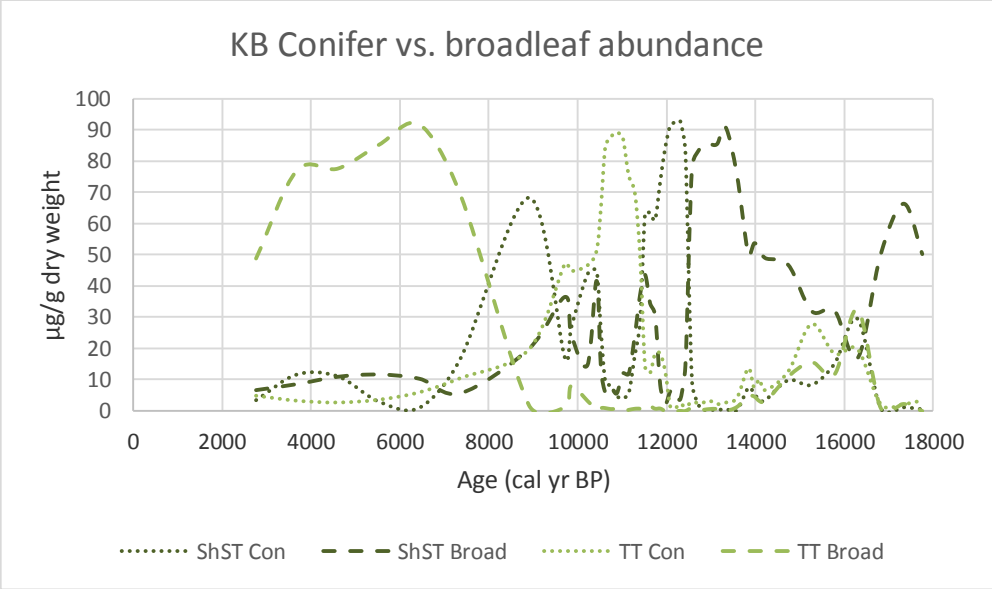

Figure 4-2: KB conifer vs. broadleaf abundance in tall trees (TT) and shrubs and small trees (ShST). Different types of trees and shrubs were prevalent at different times, depending on whether they were conifer or broadleaf species, which is not apparent in the overall pollen record.

presence of charcoal before 16.8ka indicates initial interannually dry conditions likely caused a boom in grass abundance and supported their higher-temperature burning (Westerling et al., 2003). As more persistently wetter conditions with shorter dry periods ensued, trees were able to recolonize grassland, which greatly cut down on hot fires. Qualitatively it is likely that this shift to longer wet or wetter periods was rapid, due to the rapid increase in tall trees and sharp decrease in charcoal, shrubs and grasses at 16.8ka.

4.2.2 Early deglaciation (16.8-14.7ka)

Regional temperature records show a warming trend across New Zealand during the early deglaciation 16.8-14.7ka (Alloway et al., 2007). However, the KB reconstructed temperature exhibits variability while overall remaining cool (Figure A4-1). The ecosystem reconstructions show that beginning at 16.8ka, tall trees, both broadleaf and conifer, increased in abundance. Charcoal was present in low levels and BBM levels were

higher than ever before, implying some hot fires as well as an increase in smoldering burning. The swing in ecosystem to forests with only a minor shrub presence at the same times as the emergence of smoldering fires implies increasing moisture and plausibly a change in the cycle of rain. The low resolution and variability of the BBM record between 16-13ka restricts detailed interpretation of this time period (Figure 4-1). However, the general trend implies a wetter climate overall, and possibly multiannual to decadal-term cycles of higher precipitation interspersed with periods of droughts allowing trees and shrubs to grow as well as to burn. Later in this period, the MAT reconstruction indicated a cooling at 15.7ka (McGlone et al., 2004), coinciding with the slow decrease in tall trees in favor of shrubs in the KB record, with temperatures remaining consistently colder than the Okarito record by about half a degree. The modern analogue technique used to reconstruct mean annual temperature across New Zealand was mainly populated by information from tall wet conifer forests, but the Cass Basin site and nearby locations were initially dry grass and shrubland (Wilmshurst et al., 2007). Reconstruction of KB temperature began with grassland, and as forest appeared in this area during the early deglaciation, the change in ecosystem due to changing precipitation may have then been responsible for a lowered reconstructed mean annual temperature.

This time period began with a pulse of tall tree abundance and ended as the ecosystem shifted away again from tall trees. This period was likely the beginning of a transition between the cool, dry conditions of the glacial and the warmer, wetter times of the late Holocene.

4.2.3 ACR (14.7-12.7ka)

Regionally, the ACR was a time of cooling (Alloway et al., 2007; Newnham et al., 2012), and the record from Cass Basin shows cool temperatures as well (Figure A4-1). In the KB core, there was a nearly 5-fold increase in BBM from the deglaciation co-occurring with a rapid shift from a tall tree to a broadleaf shrub and small tree ecosystem at ~14.7ka (Figure 4-2). Charcoal decreased to about 1/5 of its deglacial quantity by 14.0ka, but disappeared after a large spike in levoglucosan stereoisomers at 13.7ka. The combination of a continuing increase in BBM with diminishing charcoal suggests a shift to smoldering fires. The change in plants also suggests wetness during this time, enough for shrubs to outcompete grasses but not enough for tall trees to thrive. However, the additional increase in BBM also suggests dryness. This conundrum suggests a different pattern of wetness, plausibly a multiannual pattern with broader swings in moisture delivery, or a change in the seasonality of wetness in the area, leading to increased loss of trees and more persistent burning due to frequent dry periods. The repeated spikes in BBM continue over several thousand years, implying a continued trend of cyclical dryness that extends through the ACR into the Younger Dryas and Holocene.

An interesting point is a dip in reconstructed pollen temperature at 13.8ka coincident with a very large peak in levoglucosan stereoisomer BBM. A rapid change in both temperature reconstruction and BBM is not reflected in the temperature of the Okarito reconstruction. This may indicate an intense, large burning event local to Kettlehole Bog which influenced the temperature record to appear cooler than the actual temperature. After this, warming in KB is seen until 13.1ka despite cooling experienced widely in New Zealand during the ACR. This warming beginning around 13.7ka is signaled by a dramatic rise in broadleaf shrubs and small trees. The inconsistent warming pattern is plausibly a

response of the modern analogue technique to burning of shrubs and small trees, resulting in increased reconstructed temperature for this time.

4.2.4 Younger Dryas (12.7-11.7ka)

In the Younger Dryas, all BBM became present in still higher quantities than previous periods (Figure 4-1). Conifer shrubs and small trees rapidly increased and outcompeted broadleaf shrubs during this time before declining (Figure 4-2), which is a signal of the warming that agrees with other predictions for this period (Alloway et al., 2007) . This suggests more fine fuels, yet also a climate that supported trees. This could be the result of an increase in intensity of the intermittent dryness cycle, with wetter wet periods, drier dry periods, and a shortening of the cycle length so that the trees could become established. Alternately, the seasonality of the rain may have changed, as wetter springs and summers would promote grass growth even if the overall amount of annual moisture were still sufficient to support trees. For tall trees to dominate the pollen record, there was likely a return to cyclical precipitation with a strong wetting phase on a decadal scale. The MAT reconstruction indicates cooling occurring through most of the Younger Dryas in KB (Figure A4-1), in contrast to other temperature records for the South Island (Newnham et al., 2012; Wilmshurst et al., 2007). The Okarito record in particular (Newnham et al., 2012) displays pronounced warming during the Younger Dryas (Figure 4-3), which provides a marked contrast to the cooling in the Kettlehole Bog temperature reconstruction. As in the early deglaciation, the Younger Dryas temperature reconstructions may reported a cooler temperature because of tall conifer tree burning as indicated by elevated vanillic acid concentration.

4.2.5 Optimum (11.7-8.0ka)

From the end of the Younger Dryas until approximately 8ka, there was a marked increase in reconstructed temperature variation in the KB temperature record, with repeated swings of about two degrees in 0.5-1kyr cycles. This time period has been referred to as a climate optimum in New Zealand, and is noted by relatively consistent warming in temperature reconstructions across the North and South Islands during this time (Wilmshurst et al., 2007). In the Cass Basin at 11.2 and 9.4ka, the local temperature reconstruction was highly variable, reaching both its highest temperature of ~10°C (Figure A4-1) and lowest temperature of 7.8°C at 10.3ka. At the same time, tall conifer trees reached their peak for this core, and levoglucosan and vanillic acid spikes indicated that these trees burned in reasonable quantities through this period. The Okarito reconstruction ends at 10ka, but seems to indicate a sustained higher temperature similar to the Younger Dryas, consistent with this climate optimum. The large drop in temperature in the KB temperature record through this period of regional warming points to depressed reconstructed temperatures impacted by tall tree burning.

The pattern of multiple small BBM peaks that persisted through the ACR and Younger Dryas may have continued to persist between 10.5-9.2ka. Based on the two data points acquired during this time period, vanillic acid is present at just under 20 µg/g, and the levoglucosan stereoisomers are present in slightly smaller quantities (Figure 4-1). This implies a shift in precipitation cyclicity toward frequent dry periods allowing sustained burning without affecting the dominance of tall trees, but the data is too sparse to draw any firm conclusions.

4.2.6 Early to mid-Holocene (8.0-2.7ka)

The beginning of the Holocene represents the end of the KB record, and has a significantly lower resolution than the rest of the core. Between 8.9-2.7ka, the temperature reconstruction dropped almost 1.5 degrees from 9.2-7.6℃ (Figure A4-1), and the dominance of tall broadleaf trees, which prefer colder climates than conifers (Figure 4-4 top), indicates that this may have been a real period of cooling in KB. Around this time at 8ka the conifer shrubs of the Younger Dryas and early Holocene gave way to a large increase in tall broadleaf trees. Broadleaf trees are frequently the quickest to capitalize on fire land clearance (Coomes et al., 2005), and the burning of conifer trees or shrubs would explain the high levels of vanillic acid. This potentially indicates the burning of conifer shrubs in a tall broadleaf forest caused by wet periods persistent enough to promote tree growth and short dry periods promoting smoldering fires.

4.2.7 Cass Basin climate

An aim of this thesis was to investigate the influence of aridity on temperature reconstructions based on mean annual temperature (Wilmshurst et al., 2007; Wilmshurst unpublished data). The temperature records of Okarito and Kettlehole Bogs differed in overall pattern (Figure 4-3). Cass showed a warming in the early deglaciation and then a general cooling through the ACR and Younger Dryas. Okarito showed warming into the ACR with the warmest temperatures in the record. During the ACR, Cass experienced the coldest temperatures of the record, whereas Okarito plateaued with very slight cooling. Variable warming in KB during the early Holocene contrasts with other records, including Okarito, that show a warm climate optimum. Overall, Okarito shows a glacial to Holocene warming of over 3°C from 7 to 10℃, with warming centered in the Younger

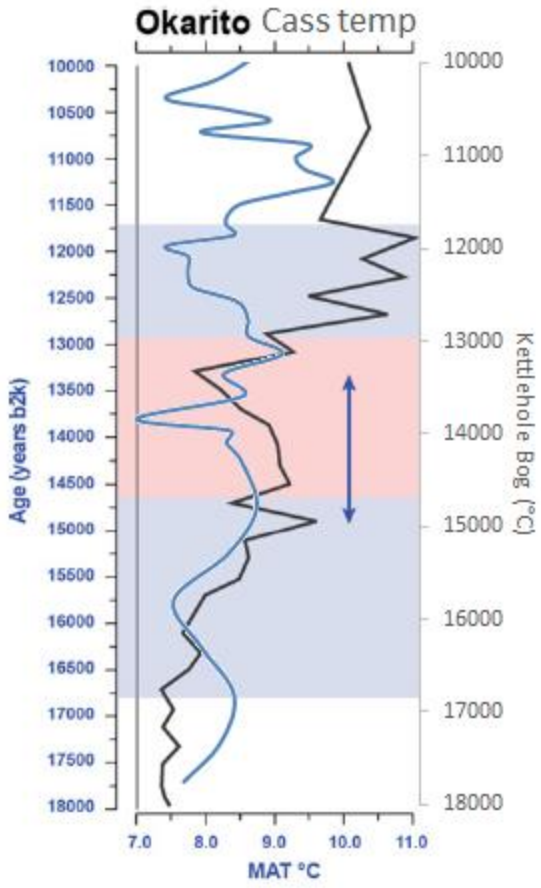

Figure 4-3: Okarito Bog pollen temperature record (right scale, black line) graphed against the Kettlehole Bog temperature record (left scale, blue line). The two temperature records tend to agree except during the 13.0-11.8ka phase, approximately the time of the Younger Dryas. (Edited from Wilmshurst et al. 2007 and Newnham et al. 2012)

Dryas. Cass Basin shows the most warming at the beginning of the Holocene, but cooled towards the modern, with a similar beginning and ending temperature of ~8°C (Figure 4-4).

Between the end of the deglaciation and the top of the core, KB reconstructed temperature is not reported to have changed more than about 3°C (Figure 4-3) with alternating periods of higher or lower temperatures than other records can account for

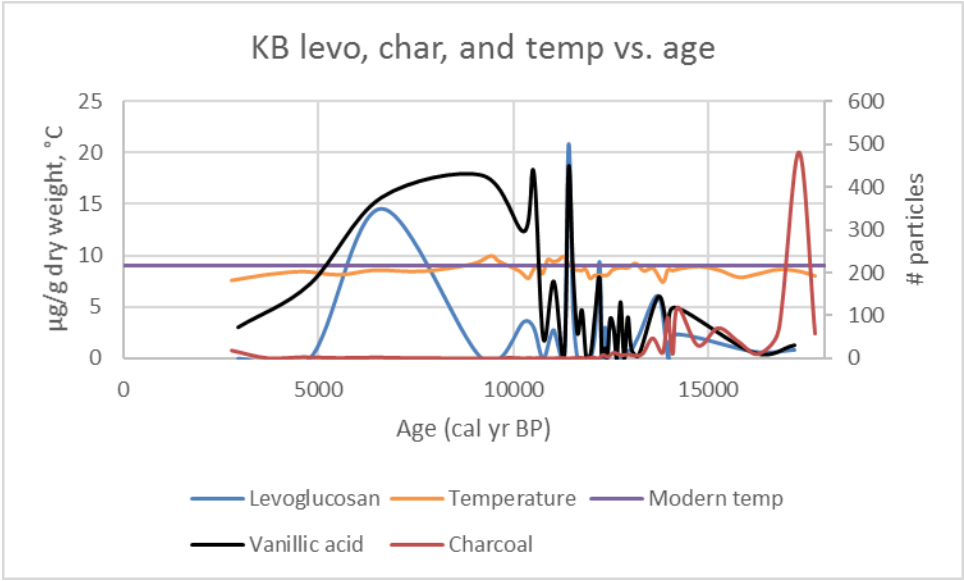

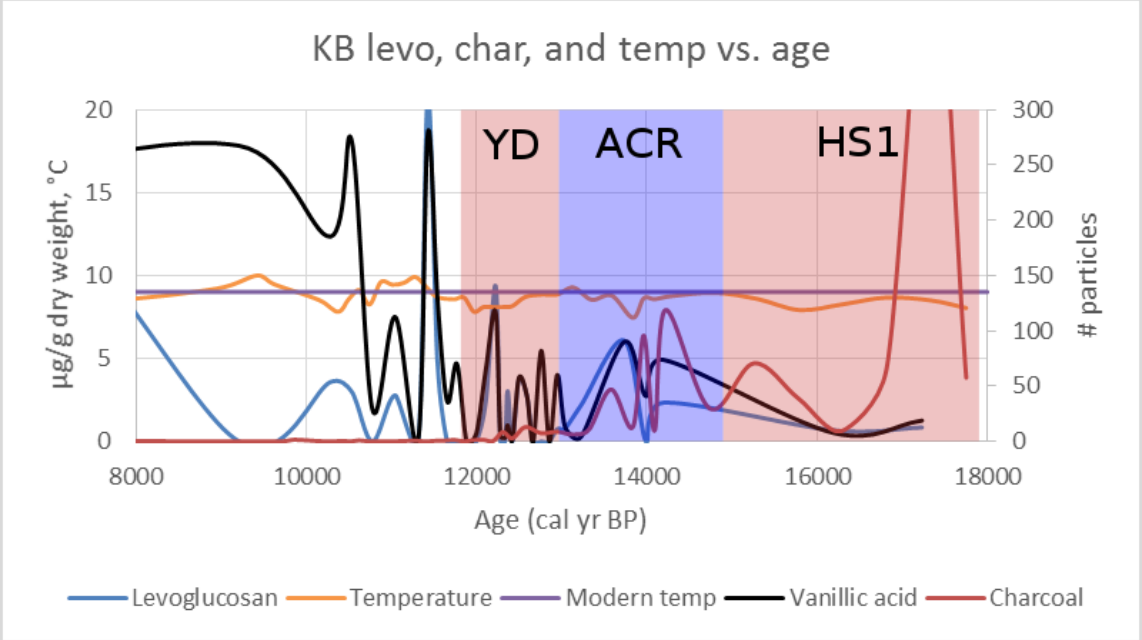

Figure 4-4: Top: Levoglucosan, charcoal, mean annual temperature reconstruction (Wilmshurst et al., 2007) and modern mean annual temperature (NIWA, 2013) for Kettlehole Bog. Bottom: An expanded view of the 10-18ky range of the center graph. Kettlehole Bog shows a hot fire (18-13ka) to cool fire (13-2ka) BBM progression and a cool (18-14ka) to warm (14ka-9ka) to cool (9ka-2ka) temperature progression.

(Alloway et al., 2007; Newnham et al., 2012; Vandergoes et al., 2008). This temperature calculation, however, seems likely to be inaccurate. The aridity measurements inferred from the BBM record since the deglaciation indicate that Cass Basin experienced a greater amount of sustained and periodic dryness than other locations in New Zealand, and in these periods of dryness the KB temperature seems to be lower than that of wetter locations. It is plausible, therefore, that during dry periods, the reconstructed temperature has been biased to cooler than was actually present at the time.

4.3 The Holocene record: ecology, temperature, and climate of the Te Anau region

The EB core provides a detailed record of the Holocene in the southern South Island. The pollen record in this core is straightforward with a consistent record of dominant tall tree forest. In contrast, there is a variable record of burning indicators with charcoal and biomarkers appearing at different levels, providing an aridity record not seen in KB, Okarito, or the North Island record (Sikes et al., 2013) due to the timescales present in those cores.

4.3.1 Mid Holocene (8.5-3.0ka)

The Eweburn Bog core temperature record began at the end of the climatic optimum at 8.5ka (Wilmshurst et al., 2007), and showed variable but high temperatures around 9-10°C for most of 8.5-6.5ka. The ecosystem record began at 7.0ka with a sudden shift in biomass from shrubs to tall trees within 100 years, around the same time as a sharp drop in temperature to around 7°C. This may represent the end of the climate optimum, with rapidly decreasing temperature and a rapid change in biomass. After this shift, tall trees made up around 90% of the ecosystem biomass, and the temperature rose again to a maximum of ~10°C at 6.4ka. While further fluctuations in temperature occurred in the

early part of the record where either charcoal or BBM's were present (Figure 4-5), there was still an overall cooling from 10-7℃ by 3.0ka.

The BBM record for the EB core began at 6.5ka, soon after the record in the Kettlehole Bog core lost resolution around 8ka. The burning indicators present show a similarly variable record as that seen in Cass Basin. There is a notable burning biomarker trend just after the highest temperature point at 6.4ka, and also a marked increase in BBM during this time, implying a shift to a drier precipitation cycle. Levoglucosan and its stereoisomers were abundant and frequently present in the core between 3.0 and 6.0ka, whereas charcoal was present at 7.0ka and after 4.2ka (Figure 4-5). This suggests a period of relative dryness marked twice through this period perhaps by still greater dryness, with more hot burning at 4.7-3.0ka. There must have been adequate cyclic precipitation between 6.0-3.0ka to sustain tall tree abundance, and to promote the fine fuels that facilitate both the burning of trees and the prevalence of charcoal-producing fires.

Temperatures suggest a trend of ~3℃ cooling throughout the record from 10℃ at 6.4ka to 7℃ at 4.3ka (Figure 4-6). The relative composition of the tall trees began to change during this period of cooling, around 4.8ka (Figure 4-7), when the conifers, which had been dominant until then, decreased as angiosperm tall trees grew to take their place. Around the same time, ~4.5ka, a very large levoglucosan spike marked the end of a period of relative abundance of BBM. This suggests a moisture increase driving this ecosystem change, as broadleaf trees such as *Nothofagus* cannot tolerate as much dryness as conifers (Wilmshurst et al., 2002). An increase in wetness would allow the broadleaf tall trees to outcompete the conifers during this time. Both warming and wetting after

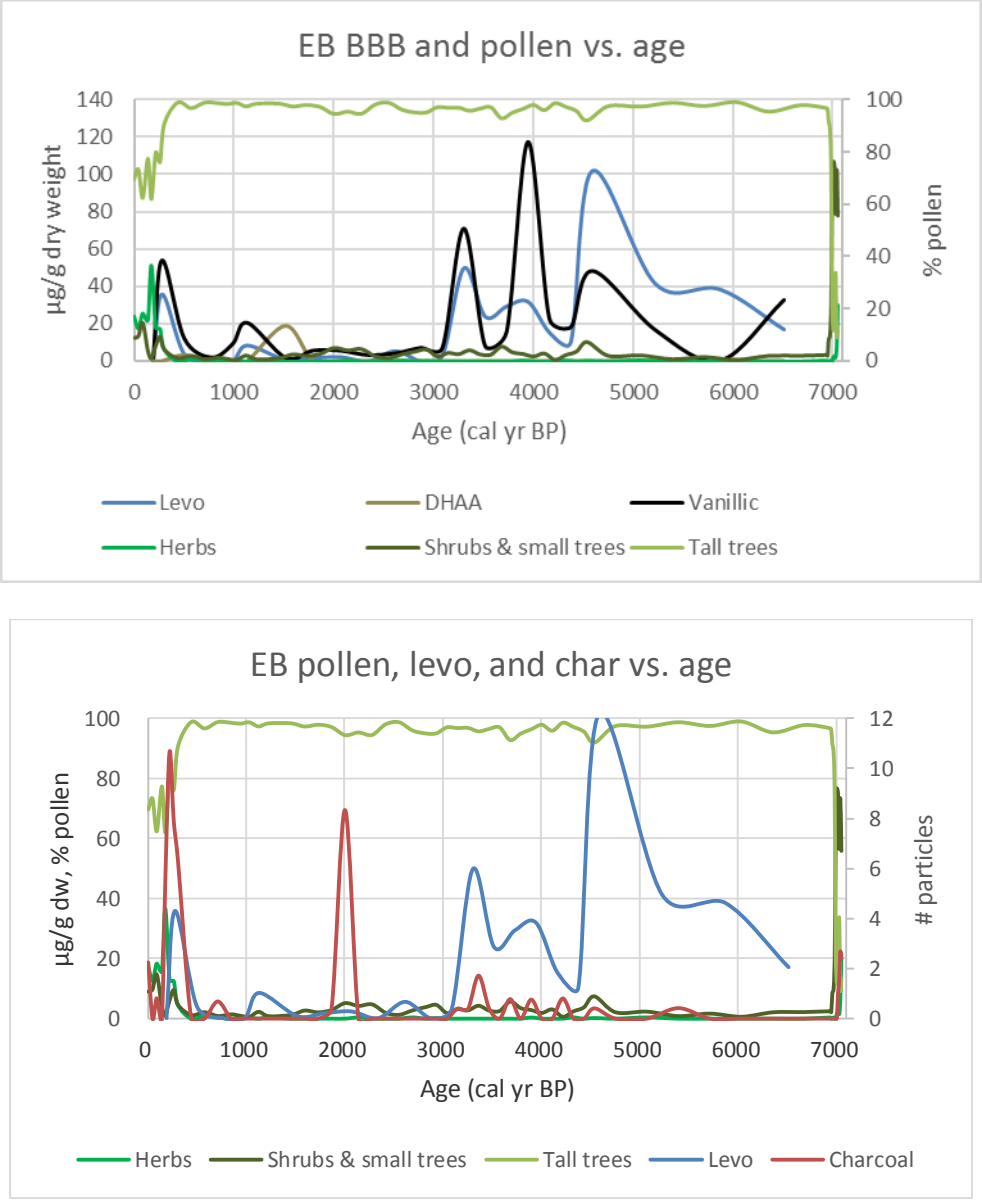

Figure 4-5: Eweburn Bog pollen ratios to age contrasted against all three major biomass burning markers (top), and against levoglucosan and charcoal (bottom). The omitted point in the bottom graph is 101.63 µg/g levoglucosan at 4.5ka. BBM abundances indicate which plants burned, while charcoal vs. levoglucosan amounts indicate heat and aridity of fires.

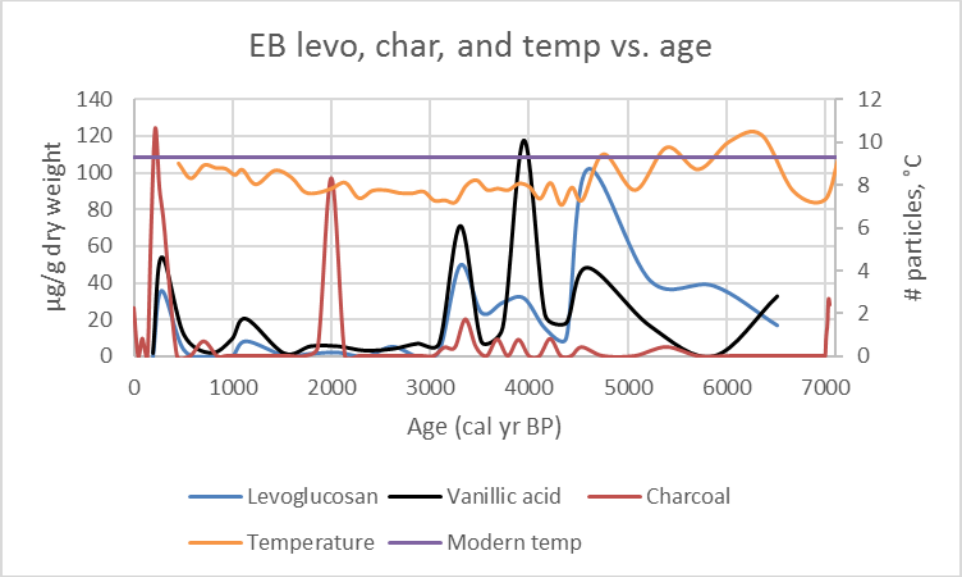

Figure 4-6: Eweburn Bog levoglucosan, charcoal, mean annual temperature, and modern temperature plotted against age in the core. There is a trend of decreasing wetness towards the modern.

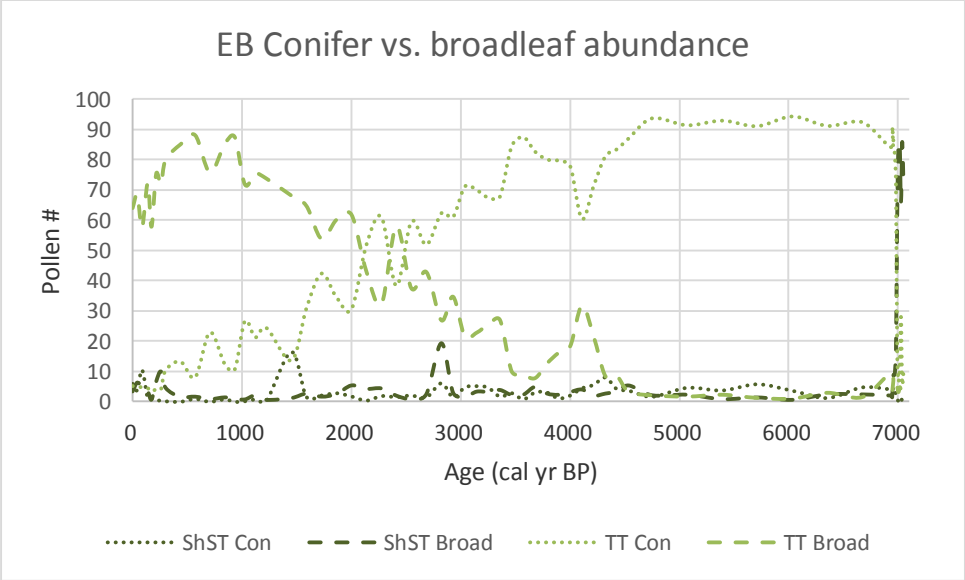

Figure 4-7: EB abundances of TT and ShST conifer and broadleaf species. The switchover from conifer to broadleaf tall trees occurs without a significant drop in overall tall tree abundance.

~4ka would have favored the angiosperms over the conifers, a trend which continued uninterrupted until the late Holocene.

4.3.2 Late Holocene (3.0-0.2ka)

The presence of all BBM at much lower levels throughout the past 3ky (Figure 4-5) suggests some fire presence throughout the late Holocene. Charcoal abundance seems to roughly correlate to small spikes in shrub and small tree abundance at 2ka and 3.2-5.3ka. This correlates with the interpretation that shrubs are more likely to grow in conditions that allow for charcoal-hot fires. During this part of the Holocene, reconstructed temperature increased nearly 2°C, from 7-9°C, toward the modern. Generally, burning events in this time period of the core did not correspond with changes in plant abundance on the ecosystem scale, although one small burning event at 1.5ka produced a DHAA spike corresponding to a temporary increase in conifer shrubs. The substantial 20% abundance drop in tall trees and contemporaneous increase in shrubs and grasses at the very top of the core is attributed to European colonization of the area (McWethy et al., 2009). Plant abundances in general resemble the modern analogue.

4.3.3 Te Anau climate

Overall, Te Anau showed three climate modes: drier and warmer but cooling from 6.5-3ka, a period of continually wet warming from 3-2ka, and the continuation of warming with an increase in aridity from 2ka to the modern. This last is evidenced by the return of sporadic BBM and charcoal peaks. The EB temperature record shows a relatively stable transition between early Holocene cooling and late Holocene warming. The proxy of surface moisture from amoeba tests supports the climate interpretation of warm and dry at the bottom of the core to cooler and wetter in the present (Wilmshurst et al., 2002). There

is evidence of burning throughout the EB core, but the Eweburn Bog temperature record does not appear to have been substantially altered by it.

4.4 Climate record of the South Island

The biomass burning record from this study shows evidence of burning in the periods where the temperature records of KB and EB differ the most (Figure 4-8). In addition, there are large changes in the ecosystem composition of KB where its temperature differs from that of Okarito. From this we conclude that temperature reconstructions in the KB record may have measurable bias caused by plant burning. During the time of large grass fires, temperature reconstructions are warmer than Okarito would predict. In contrast, during times when mainly shrubs and tall trees are burning, the temperature reconstructions are cooler than that of Okarito. This is crucial to reconstructing climate patterns in Cass Basin.

The Eweburn Bog record picks up in time at approximately 8.5ka in the early Holocene, which is at the end of the climate optimum (Wilmshurst et al., 2007). The presence of large peaks of BBM with very low levels of charcoal and persistent presence of trees points to a more equally wet and dry cycle, with sufficient interannual dryness to allow understory to burn and wetness to keep the conifer trees alive while smoldering. There was no significant change in plant abundance ratio, suggesting no drastic change in climate.

4.5 Climate of the NZ region

4.5.1 Temperate climate in New Zealand

The regional signature of temperature change is of an overall warming from the last glaciation to the Holocene (Alloway et al., 2007). The sea surface temperature (SST) record

on the Chatham Rise, an area of raised sea floor off the eastern coast of the South Island (Figure 4-9), provides an important reference for the climate of Kettlehole Bog, and the South Island in general. The subpolar and subtropical water masses there are separated by the STF, which did not cross the rise (Stevens and Chiswell, 2013), nor did it migrate off the Rise in the last glaciation (Sikes et al., 2002). The SST of the Chatham Rise was reconstructed using several techniques: faunal assemblages, alkenone ratios, Mg/Ca ratios and Uk37 (Pahnke et al., 2003; Sikes et al., 2002). The alkenones suggest an average temperature difference between the Chatham Rise and Cass Basin of about 6°C. Alkenones have been shown to record summer temperatures (Sikes et al., 2005), whereas pollen records are calibrated to estimate mean annual temperature, so the 3-7°C temperature difference in actual temperature between the two records is not unexpected. However, the magnitude of change being greater in the ocean is somewhat more problematic. SST rose consistently between 17.8-11.6ka, to the early Holocene maximum, and then cooled from 11.6-2ka. The decrease in SST after the optimum was only ~2°C, so the Holocene SST is still 4°C warmer than the glaciation. This overall warming is very similar to Okarito, with the exception that the terrestrial record has more pronounced cooling in the ACR. The terrestrial temperature record from Cass Basin is largely inconsistent with these records through the latter half of the record. Temperature reconstructions in KB have a maximum range of about 3°C, which is inconsistent with the 4 and 6°C change seen in Okarito and SST, respectively. In addition, the temperature essentially does not change in KB from deglaciation to the present (Figures 4-8 and 4-9), in contrast to SST that shows an overall 2°C of warming from deglaciation to present.

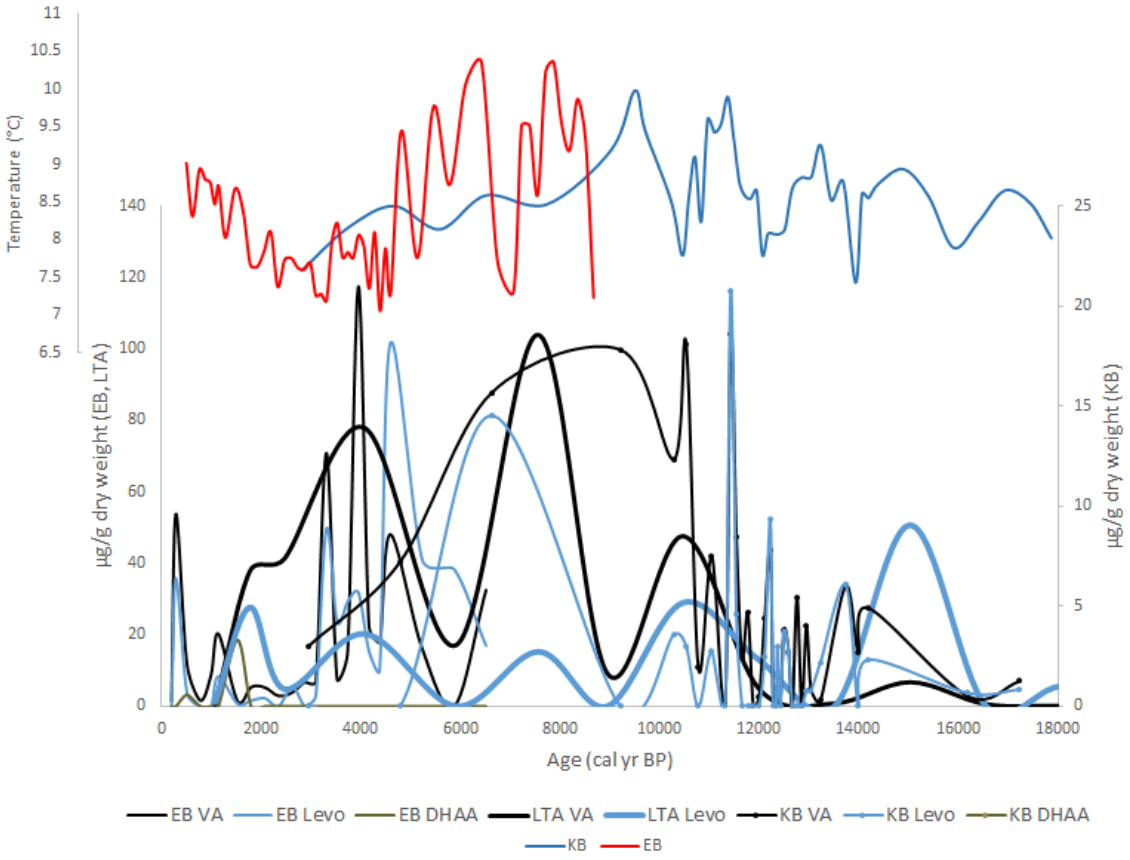

Figure 4-8: KB, EB, and LTA BBM, and MAT from KB and EB, plotted against time.

The discrepancy of the Kettlehole Bog temperature reconstruction from the regional may be explained if the interaction of burning with the ecosystem affected the temperature reconstructed from pollen abundances. Terrestrial plants are governed by aridity, and have been demonstrated to react to burning pressures (Rogers et al., 2013; Westerling et al., 2003). Okarito can be assumed to have been less affected by dryness due to its consistently wet history. In general, reconstructed temperature for KB appears to be biased cooler during times of smoldering burning while trees persisted, and possibly biased to warmer during times when grasses and shrubs dominated and hotter fires occurred. Tall trees proliferated and appear to have burned as temperatures warmed, as evidenced in the regional record (Newnham et al., 2012; Sikes et al., 2005). This pattern may have been

caused by a shift from persistent dryness in the glaciation toward longer periods of increased precipitation with cycles of shorter but regular dry periods. Assuming the climate was mainly wet with periodic dry times, trees grow and burn. Grasses grow and burn under conditions of seasonal or interannual periods of wet and dry, and typical shrub burning seems to occur during either climate regime. From the KB record, it can be tentatively inferred that shorter aridity cycles can lead to inflation in temperature reconstructions using the modern analogue technique, and the factors behind longer aridity cycles can lead to temperature depression (Figure 4-10). Further investigation is required to determine the factors behind this influence.

During the ACR, cooling occurred in both terrestrial records and not the ocean record, while ocean fronts varied very little on this timescale (Sikes et al., 2002). A probable cause of this cooling would be shifting winds, which would have a strong

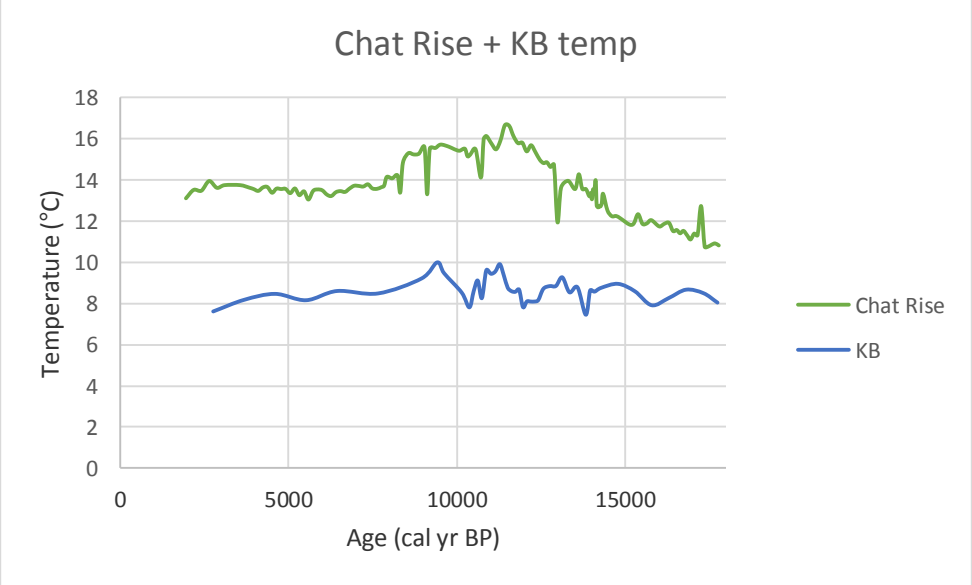

Figure 4-9: Pollen temperature record for KB and alkenone SST for South Chatham Rise. The Chatham Rise record has a 5°C temperature difference, and rises consistently into the Holocene, after which it declines to modern temperatures. The KB record has a smaller temperature difference, and rises and falls erratically.

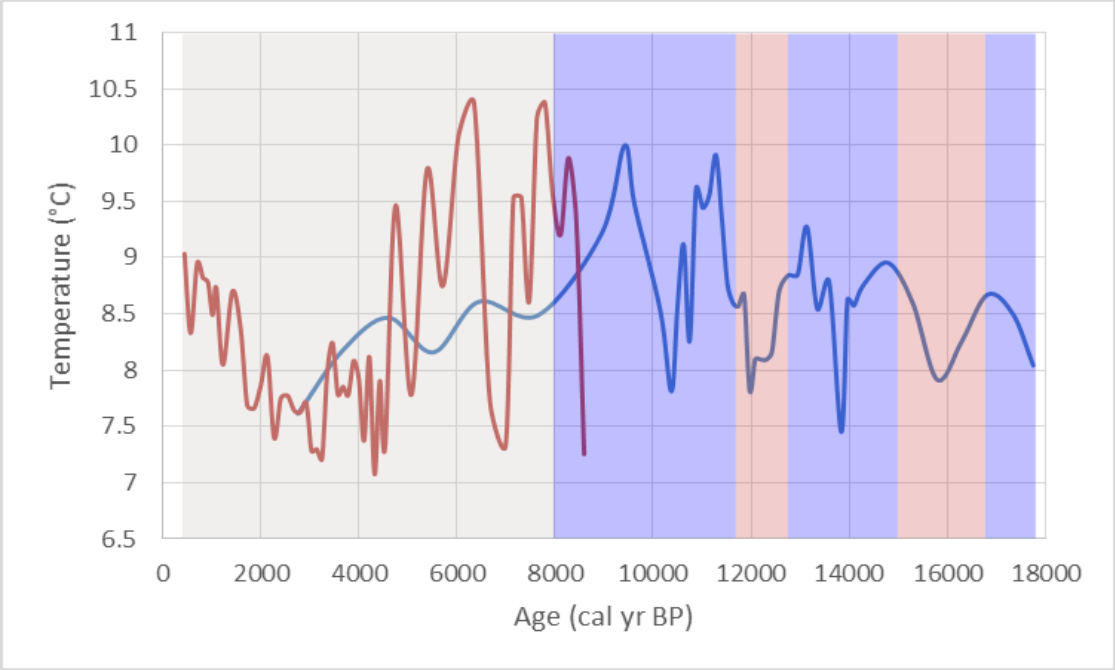

Figure 4-10: KB (blue) and EB (red) temperature overlain with the proposed errors in temperature reconstruction. Blue boxes indicate time periods when the actual temperature is expected to be cooler than the reconstruction shows, and red boxes indicate when the actual temperature is expected to be warmer. The grey box covering most of the Holocene indicates that the reconstruction seems to match actual temperature.

aridity effect on both the survival and burning of land plants. This could be the factor behind climate growing wetter after the glaciation, but still with enough cyclic dryness to provide fuel. There is evidence that wind shifts in the ACR caused glaciers to readvance in the South Island (Putnam et al., 2010) along with general cooling (Vandergoes et al., 2008). Burning patterns from KB suggest that it was also dry during this time.

During the Younger Dryas, KB cooled while regionally other records suggest warming (Alloway et al., 2007; Newnham et al., 2012). At KB the Younger Dryas was also marked by an ecosystem change to tall trees dominating after a temporary increase in conifer shrub abundance. Smoldering burning also increased during the Younger Dryas relative to the ACR, suggesting a shift towards a cycle of more wetness than dryness.

Plausibly, continued burning of underbrush prevented tall conifers from propagating, biasing the reconstruction to colder.

Following the Younger Dryas, regional records warm into the Holocene optimum. Okarito appears to cool by about 1°C, though its Holocene temperature appears to have been about 3°C warmer than the late glaciation. In contrast, KB temperature fell back to glacial levels of 7.5°C, punctuated by 3°C swings to 10°C. This may reflect continuing burning influencing the temperature reconstruction. The BBM record is too coarse to draw any specific conclusions, but the general trend appears to be continued smoldering burning into the mid-Holocene.

After the Holocene optimum, the Eweburn burning record shows the continued presence of BBM from 7-3ka. This implies a shift toward dryer cycles with sufficient periodic wetness to promote the continued burning of understory.

4.5.2 Comparison to North Island records

Onepoto maar in the Auckland area provides another BBM record from the North Island, giving an important comparison to the records in this study from the South Island (Sikes et al., 2013). That site is fully subtropical and has strong seasonality in the rainfall pattern today, with wet winters and dry summers. The temperature has a seasonal range of about 8.5°C (Table 1-1).

Reconstructed temperatures in the Auckland area and both Okarito and KB were similar at the LGM, just under 8°C (Figures 4-4 and 4-11). In the North Island temperatures warmed earlier at approximately 16.6ka and climbed rapidly, while both

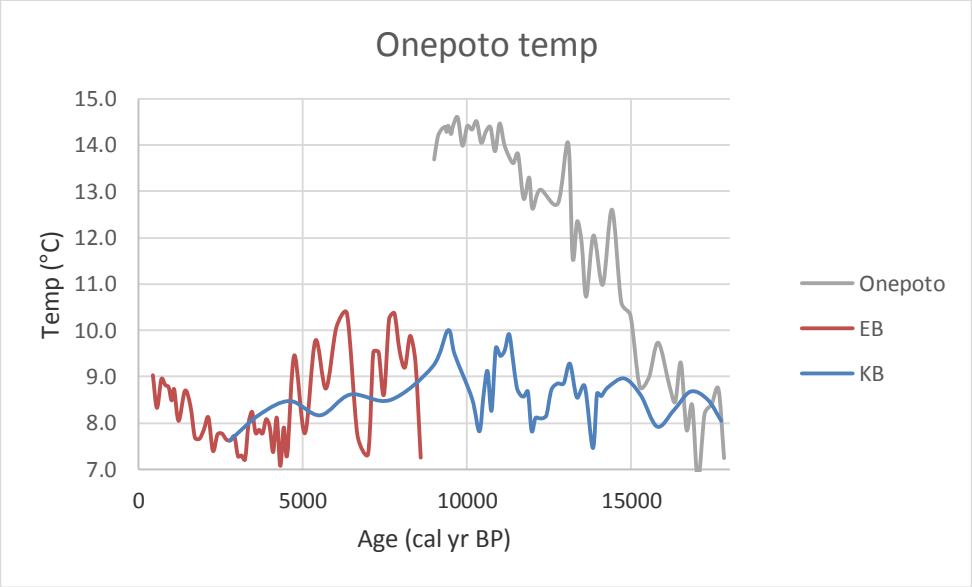

Figure 4-11: Onepoto temperature graphed with EB and KB temperature records. There is a vast temperature difference between the North Island and South Island, likely due to southern westerly wind relaxation.

South Island records Okarito and KB warmed around 1℃, staying near 9℃. At the beginning of the ACR around 14.4ka, Onepoto temperature had warmed to ~12℃. Across the ACR all three bog temperature records cooled ~1℃, with perhaps greater cooling in the South Island records.

Following the ACR and through the Younger Dryas, Onepoto and Okarito warmed, with the North Island warming by 4℃, twice the ~2℃ warming that the South Island experienced during that time. KB temperatures cooled and fluctuated through this period, which may have been due to KB returning to drier conditions more similar to the glaciation than to the ACR. A shift in global wind patterns towards the north, but not to the northern extent at which these patterns lie in the Holocene, may have caused this. This is supported by the differences in the temperature records of Onepoto and Okarito, and the North Island experiencing more warming after the ACR than the South Island.

After the Younger Dryas, North Island temperatures plateaued, whereas Okarito cooled by ~1°C. The KB record warms and also fluctuates, suggesting that increased and fluctuating moisture leading to burning may have continued to bias the reconstruction.

Overall, the South Island experienced less warming than the North Island, with the South Island sites showing greater responses to the millennial climatic events of the ACR and Younger Dryas. This suggests that the drivers of these events were more high-latitude in their forcing, and the biomass burning markers from Onepoto can shed light on this (Figure 4-12). The patterns of climate events there are distinct from the KB record. Onepoto had greater grass and charcoal counts in the LGM (Figure 4-13), implying dryness. The other BBM were present and remained in high quantities from the LGM and HS1 dryness signal (Sikes et al., 2013). This is consistent with previous studies of New

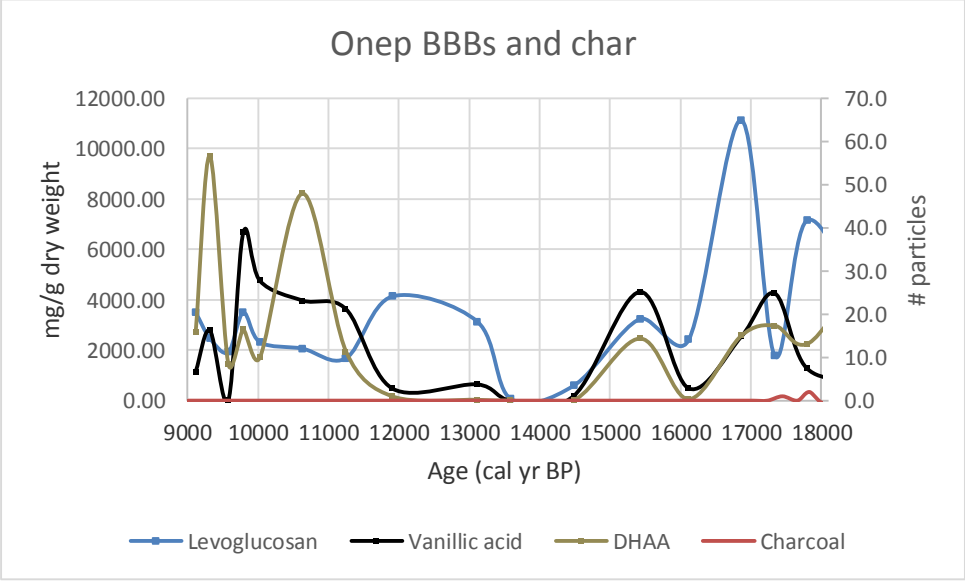

Figure 4-12: Biomarker records for Onepoto maar, including charcoal. The most levoglucosan occurs at the onset of heightened temperature rise.

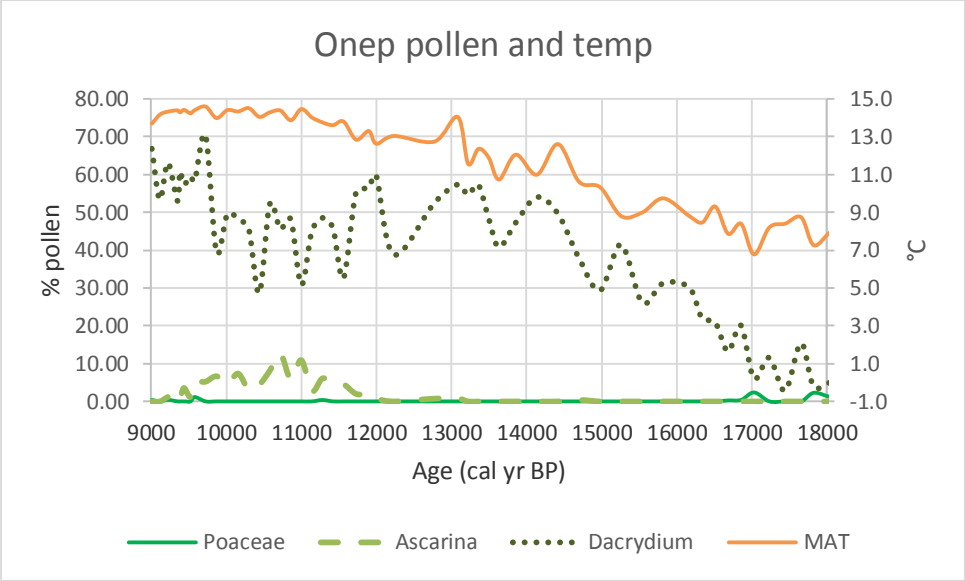

Figure 4-13: Onepoto pollen and temperature records. Dacrydium = tall tree (conifer), Ascarina = shrub (broadleaf), and Poaceae = grass species that are the dominant species of their type in the region. Tall trees increase with increasing temperature, until they dip in abundance around 12ka in favor of shrubs.

Zealand seasonality changes using $\delta^{13}C$ of plant leaf waxes that suggest wetting springs with summers remaining dry in Onepoto during this time (Sikes et al., 2013). Due to the similar location and climate of the South Island, however, it can be assumed that its seasonality likely varied in a similar way to the North Island.

In the Onepoto core, BBM showed rapid wetting from the glaciation of first springs and then summers into the ACR. The ACR was very wet and cool in the Auckland area. This is in contrast to the Cass Basin, which was cooler but also moderately dry, consistent with wind fronts moving south in the early deglaciation. After the ACR, BBM in Auckland returned, suggesting a return to seasonal or cyclical dryness through the Younger Dryas and Holocene (Sikes et al., 2013), with enough periods of wetting to produce smoldering

fires. Relatively wet springs and moderately dry summers could have produced this pattern (Sikes et al., 2013). This contrasts with the aridity implied in KB through the deglaciation.

Around the LGM was the time that grasses were at their highest abundance in Onepoto, so it is likely that grasses typically produced the most charcoal, as in KB. *Dacrydium* conifer pollen ratios seem to decrease at times of high DHAA in the core, which likely means that the shrubs that took over while the trees were decreasing were at least partly conifers.

4.5.3 Winds

The oceanic fronts surrounding New Zealand move very little on glacial scales, leaving shifts in air masses to control the subtleties of climate. At the beginning of the deglaciation, a northward shift occurred in global atmospheric fronts such as the ITCZ, as well as a relaxation of the southern westerly winds that typically contribute to cooling and drying of New Zealand climate (Lamy et al., 2010). Temperature (Figure 4-14) and overall climate (Tables 4-1 and 4-2) trends for KB and EB were likely affected by these shifts.

The southern westerly wind (SWW) belt is comprised of a band of cold, dry air with a consistently wet northern edge (Lamy et al., 2010). It can be inferred that the northern edge would be responsible for causing climatic cycles high in precipitation for the area below it, either periods of longer wetness and shorter dryness, or periods with a higher volume of precipitation. The band of dry air to the south would correspondingly cause cyclical dryness with low or infrequent periods of precipitation.

These influences of the SWW are reflected in the North Island records at Onepoto by the initial cool and dry conditions at the LGM followed by rapid warming and increasing

spring wetness and summer dryness. In the South Island, conditions began only slightly colder but persistently drier than in the north. The drop in charcoal and abundance of BBM indicate that conditions then switched to wetter cycles and less dryness, but not much warmer. It is likely that spring in particular was wetter, by analogy to the US and North Island studies (Sikes et al., 2013; Westerling et al., 2003). The increasing wetness and warming in the North Island at the same time as the South Island showed slightly increased wetness without warming may have both resulted from the presence of the northern edge of the westerly wind belt moving southward (Lamy et al., 2010). After sitting over the North Island in the glaciation, it is plausible that the SWW's northern edge moved into the vicinity of Kettlehole Bog between the deglaciation and the ACR.

During the ACR, the winds likely moved north again. Onepoto showed cooling and a marked reduction of all BBM indicating wetting during the ACR (Sikes et al., 2013). This implies the return of cool, persistently wet conditions to Onepoto as the northern rain front moved north again over the North Island (Sikes et al., 2013). The expanding of glacial moraines in New Zealand during this time corroborates this interpretation (Putnam et al., 2010). The South Island records showed a climatic shift toward cooler temperatures and a drier cycle with multiannual wetness, evidenced by a major ecosystem change to shrub dominance and a much sharper temperature swing. This is consistent with the SWW moving northward away from the KB region during the ACR.

After the ACR, North Island summers became more arid, with springs remaining relatively wet (Sikes et al., 2013). Reconstructed temperature continued to rise until its plateau at 11.5ka. Kettlehole Bog's climate appears to have shifted to shorter cycles of increased wetness and dryness, and experienced a temporary dip in temperature but

warmed overall. This suggests that either the SWW moved slightly south during this time, just enough to affect both locations; or the wind belt may have moved more south over Kettlehole Bog, reducing the cooling, drying effect of the southern portion of the wind belt, and a different wind pattern is responsible for climate effects in the North Island after this point.

After this time, the record continues where EB and KB overlap. Both cores begin warm at the end of the optimum and cool toward the late Holocene. KB experiences a shift toward persistent wetness from 4.8ka to the top of the record at 2.9ka, and EB echoes this with wetting of its own from the bottom to the top of the core. This supports a southward trend in the SWW, bringing first cold conditions followed by wetness to both locations.

Overall, shifts in the cyclicity of aridity vs. precipitation in New Zealand since the glaciation may be attributable to north-south fluctuations in the SWW. In general, the SWW moved southward from the deglaciation to the Holocene, with one potential northward shift during the ACR. The proposed position of the border between the wet northern edge and the dry southern winds as between Auckland and Cass Basin may explain the locations' varying reactions to various deglacial millennial events.

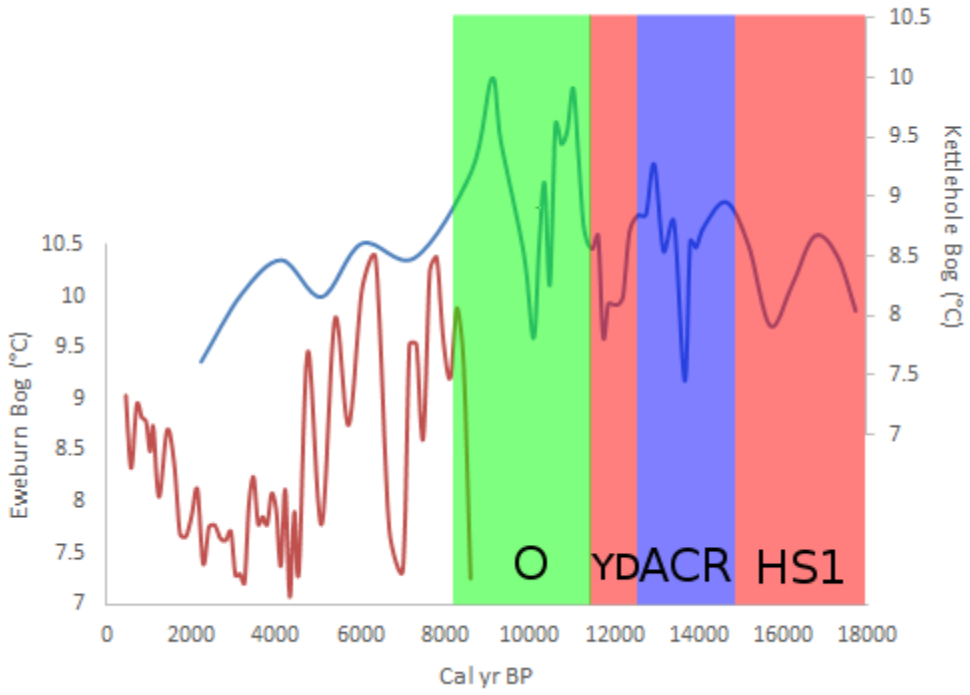

Figure 4-14: KB and EB core temperatures, related to millennial deglacial events.

KB	Holocene	Optimum	YD	ACR	(ED) Early deglaciation	(EG) End of glaciation
Age (ka)	2.7-8	8-11.7	11.7-12.7	12.7-14.7	14.7-16.8	16.8-17.7
Charcoal	0	0	0	+	++	+
Levoglucosan	+++	+++	++	++	+	0
Vanillic acid	+++	+++	++	+	+	0
Reconstructed temperature (°C)	7.6-8.5	7.8-10.0	7.8-8.5	7.5-9.5	8.0-9.0	8.0
Actual temperature	Same	Cooler	Warmer	Cooler	Warmer	Cooler
Pollen	TT>>ShST>G	TT>>ShST>G	Transition from ShST>H>TT to TT>>ShST>G	ShST>G>TT	TT>ShST>G	ShST>G>TT
Interpretation	Optimum-like first, shading into cool, persistent wet/mild dry	YD-like first, sharp switch to warm, decadal cycles of equal strong dry/ strong wet	ACR-like first, sharp switch to warm, decadal cycles of moderate wet/ moderate dry	ED-like first, shading into cool, multiannual cycles of persistent dry/mild wet	Cool, decadal cycles of middling wet/ intermittent dry	Cool, annual cycles of persistent dry/mild wet

Table 4-1: Summary of KB biomarkers, ecology, and temperature into an overall climate interpretation. TT = tall trees, ShST = shrubs and small trees, G = grasses. 0 = none, + = small amounts, ++ = moderate amounts, +++ = large amounts. "Levoglucosan" refers to all three stereoisomers. The interpretation tab lists the major mode of precipitation first (wet, dry) followed by the deviation (dry, wet) that likely leads to the observed climate signal.

EB	Late Holocene	Early Holocene
Age (ka)	0.2-3	3-8
Charcoal	0	+
Levoglucosan	+	+++
Vanillic acid	+	+++
Reconstructed temperature (°C)	7.3-9.0	7.0-10.3
Actual temperature	Same	Same
Pollen	TT>>ShST>G	Start ShST>>G>TT, then TT>>ShST>G
Interpretation	Cool, cycles of persistent wet/mild dry	Warm, Optimum-like cycles of equal strong wet/strong dry within cycles of wet/half-dry

Table 4-2: Summary of EB biomarkers, ecology, and temperature into an overall climate interpretation. TT = tall trees, ShST = shrubs and small trees, G = grasses. 0 = none, + = small amounts, ++ = moderate amounts, +++ = large amounts. "Levoglucosan" refers to all three stereoisomers.

V. CONCLUSIONS

The climatic history of New Zealand since the LGM indicates that temperature and aridity have been affected by both wind variability and ocean stability. The deglacial records of temperature in the South Island show a smaller change in temperature than the North Island (Sikes et al., 2013; Wilmshurst et al., 2007). Records from the present study suggest that in areas with significant aridity, changes in South Island temperature reconstructions may have been affected by aridity as represented by burning events. Our analysis of biomass burning markers indicate times where reconstructed temperatures do not match regional trends, which may indicate where smoldering fires may have affected ecosystems and, by extension, temperature reconstructions. Taking burning to be correlated to moisture patterns, climate in the South Island went from cooler and drier in the LGM through a period of overall moderate warming and wetting. This thesis comes to the following specific conclusions:

- Biomass burning biomarkers levoglucosan, mannosan, galactosan, DHAA, and vanillic acid provide a record of burning that is distinct from the record of charcoal. They provide a new record of lower-temperature burning in deglacial and Holocene South Island, New Zealand. Smoldering fires (BBM's) tended to have an inverse relationship to hot fires (charcoal). These cooler fires were prevalent in the Younger Dryas and ACR in the Cass Basin region, and in the mid-late Holocene in the Te Anau region.

- The temperature reconstructions created from pollen assemblages in these cores were affected by this burning. The temperatures reconstructed in the KB core differ from the regional temperature patterns with fire biasing temperature to cooler in the

early deglaciation and Younger Dryas, and toward high variability during the ACR and climate optimum.

- BBM as proxies of aridity can be used to qualitatively assess climatic aridity. Additionally, in combination with ecosystem changes, they may be able to discern changing patterns of moisture delivery.

- The patterns in this record suggest that the early deglaciation was persistently dry but characterized by interseasonal/interannual wetness, leading to longer cycles of increased wetness with distinct dry periods in the early deglaciation. The cycles shifted drier and shorter from the Younger Dryas to the early Holocene, and then to persistent wetting again towards the modern.

- The North and South Islands appeared to have similar temperatures at the end of the glaciation. The North Island warmed rapidly and considerably, whereas it appears that the South Island warmed less but trended to wetter conditions and more variable cyclicity in the delivery of that moisture.

- The climate record constructed by the BBM in this thesis suggest north-south variability of moisture delivery, which is interpreted as variability of the southern westerly winds. A southward motion at the end of the glaciation brought subtropical conditions to the North Island, with continued cooler dry conditions in the South Island. The wind belt shifted north in the ACR and then south from the Younger Dryas to the Holocene, bringing alternating periods of wet and dry summers to the South Island.

VI. REFERENCES

Abas, M., Simoneit, B.R.T., Elias, V.O., Cabral, J.A. and Cardoso, J.N. (1995) Composition of higher molecular weight organic matter in smoke aerosol from biomass combustion in Amazonia. Chemosphere 30, 995-1015.

Alloway, B.V., Lowe, D.J., Barrell, D.J.A., Newnham, R.M., Almond, P.C., Augustinas, P.C., Bertler, N.A.N., Carter, L., Litchfield, N.J., McGlone, M.S., Schulmeister, J., Vandergoes, M.J., Williams, P.W. and NZ-INTIMATE (2007) Towards a climate event stratigraphy for New Zealand over the past 30 000 years (NZ-INTIMATE project). Journal of Quaternary Science 22, 9-35.

Augustinus, P.C., Cochran, U., Kattel, G., D'Costa, D. and Shane, P. (2011) Late Quaternary paleolimnology of Onepoto maar, Auckland, New Zealand: Implications for the drivers of regional paleoclimate. , doi:10.1016/j.quaint.2011.02.028. Quaternary International, doi:10.1016/j.quaint.2011.1002.1028.

Bartlein, P.J., Anderson, K.H., Anderson, P.M., Edwards, M.E., Mock, C.J., Thompson, R.S., Webb, R.S., Webb, T. and Whitlock, C. (1998) Paleoclimate simulations for North America over the past 21,000 years: features of the simulated climate and comparisons with paleoenvironmental data Quaternary Science Reviews 17, 549-585.

Belkin, I.M. and Gordon, A.L. (1996) Southern Ocean fronts from the Greenwich meridian to Tasmania. Journal of Geophysical Research 101, 3675-3696.

Bi, X., Simoneit, B.R.T., Sheng, G., Ma, S. and Fu, J. (2008) Composition and major sources of organic compounds in urban aerosols. Atmospheric Research 88, 256-265.

Blunier, T., Schwander, J., Stauffer, B., Stocker, T., Dallenbach, A., Indermuhle, A., Tschumi, J., Chappellaz, J., Raynaud, D. and Barnola, J.-M. (1997) Timing of the Antarctic cold reversal with respect to the Younger Dryas event. Geophysical Research Letters 24, 2683-2686.

Broecker, W.S. (1998) Paleocean circulation during the last deglaciation: A biopolar seesaw? Paleoceanography 13, 119-121.

Burrows, C.J. (1983) Radiocarbon dates from Late Quaternary deposits in the Cass District, Canterbury, New Zealand. New Zealand Journal of Botany 21, 443-454.

Clark, R.L. (1982) Point count estimation of charcoal in pollen preparations and thin sections of sediments. Pollen et Spores 25, 523-535.

Coomes, D.A., Allen, R.B., Bentley, W.A., Burrows, L.E., Canham, C.D., Fagan, L., Forsyth, D.M., Gaxiola-Alcantar, A., Parfitt, R.L., Ruscoe, W.A., Wardle, D.A., Wilson, D.J. and Wright, E.F. (2005) The hare, the tortoise and the crocodile: the ecology of angiosperm dominance, conifer persistence and fern filtering. Journal of Ecology 93, 918-935.

Denton, G.H., Anderson, R.F., Toggweiler, J.R., Edwards, R.L., Schaefer, J.M. and Putnam, A.E. (2010) The Last Glacial Termination. Science 328, 1652-1656.

Denton, G.H. and Hendy, C.H. (1994) Younger Dryas age advance of Franz Josef Glacier in the Southern Alps of New Zealand. Science 264, 1434-1437.

Elias, V.O., Simoneit, B.R.T., Cordeiro, R.C. and Turcq, B. (2001) Evaluating levoglucosan as an indicator of biomass burning in Carajás, Amazônia: A comparison to the charcoal record. Geochim. Cosmochim. Acta 65, 267–272.

Grimshaw, J. (1976) Depsides, hydrolysable tannins, lignans, lignin and humic acid., in: Coffey, S. (Ed.), Rodd's Chemistry

of Carbon Compounds, 2nd ed. Elsevier, Amsterdam, pp. 203-278.

Hajdas, I., Lowe, D.J., Newnham, R.M. and Bonani, B. (2006) Timing of the late-glacial climate reversal in the Southern Hemisphere using high-resolution radiocarbon chronology for Kaipo bog, New Zealand. Quaternary Research 65, 340-345.

Hellstrom, J.C. and McCulloch, M.T. (2000) Multi-proxy constraints on the climatic significance of trace element records from a New Zealand speleothem. Earth and Planetary Science Letters 179, 287-297.

Kaplan, M.R., Schaefer, J.M., Denton, G.H., Barrell, D.J.A., Chinn, T.J.H., Putnam, A.E., Andersen, B.G., Finkel, R.C., Schwartz, R. and Doughty, A.M. (2010) Glacier retreat in New Zealand during the Younger Dryas stadial. Nature 467, 194-197.

Kohfeld, K.E., Graham, R.M., Boer, A.M.d., Sime, L.C., Wolff, E.W., Quéré, C.L. and Bopp, L. (2013) Southern Hemisphere westerly wind changes during the Last Glacial Maximum: paleo-data synthesis. Quaternary Science Reviews 68, 76-95.

Kuo, L.-J., Herbert, B.E. and Louchouarn, P. (2008) Can levoglucosan be used to characterize and quantify char/charcoal black carbon in environmental media? Organic Geochemistry 39, 1466–1478.

Lamy, F., Kaiser, J., Arz, H.W., Hebbeln, D., Ninnemann, U., Timm, O., A.Timmermann and Toggweiler, J.R. (2007) Modulation of the bipolar seesaw in the Southeast Pacific during Termination 1. Earth and Planetary Science Letters 259, 400-413.

Lamy, F., Kilian, R., Arz, H.W., Francois, J.-P., Kaiser, J., Prange, M. and T.Steinke (2010) Holocene changes in the position and intensity of the southern westerly wind belt. Nature Geosci 3, 695-699.

Lee, S.Y., Chiang, J.C.H., Matsumoto, K. and Tokos, K.S. (2011) Southern Ocean wind response to North Atlantic cooling and the rise in atmospheric CO_2: Modeling perspective and paleoceanographic implications. Paleoceanography 26, PA1214, doi:1210.1029/2010PA002004.

Lobert, J.M. and Warnatz, J. (1993) Emissions from the combustion process in vegetation. Fire in the Environment 13, 15-37.

Lowe, D.J. and Newnham, R.M. (1999) Advances in Quaternary tephrostratigraphy and tephrachronology in New Zealand. Quaternary Australasia 17, 12-19.

McGlone, M.S., Turney, C.S.M., M.Wilmshurst, J., Renwick, J. and Pahnke, K. (2010) Divergent trends in land and ocean temperature in the Southern Ocean over the past 18,000 years. Nature Geoscience 3, 622-626.

McGlone, M.S., Turney, C.S.M. and Wilmshurst, J.M. (2004) Lateglacial and Holocene vegetation and climatic history of the Cass Basin, central South Island, New Zealand. Quaternary Research 62, 267–279.

McWethy, D.B., Whitlock, C., Wilmshurst, J.M., McGlone, M.S. and Li, X. (2009) Rapid deforestation of South Island, New Zealand, by early Polynesian fires. The Holocene 19, 883-897.

Medeiros, P.M., Sikes, E.L., Thomas, B. and Freeman, K.H. (2012) Flow discharge influences on input and transport of particulate and sedimentary organic carbon along a small temperate river Geochim. Cosmochim. Acta 77, 317-334.

Medeiros, P.M. and Simoneit, B.R.T. (2008) Multi-biomarker characterization of sedimentary organic carbon in small rivers draining the northwestern United States. Organic Geochemistry 39, 52-74.

Meyers, P.A. (1997) Organic geochemical proxies of paleoceanographic, paleolimnologic, and paleoclimatic processes. Organic Geochemistry 27, 213-250.

Moar, N.T. (1971) Contributions to the quaternary history of the New Zealand flora: 6. Aranuian pollen diagrams from Canterbury, Nelson, and North Westland, South Island. New Zealand Journal of Botany 9, 80-145.

Newnham, R., Vandergoes, M.J., Hendy, C., Lowe, D.J. and Preusser, F. (2007) A terrestrial palynological record for the last two glacial cycles from southwestern New Zealand. Quaternary Science Reviews 26, 517-535.

Newnham, R.M. and Lowe, D.J. (2000) Fine resolution pollen record of late glacial climate reversal from New Zealand. Geology 28, 759-762.

Newnham, R.M., Vandergoes, M.J., Sikes, E., Carter, L., Wilmshurst, J.M., Lowe, D.J., McGlone, M.S. and Sandiford, A. (2012) Does the bipolar seesaw extend to the terrestrial southern mid-latitudes? Quaternary Science Reviews 36, 214–222.

NIWA (2013) Overview of New Zealand Climate, http://www.niwa.co.nz/education-and-training/schools/resources/climate/overview.

Oros, D.R. and Simoneit, B.R.T. (2001) Identification and emission factors of molecular tracers in organic aerosols from biomass burning. Part 1. Temperate climate conifers. Applied Geochemistry 16, 1513-1544.

Pahnke, K., Zahn, R., Elderfield, H. and Schulz, M. (2003) 340,000-Year Centennial-Scale Marine Record of Southern Hemisphere Climatic Oscillation. Science 301, 948-952.

Putnam, A.E., Denton, G.H., Schaefer, J.M., Barrell, D.J.A., Andersen, B.G., Finkel, R.C., Schwartz, R., Doughty, A.M., Kaplan, M.R. and Schlüchter, C. (2010) Glacier advance in southern middle-latitudes during the Antarctic Cold Reversal. Nature Geoscience 3, 700-704.

Rogers, B.M., Randerson, J.T. and Bonan, G.B. (2013) High-latitude cooling associated with landscape changes from North American boreal forest fires. . Biogeosciences 10, 699-718.

Rogers, B.M., Soja, A.J., Goulden, M.L. and Randerson, J.T. (2015) Influence of tree species on continental differences in boreal fires and climate feedbacks. Nature Geoscience 8, 228-234.

Saiz-Jimenez, C. and Leeuw, J.W.d. (1986) Lignin pyrolysis products: Their structures and their significance as biomarkers. Organic Geochemistry 10, 869-876.

Samson, C.R., Sikes, E.L. and Howard, W.R. (2005) Deglacial paleoceanographic history of the Bay of Plenty, New Zealand. Paleoceanography 20, doi:10.1029/2004PA001088.

Shafizadeh, F. (1984) The chemistry of pyrolysis and combustion. American Chemical Society, Washington, DC, ETATS-UNIS.

Shulmeister, J., Goodwin, I., Renwick, J., Harled, K., Armand, L., McGlone, M.S., Cook, E., Dodsonh, J., Hesse, P.P., Mayewski, P. and Curran, M. (2004) The Southern

Hemisphere westerlies in the Australasian sector over the last glacial cycle: a synthesis. Quaternary International 118-119, 23–53.

Sikes, E.L., Howard, W.R., Neil, H.L. and Volkman, J.K. (2002) Glacial-interglacial sea surface temperature changes across the subtropical front east of New Zealand based on alkenone unsaturation ratios and foraminiferal assemblages. Paleoceanography 17, 10.1029/2001PA000640.

Sikes, E.L., Howard, W.R., Samson, C.R., Mahan, T.S., Robertson, L.G. and Volkman, J.K. (2009a) Southern Ocean seasonal temperature and Subtropical Front movement on the South Tasman Rise in the Late Quaternary. Paleoceanography 24, PA2201, doi:2210.1029/2008PA001659.002009.

Sikes, E.L., Medeiros, P.M., Augustinas, P., Wilmshurst, J. and Freeman, K. (2013) Seasonal variations in aridity and temperature characterize changing climate during the last deglaciation in New Zealand. Quaternary Science Reviews 74, 246-256.

Sikes, E.L., Nodder, S.D., O'Leary, T. and Volkman, J.K. (2005) Alkenone temperature records and biomarker flux at the subtropical front on the Chatham Rise, SW Pacific Ocean. Deep Sea Research I 52, 721-748.

Sikes, E.L., Uhle, M.E., Nodder, S.D. and Howard, M.E. (2009b) Sources of organic matter in a coastal marine environment: Evidence from n-alkanes and their d13C distributions in the Hauraki Gulf, New Zealand. Marine Chemistry 113, 149-163.

Simoneit, B.R.T. (2002) Biomass burning — a review of organic tracers for smoke from incomplete combustion. Applied Geochemistry 17, 129-162.

Simoneit, B.R.T., Schauer, J.J., Nolte, C.G., Oros, D.R., Elias, V.O., Fraser, M.P., Rogge, W.F. and Cass, G.R. (1999) Levoglucosan, a tracer for cellulose in biomass burning and atmospheric particles. Atmospheric Environment 33, 173-182.

Singer, C., Shulmeister, J. and McLea, B. (1998) Evidence against a significant Younger Dryas cooling event in New Zealand. Science 281, 812-814.

Sokolov, S. and Rintoul, S. (2009) Circumpolar structure and distribution of the Antarctic Circumpolar Current fronts: 1. Mean circumpolar paths. Journal of Geophysical Research 114.

Stevens, C. and Chiswell, S. (2013) Ocean currents and tides - Currents, Te Ara - the Encyclopedia of New Zealand.

Stuiver, M., Reimer, P.J. and Reimer, R. (2013) CALIB Radiocarbon Calibration, 7.0.4 ed. Quaternary Isotope Laboratory, University of Washington.

Toggweiler, J.R., Russell, J.L. and Carson, J.R. (2006) Mid-latitude westerlies, atmospheric CO_2, and climate changes during the ice ages. Paleoceanography 21, doi8:10.1029/2005PA001154.

Turney, C.S.M., McGlone, M. and Wilmshurst, J.M. (2003) Asynchronous climate change between New Zealand and the North Atlantic during the last deglaciation. Geology 31, 223-226.

Vandergoes, M.J., Dieffenbacher-Krall, A.C., Newnham, R.M., Denton, G.H. and Blaauw, M. (2008) Cooling and changing seasonality in the Southern Alps, New Zealand during the Antarctic Cold Reversal Quaternary Science Reviews 27, 589-601.

Vandergoes, M.J. and Fitzsimons, S.J. (2003) The Last Glacial–Interglacial Transition (LGIT) in south Westland, New Zealand: paleoecological insight into mid-latitude Southern Hemisphere climate change. Quaternary Science Reviews 22, 1461-1476.

Wards, I. (1976) New Zealand Atlas. A.R. Shearer Government Printer, Wellington, New Zealand, p. 292.

Weaver, P.P.E., Carter, L. and Neil, H.L. (1998) Response of surface water masses and circulation to late Quaternary climate change east of New Zealand. Paleoceanography 13, 70-83.

Westerling, A.L. (2009) Climate Change Impacts on Wildfire, in: Schneider, Mastrandrea, Rosencranz, Kuntz-Duriseti (Eds.), Climate Change Science and Policy. Island Press.

Westerling, A.L., Gershunov, A., Brown, T.J., Cayan, D.R. and Dettinger, M.D. (2003) Climate and Wildfire in the Western United States. Bulletin of the American Meteorological Society 84, 595-604.

Westerling, A.L., Turner, M.G., Smithwick, E.A.H., Romme, W.H. and Ryan, M.G. (2011) Continued warming could transform Greater Yellowstone fire regimes by mid-21st century. PNAS 108, 13165-13170.

Wilmshurst, J., McGlone, M. and Charman, D.J. (2002) Holocene vegetation and climate change in southern New Zealand: linkages between forest composition and quantitative surface moisture reconstructions from an ombrogenous bog. Journal of Quaternary Science 17, 653-666.

Wilmshurst, J.M., McGlone, M.S., Leathwick, J.R. and Newnham, R.M. (2007) A pre-deforestation pollen-climate calibration model for New Zealand and quantitative temperature reconstructions for the past 18 000 years BP. . Journal of Quaternary Science 22, 535-547.

Wilmshurst, J.M., Wiser, S.K. and Charman, D.J. (2003) Reconstructing Holocene Water Tables in New Zealand Using Testate Amoebae: Differential Preservation of Tests and Implications for the Use of Transfer Functions. Holocene 13, 61-72.

VII. APPENDICES

APPENDIX 1: Core sampling list.

Core	Depth (cm)	Age (cal yr BP)	Sed dry weight (g)	Date ASE extracted	Date GCMS run	Levoglucosan (µg/g dw)	Mannosan (µg/g dw)	Galactosan (µg/g dw)	Vanillic acid (µg/g dw)	DHAA (µg/g dw)
EB	45	195	0.138	13-Nov-13	2-Sep-14	0.00	0.00	0.00	1.54	0.00
	65	281	0.3822	12-Sep-12	20-Jan-15	35.78	21.18	47.76	53.85	0.00
	85	505	0.351	12-Sep-12	20-Jan-15	3.82	0.93	0.00	11.85	3.18
	105	774	0.123	13-Nov-13	19-Jun-14	0.00	3.91	4.51	1.62	0.00
	126	989	0.199	9-Sep-13	11-Jul-14	0.00	2.37	5.30	8.90	0.00
	145	1135	0.272	12-Sep-12	22-Jan-15	8.42	3.63	10.83	20.32	0.00
	165	1521	1.848	13-Nov-13	6-Nov-14	0.72	0.86	0.38	1.45	18.59
	185	1796	0.201	9-Sep-13	11-Jul-14	1.65	3.48	1.79	5.40	0.00
	205	2070	0.595	13-Nov-13	29-Aug-14	2.26	4.94	3.53	5.30	0.00
	225	2344	0.188	16-Oct-13	1-Sep-14	0.00	2.53	0.80	2.95	0.00
	245	2618	0.149	13-Nov-13	3-Sep-14	5.45	2.24	0.00	3.87	0.00
	265	2877	0.129	16-Oct-13	3-Sep-14	0.00	1.84	0.00	6.84	0.00
	285	3091	0.216	16-Oct-13	11-Jul-14	3.03	32.92	16.22	6.86	0.00
	305	3306	0.417	12-Sep-12	22-Jan-15	49.69	43.17	72.06	70.91	0.00
	325	3520	0.164	13-Nov-13	18-Feb-14	23.79	7.56	1.68	7.63	0.00
	345	3734	0.149	16-Oct-13	29-Oct-13	29.30	10.60	7.53	15.38	0.00
	365	3948	0.215	13-Nov-13	8-Sep-14	31.82	108.27	81.10	117.51	0.00
	385	4163	0.195	16-Oct-13	31-Oct-14	15.36	27.59	14.74	22.41	0.00
	405	4377	0.242	13-Nov-13	5-Sep-14	10.14	16.28	13.81	17.95	0.00
	425	4591	0.3256	12-Sep-12	6-Feb-15	101.63	29.78	57.03	48.15	0.00
	445	5232	0.361	9-Sep-14	14-Jul-14	41.00	52.65	24.03	16.10	0.00

Core	Depth (cm)	Age (cal yr BP)	Sed dry weight (g)	Date ASE extracted	Date GCMS run	Levoglucosan (µg/g dw)	Mannosan (µg/g dw)	Galactosan (µg/g dw)	Vanillic acid (µg/g dw)	DHAA (µg/g dw)
	465	5872	0.275	6-Dec-13	21-Mar-14	38.39	19.96	9.13	0.00	0.00
	485	6513	0.5971	12-Sep-12	6-Feb-15	16.98	12.98	21.50	32.56	0.00
KB	32	2944	0.828	2-Jan-14	18-Apr-14	0.00	0.00	1.77	3.00	0.00
	52	4785	1.7073	12-Sep-12	10-Feb-15	0.00	0.00	0.00	7.22	0.00
	72	6625	0.575	6-Sep-13	20-Mar-14	14.53	6.82	11.53	15.66	0.00
	92	9210	1.000	12-Sep-12	10-Feb-15	0.00	0.00	0.00	17.82	0.00
	112.5	10279	0.701	6-Sep-13	16-Jul-14	3.57	7.87	5.71	12.34	0.00
	132.5	10533	0.6928	12-Sep-12	16-Feb-15	3.01	9.28	33.49	18.12	6.12
	152.5	10776	0.799	6-Sep-13	17-Jul-14	0.00	0.53	0.26	1.95	0.00
	172.5	11046	0.311	6-Dec-13	24-Feb-14	2.78	10.03	4.58	7.50	0.00
	192.5	11315	1.069	6-Sep-13	17-Jul-14	0.00	0.49	0.37	0.12	0.00
	202.5	11429	0.335	6-Dec-13	20-Mar-14	20.78	25.81	23.64	18.61	0.00
	212.5	11543	0.585	6-Sep-13	18-Jul-14	4.62	7.01	3.89	8.50	0.00
	222.5	11656	0.8504	12-Sep-12	16-Feb-15	0.00	0.00	0.00	2.42	9.13
	232.5	11770	0.456	6-Dec-13	21-Mar-14	0.00	1.81	4.08	4.68	0.00
	242.5	11883	0.484	6-Dec-13	21-Mar-14	0.00	0.00	0.00	0.00	0.00
	252.5	11997	0.534	6-Dec-13	5-Sep-14	0.00	0.00	0.00	0.46	0.00
	262.5	12110	0.760	6-Sep-13	18-Mar-14	2.44	4.31	5.70	4.37	0.00
	272	12218	0.412	2-Jan-14	17-Oct-14	9.37	11.02	17.67	7.81	0.00
	277	12275	0.921	2-Jan-14	5-Sep-14	0.00	0.24	0.70	0.34	0.00
	282	12331	0.624	2-Jan-14	18-Apr-14	0.00	2.38	2.78	0.22	0.00
	285	12366	0.815	2-Jan-14	21-Oct-14	3.02	0.71	0.64	0.97	0.00
	290	12422	1.244	6-Sep-13	21-Jul-14	0.00	0.33	0.51	0.09	0.00
	296	12498	0.476	2-Jan-14	24-Oct-14	3.73	3.03	3.82	3.84	0.00
	301	12592	0.810	2-Jan-14	24-Oct-14	2.73	2.16	3.49	2.73	0.00

Core	Depth (cm)	Age (cal yr BP)	Sed dry weight (g)	Date ASE extracted	Date GCMS run	Levoglucosan (µg/g dw)	Mannosan (µg/g dw)	Galactosan (µg/g dw)	Vanillic acid (µg/g dw)	DHAA (µg/g dw)
	305	12667	0.802	2-Jan-14	18-Apr-14	0.00	3.01	3.27	0.00	0.00
	310	12761	0.948	2-Jan-14	12-Sep-14	0.00	0.71	1.43	5.47	0.00
	315	12855	0.842	7-Jan-14	1-May-14	0.00	2.43	4.92	0.00	0.00
	320	12949	1.8259	12-Sep-12	19-Feb-15	0.75	2.88	7.32	4.00	0.00
	325	13043	0.845	7-Jan-14	1-May-14	0.80	3.69	6.18	0.84	0.00
	335	13231	1.065	7-Jan-14	8-Sep-14	2.21	2.33	3.43	0.30	0.00
	356	13734	0.799	7-Jan-14	2-May-14	6.08	22.40	34.31	6.01	0.00
	366	13990	1.160	7-Jan-14	2-May-14	0.00	2.47	3.17	2.72	0.00
	374	14194	1.299	7-Jan-14	12-Sep-14	2.33	4.78	7.17	4.91	0.00
	394	16194	1.432	7-Jan-14	30-Oct-14	0.67	0.71	0.77	0.51	0.00
	404	17232	1.381	7-Jan-14	30-Oct-14	0.84	0.83	0.99	1.26	0.00
LTA	55	1069	0.349	21-Aug-13	9-Jul-14	1.18	1.18	0.87	0.45	0.00
	65	1768	0.848	1-Jun-15	7-Jun-15	27.71	31.76	18.12	37.84	0.00
	75	2466	0.435	21-Aug-13	3-Oct-14	4.82	12.23	2.37	41.39	0.00
	85	4075	1.218	8-May-15	7-Jun-15	20.31	56.23	33.12	77.90	0.00
	95	5912	0.438	21-Aug-13	2-Oct-14	0.00	6.45	2.39	17.14	0.00
	104	7565	1.617	8-May-15	8-Jun-15	15.30	87.04	65.34	103.97	0.00
	112.5	8952	0.219	21-Aug-13	8-Oct-14	0.00	0.00	0.00	9.15	0.00
	122.5	10472	1.073	8-May-15	8-Jun-15	29.03	131.16	56.36	47.64	0.00
	132.5	11992	0.807	8-May-15	8-Jun-15	13.05	10.22	5.32	4.96	0.00
	142.5	13512	0.373	21-Aug-13	8-Oct-14	0.00	1.98	1.45	0.85	0.00
	152.5	15032	0.899	8-May-15	8-Jun-15	50.72	217.43	208.56	6.76	0.00
	162.5	16552	0.522	21-Aug-13	9-Oct-14	0.15	1.55	1.53	0.63	0.00
	172.5	18072	3.269	8-May-15	9-Jun-15	5.62	23.91	18.28	0.18	0.00
	182.5	19592	1.947	21-Aug-13	8-Jul-14	0.00	0.56	0.58	0.00	0.00

Core	Depth (cm)	Age (cal yr BP)	Sed dry weight (g)	Date ASE extracted	Date GCMS run	Levoglucosan (µg/g dw)	Mannosan (µg/g dw)	Galactosan (µg/g dw)	Vanillic acid (µg/g dw)	DHAA (µg/g dw)
	192.5	21112	5.401	8-May-15	9-Jun-15	5.99	43.23	66.29	0.25	0.00
	199	22100	2.811	21-Aug-13	8-Jul-14	0.00	0.22	0.33	0.02	0.00

APPENDIX 2: Supporting mean annual temperature data. Ages were calculated in this thesis, but depths and temperatures reported in this thesis are previously published (Pahnke et al., 2003; Sikes et al., 2002; Sikes et al., 2013; Wilmshurst et al., 2003) except for Eweburn Bog MAT (Wilmshurst, unpublished data).

Depth (EB)	Age	MAT (°C)	Depth (KB)	Age	MAT (°C)	Depth (Onepoto)	Age	MAT (°C)	Depth (C. Rise)	Age	MAT
80	449	9.03	30	2760	7.61	1	9009	13.7	22.5	1950	13.11
90	572	8.33	40	3680	8.18	6	9116	14.2	24.5	2180	13.52
100	707	8.95	50	4601	8.47	11	9223	14.3	26.5	2410	13.48
110	825	8.82	60	5521	8.16	16	9352	14.4	28.5	2640	13.95
120	928	8.78	70	6441	8.61	18.5	9384	14.3	30.5	2870	13.62
130	1020	8.49	80	7659	8.49	21	9437	14.4	32.5	3100	13.75
140	1097	8.73	90	8952	9.21	23.5	9523	14.2	36.5	3560	13.75
150	1232	8.05	96	9419	10.00	26	9581	14.4	40.5	3830	13.63
160	1425	8.70	100	9627	9.46	28.5	9725	14.6	42.5	3960	13.56
170	1590	8.38	110	10149	8.53	31	9870	14.0	44.5	4100	13.47
180	1727	7.69	120	10374	7.81	33.5	10015	14.4	46.5	4240	13.64
190	1865	7.66	130	10501	8.58	36	10159	14.3	48.5	4370	13.66
200	2002	7.86	140	10624	9.12	38.5	10301	14.5	50.5	4510	13.38
210	2139	8.12	150	10746	8.26	41	10441	14.0	52.5	4640	13.58
220	2276	7.40	160	10877	9.61	43.5	10581	14.3	54.5	4780	13.56
230	2413	7.75	170	11012	9.44	46	10721	14.4	56.5	4910	13.57
240	2550	7.77	180	11147	9.56	48.5	10861	13.9	58.5	5050	13.36
250	2683	7.64	190	11281	9.91	51	11002	14.5	60.5	5190	13.59
260	2812	7.63	200	11401	9.35	53.5	11142	14.0	62.5	5320	13.26
270	2931	7.71	210	11515	8.77	56	11282	13.8	64.5	5460	13.45

Depth (EB)	Age	MAT (°C)	Depth (KB)	Age	MAT (°C)	Depth (Onepoto)	Age	MAT (°C)	Depth (C. Rise)	Age	MAT
280	3038	7.28	220	11628	8.60	58.5	11422	13.6	66.5	5590	13.05
290	3145	7.30	230	11742	8.57	61	11562	13.8	68.5	5730	13.47
300	3252	7.21	240	11855	8.67	63.5	11730	12.8	70.5	5860	13.54
310	3360	7.99	250	11969	7.82	66	11898	13.3	72.5	6000	13.50
320	3467	8.24	260	12082	8.10	67.5	11999	12.6	74.5	6140	13.29
330	3574	7.78	270	12195	8.10	71	12235	13.0	76.5	6270	13.22
340	3681	7.85	280	12309	8.09	79	12773	12.7	78.5	6410	13.41
350	3788	7.78	290	12422	8.16	84	13085	14.0	80.5	6540	13.46
360	3895	8.08	300	12573	8.71	86.5	13222	11.6	82.5	6680	13.42
370	4002	7.93	310	12761	8.84	89	13359	12.4	84.5	6810	13.58
380	4109	7.37	320	12949	8.85	91.5	13497	11.9	86.5	6950	13.72
390	4217	8.12	330	13137	9.27	94	13634	10.7	88.5	7090	13.71
400	4324	7.07	340	13351	8.54	96.5	13858	12.0	90.5	7220	13.68
410	4431	7.90	350	13590	8.79	99	14138	11.0	92.5	7360	13.79
420	4538	7.32	360	13836	7.45	101.5	14419	12.6	94.5	7490	13.59
430	4751	9.46	365	13964	8.63	104	14700	10.6	96.5	7630	13.57
440	5072	7.78	370	14092	8.57	106.5	14981	10.3	98.5	7760	13.65
450	5392	9.78	375	14294	8.76	109	15262	8.8	100.5	7840	13.72
460	5712	8.75	380	14794	8.95	111.5	15543	9.0	102.5	7920	14.15
470	6032	10.08	385	15294	8.59	114	15824	9.7	106.5	8080	14.08
480	6353	10.37	390	15794	7.91	119	16169	8.8	110.5	8240	14.22
490	6673	7.73	395	16298	8.26	121.5	16342	8.5	112.5	8320	13.38
500	6994	7.33	400	16817	8.67	124	16514	9.3	114.5	8400	14.84
505	7154	9.53	405	17336	8.50	126.5	16687	7.9	118.5	8560	15.30
510	7314	9.54	409	17751	8.04	129	16859	8.4	122.5	8720	15.24

Depth (EB)	Age	MAT (°C)	Depth (KB)	Age	MAT (°C)	Depth (Onepoto)	Age	MAT (°C)	Depth (C. Rise)	Age	MAT
515	7475	8.61				131.5	17032	6.8	126.5	8880	15.28
520	7635	10.25				134	17235	8.2	130.5	9040	15.60
525	7795	10.38				136.5	17447	8.4	132.5	9120	13.30
530	7955	9.56				139	17659	8.7	134.5	9200	15.53
535	8116	9.20				141	17828	7.3	138.5	9360	15.55
540	8276	9.89							142.5	9520	15.72
545	8436	9.32							148.5	9760	15.62
550	8596	7.25							152.5	9920	15.50
									156.5	10080	15.42
									160.5	10240	15.52
									162.5	10320	15.15
									164.5	10400	15.23
									168.5	10560	15.49
									172.5	10720	14.12
									174.5	10800	15.98
									176.5	10880	16.14
									180.5	11040	15.75
									182.5	11170	15.49
									184.5	11300	15.92
									186.5	11430	16.66
									188.5	11560	16.63
									190.5	11690	16.12
									192.5	11820	15.79
									194.5	11950	15.81
									196.5	12080	15.39

Depth (EB)	Age	MAT (°C)	Depth (KB)	Age	MAT (°C)	Depth (Onepoto)	Age	MAT (°C)	Depth (C. Rise)	Age	MAT
									198.5	12210	15.69
									200.5	12340	15.35
									202.5	12470	14.98
									204.5	12580	14.82
									206.5	12680	14.86
									208.5	12790	14.63
									210.5	12890	14.75
									212.5	12995	11.95
									214.5	13100	13.62
									218.5	13310	13.96
									222.5	13520	13.56
									224.5	13630	14.28
									226.5	13730	13.57
									228.5	13840	13.56
									230.5	13940	13.21
									232.5	13980	13.36
									234.5	14020	13.06
									236.5	14050	13.54
									238.5	14090	13.48
									240.5	14130	13.98
									242.5	14160	12.76
									244.5	14200	12.67
									246.5	14240	12.75
									248.5	14270	12.71
									250.5	14310	12.85

Depth (EB)	Age	MAT (°C)	Depth (KB)	Age	MAT (°C)	Depth (Onepoto)	Age	MAT (°C)	Depth (C. Rise)	Age	MAT
									252.5	14350	13.33
									254.5	14480	12.52
									256.5	14610	12.24
									258.5	14740	12.25
									260.5	14870	12.13
									264.5	15130	11.84
									266.5	15260	11.88
									268.5	15390	12.34
									270.5	15520	11.87
									272.5	15650	11.89
									274.5	15780	12.05
									277.5	15980	11.78
									278.5	16050	11.74
									280.5	16180	11.88
									282.5	16310	11.92
									284.5	16430	11.52
									286.5	16540	11.57
									288.5	16640	11.41
									290.5	16740	11.53
									292.5	16850	11.31
									294.5	16950	11.11
									296.5	17060	11.4
									298.5	17160	11.32
									300.5	17265	12.73
									302.5	17370	10.76

Depth (EB)	Age	MAT (°C)	Depth (KB)	Age	MAT (°C)	Depth (Onepoto)	Age	MAT (°C)	Depth (C. Rise)	Age	MAT
									304.5	17480	10.77
									306.5	17580	10.86
									308.5	17680	10.92
									310.5	17790	10.82

APPENDIX 3: Eweburn Bog core details

Wilmshurst et al. (2002) divide the core into 4 zones based on testate amoeba assemblages within the core, with two subdivisions per zone to put finer detail into pollen records from each period. Samples were taken for ^{14}C dating throughout the core.

Zone 1 covers the bottom 550–495cm of the core, representing ca. 11000–7000 calendar years before present (BP). The core consists of highly humified peat, with no testate amoeba occurring until 500cm. The basal sediments were fine silts and clays left behind from retreating glacier meltwater, which were not sampled. Subzone 1a (550–525 cm; ca. 11000 (extrapolation) − 8700 cal. yr BP) is dominated by pollen from shrubs and small trees, with abundant grasses and ferns but forest taxa making up less than 30% of total pollen count. Traces of charcoal are present throughout the zone. Subzone 1b (525–495 cm; ca. 8700–7000 cal. yr BP) sees a rapid rise in forest taxa, especially tall podocarps, with a corresponding decline in most shrubs, grasses, and ferns.

Zone 2 (495–310 cm; ca. 7000–3400 cal. yr BP) contains more species of testate amoeba and *Sphagnum* becomes more common. Subzone 2a (495–415 cm; ca. 7000–4600 cal. yr BP) displays the peak of forest taxa, with the first presence of *Nothofagus* tall trees increasing from traces to less than 5% of total pollen. Total small trees, shrubs, grasses, and ferns remain present but very low. Subzone 2b (415–310 cm; ca. 4600–3400 cal. yr BP) shows a local peak of Nothofagus up to about 40% total, with a subsequent drop-off to less than 10% as other tall trees rise to take its place. Shrubs are consistently present but in low percentages, while wetland taxa are in highest abundance during this time.

Zone 3 (310–75 cm; ca. 3400–400 cal. yr BP) contains a sharp transition to drier species of testate amoeba, showing marked surface dryness along with lowered water table estimates and a decrease in *Sphagnum* abundance. Subzone 3a (310–125 cm; ca. 3400–1300 cal. yr BP) shows *Nothofagus* declining while other tall trees increase in prevalence. Some grasses flourish, while most small trees and shrubs show very little signs of thriving. A charcoal band at 200cm corresponds to some wetter plants decreasing in abundance, although plants requiring dry conditions do not necessarily increase in exchange. Subzone 3b (125–75 cm; ca. 1300–400 cal. yr BP) depicts a decline in podocarp trees as well as shrubs requiring wetter conditions.

Zone 4 (75–0 cm; ca. 400 cal. yr BP to present) contains a rapid change back to wetter conditions at 60cm, with higher *Sphagnum* abundance, amoeba tests indicating the increased prevalence of wet-tolerant species, and humification becoming poorer with decreasing depth. Subzone 4a (75–35 cm; ca. 400–130 cal. yr BP) chronicles the onset of deforestation in the region, with tree taxa as a whole sharply decreasing in abundance in favor of ferns and shrubs. A large charcoal presence indicates human-derived forest clearing during this time (McWethy et al., 2009). Subzone 4b (35–0 cm: ca. 130 cal. yr BP to the present) contains the appearance of introduced species brought to the region during settlement alongside further declines in most tall trees and wetland species, with small trees, shrubs, and grasses proliferating to take their place.

APPENDIX 4: Supporting data: pollen assemblages and pollen temperatures

The cores upon which the present study was based were initially studied for pollen records by Matt McGlone and Janet Wilmshurst, and these records were subsequently reanalyzed for temperature records by Janet Wilmshurst. The pollen results from these previous studies of Kettlehole and Eweburn Bogs have been previously published (McGlone et al., 2004; Wilmshurst et al., 2002). The temperature results are based on seven temperature reconstructions from pollen assemblages taken from sites across the South Island of New Zealand (Figure 1-3). These reconstructions are thought to be biased due to pollen not accurately representing changes in local aridity. Eweburn mean annual temperature data was collected and calculated during the same study as the Kettlehole temperature data (Wilmshurst et al., 2007), but has not been previously published. All pollen records are reported in percent fraction of total pollen counted in a given sample (McGlone et al., 2004; Wilmshurst et al., 2002).

A4.1 Kettlehole Bog

Kettlehole Bog contains a complex pollen record. The base of the pollen record at 17.7ka has high concentrations of shrubs and small trees (43.5-56.7%) and grasses (16.7-26.4%), with a very low abundance of tall trees (4.1-4.8%). Between 16.8-16.3ka, however, this ecosystem underwent an abrupt change, with tall trees taking over at 80.0% abundance, with shrubs and grasses declining (14.5% and 3.0% respectively). After this abrupt change, shrubs and grasses both gradually increased to 43.6 and 28.4% abundance (respectively) by 14.1ka, as the tall trees declined once again to 12.8%. This trend continued until 13.3ka, and from then to 12.4ka when shrubs achieved their maximum abundance (82.2-91.6%), and tall trees dipped to their minimum abundance (2.6-6.3%). Herbs and grasses continued

to decline in abundance (5.3% at the beginning of this period to 1.3% at the end). At 12.4ka, another extreme shift occurred when tall trees suddenly surpassed shrubs and small trees to become the dominant plant type (74.6-98.2%), a pattern that persists until the top of the core (~2ka). Shrub abundance decreased correspondingly (1.7-23.9%), and grasses became nearly nonexistent (0-1.4%). There are a few fluctuations following this at 11.6ka and 9.7ka, but they are relatively minor (Figure A4-1). These excursions from the norm did not involve grass and herb abundances. At the top of the core (2.8ka), the pollen ratios experience a shift that is relatively small, with tall trees dropping from 91.7% to 56.7%, shrubs remaining relatively constant from 6.8 to 4.7%, and grasses rising from 0.9% to 14.4%, their highest relative abundance in 10,000 years.

The characteristic warming of the HS1 beginning at 17.5ka is barely present (Figure A4-1), obscured by a cooling regression from 8.6°C at 16.8ka to 7.9°C at 15.8ka that is only just overcome at 14.6ka and 8.9°C before the predicted start of the ACR at 14.7ka. An increase in temperature occurs during the supposedly cooling ACR, to a maximum of 9.3°C at 13.1ka, followed by more cooling, reaching 8.8°C by 12.8ka. Further cooling followed to a minimum of 7.8°C as the warming of the Younger Dryas occurred elsewhere in the southern hemisphere. Finally, at 12.0ka, warming begins in earnest until 11.4ka, after which the climate drops and rises again until the end of the climate optimum, which appears to be at 9.4ka, hitting an all-time maximum of 10.0°C. From then to the top of the core, the Kettlehole temperature reconstruction generally decreases to a minimum of 7.6°C at 2.7ka.

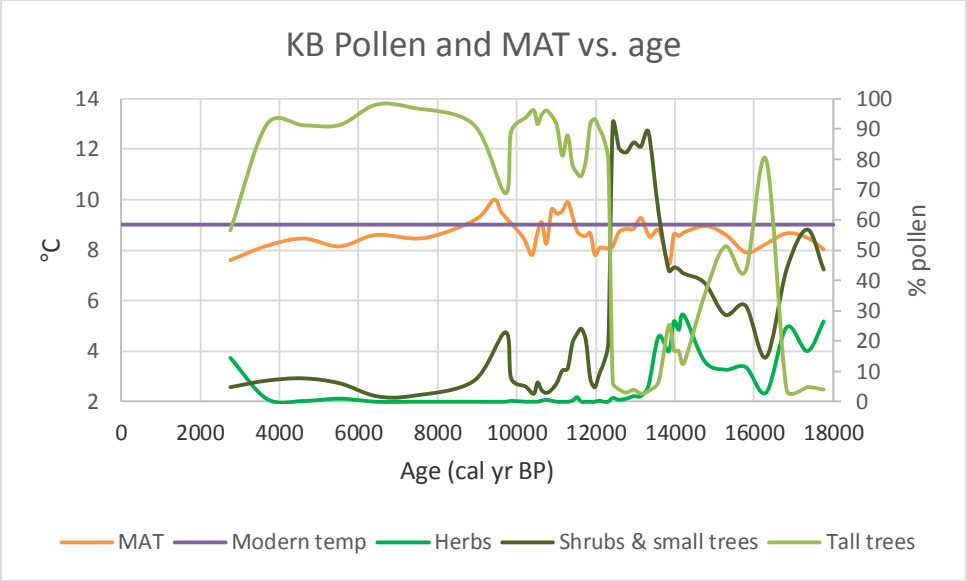

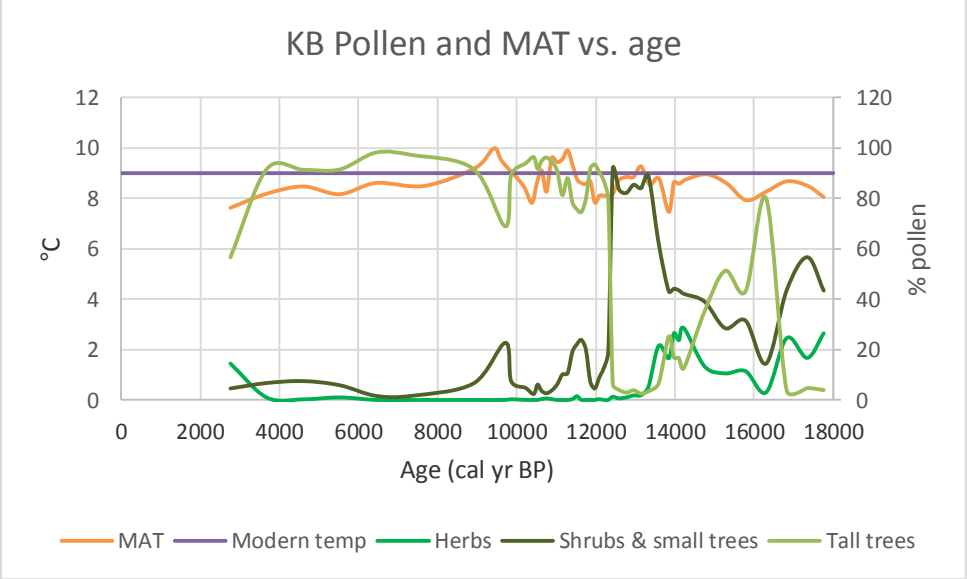

Figure A4-1: Top: Kettlehole Bog pollen percentages and mean annual temperature plotted against age (cal yr BP). MAT stands for modern analog technique, which was used to calculate mean annual temperature over this time period. Bottom: The same graph with axes arranged to best display the apparent negative correlation between tall tree pollen percentage and MAT from 12.4-7.7ka (McGlone et al., 2004; Wilmshurst et al., 2002).

Kettlehole Bog spans nearly the entire deglaciation, which allows temperature, ecology, and aridity to be compared from the LGM through such important deglacial millennial events as the ACR and the Younger Dryas. The core contains a complex pollen record that is an important component of the BBM record constructed in this thesis. From the LGM to the Holocene, the temperature of the bog changed very little, despite large shifts in both pollen abundance ratios and burning biomarker concentrations.

A4.2 Eweburn Bog

Eweburn Bog, which only covers the Holocene, had a simpler pollen record in contrast to the more complex BBM history discussed above. The pollen ratios between tall trees (91-99%), grasses (0-1%), and short trees and shrubs (0.6-7.3%) remained relatively constant (Figure A4-2) between the bottom of the core record at about 7ka and the modern (Wilmshurst et al., 2002). There was a minor dip in tall tree abundance percentage from 97.8-95.4% and back up to 99.0%. That came just before the large levoglucosan spike at 6ka, as well as separate dips in tall tree abundance just before (97.5-92.0% at 4.5ka and then back to 95.6%) and after (95.0-92.8% at 3.7ka and then back to 97.0%) large spikes in both levoglucosan and vanillic acid at 4ka. The sharp decrease in tall trees at approximately 200 years has been ascribed to anthropogenic deforestation and widespread land burning during European colonization of the country (McWethy et al., 2009).

The mean annual temperature reconstruction of Eweburn Bog exhibits a gradual curve from high at the bottom of the core, to low in the middle of the core, to about modern temperatures by the top. The lowest points in the core, where the pollen record

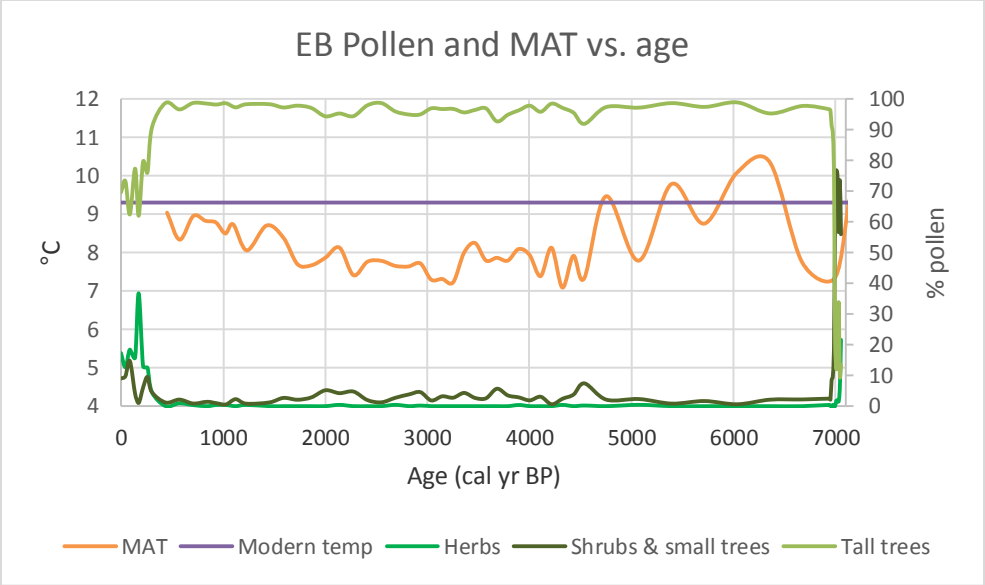

Figure A4-2: Eweburn Bog pollen percentages and mean annual temperature plotted against age (cal yr BP). MAT stands for modern analog technique. Ratios of tall trees, shrubs, and grasses remain essentially stable between 7.0-0.4ka, despite the oscillating temperature.

begins, swing from 9.5°C at 7.1ka to 7.3°C at 7.0ka to 10.3°C at 6.3ka, from one of the lowest temperatures recorded to the highest. This temperature dip appears at the time that a major ecosystem reorganization occurs in the pollen record. From 6.3ka, the temperature reconstruction fluctuates but cools overall to the lowest temperature of 7.1°C at 4.3ka. The reconstructed temperature plateaus from 4.3-3.3ka, warming to the top of the core with less fluctuation than the previous cooling exhibited. The youngest reconstructed temperature is 9.0°C at 0.4ka, which is only slightly cooler than the modern mean annual temperature of 9.2°C.

Overall, the temperature in Eweburn Bog did not appear to affect the biomass much at all. The only relevant changes to biomass were at the time of European colonization in the modern, and at the base of the core, but without BBM records during this time the cause

and effect relationship between temperature reconstruction and biomass cannot be determined.

A4.3 Mean annual temperature for KB and EB cores over time

Where the two temperature reconstructions overlap, they seem to agree in overall trend of warming or cooling, if not in magnitude {Wilmshurst, 2007 #2842; Wilmshurst, unpublished data}.